ANDRA BGR CHEVRON CRIEPI ENRESA ENSI GRS IRSN
JAEA NAGRA NWMO OBAYASHI SCK•CEN SWISSTOPO

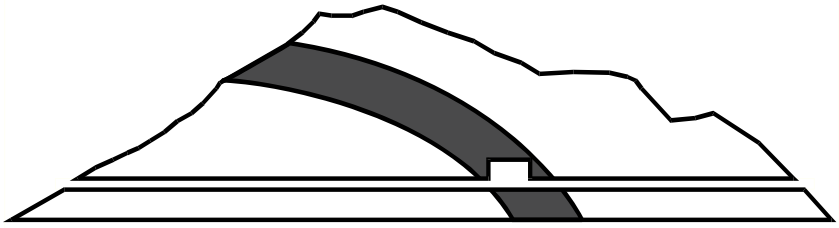

Mont Terri Project

TECHNICAL REPORT 2009-07

July 2010

LT Experiment:
Mechanical Behavior of Opalinus Clay, Final report from Phases 6 – 14

W. Gräsle and I. Plischke

BGR, Germany

Distribution:

Standard distribution:

ANDRA (J. Delay)

BGR (K. Schuster)

CHEVRON (P. Connolly)

CRIEPI (K. Kiho)

ENRESA (J.C. Mayor)

ENSI (E. Frank)

GRS (T. Rothfuchs)

IRSN (J.-M. Matray)

JAEA (K. Aoki)

NAGRA (T. Vietor)

NWMO (B. Belfadhel)

OBAYASHI (H. Kawamura, T. Ishida)

SCK•CEN (G. Volckaert)

SWISSTOPO (P. Bossart, A. Möri and Ch. Nussbaum)

Additional distribution:

Every organisation & contractor takes care of their own distribution.

TABLE OF CONTENTS

1 INTRODUCTION

The long-term safety of repositories for radioactive or toxic wastes can be predicted if the mechanical behavior and hydraulic properties of the host rock can be described reliably. For this purpose laboratory tests were performed on the Opalinus Clay formation (shaly facies) from the Mont Terri Rock Laboratory.

The LT (laboratory temperature testing) experiment started in project phase 6 (2001 – 2002) with the general objective of the "description and characterization of creep, dilation, healing, strength and permeability of Opalinus Clay at various temperatures." The associated laboratory experiments have been performed by BGR in its geomechanical facilities.

During phase 6, 7 & 8 and 12, 13 & 14 this experiment was supported by BGR and NAGRA, whereas Phases 9 up to 11 were solely performed by BGR.

The results of associated strength tests are described in SCHNIER (2005). Additional results from triaxial Karman tests at BGR during phase 8 and 9 that include failure and post failure strengths, elastic deformation parameters, influence of the bedding and water content as well as deformations due to temperature changes are reported by SCHNIER & STÜHRENBERG (2007).

Phases 9 and 10 focused on the results of true triaxial experiments with respect to the deformation behavior under isostatic and shear loading and anisotropies of strength and dilatancy of Opalinus Clay. The results are reported by NAUMANN & PLISCHKE (2006).

Starting in phase 11 up to phase 14 long-term multistep creep tests on samples from the shaly facies were carried out. The tests were performed under drained and undrained conditions. During this time a new type of triaxial test using a complex process path was carried out, investigating the limit of linear elastic behavior, the shear failure limit, and the residual strength as functions of minimum principal stress or mean normal stress respectively. The tests were performed under undrained conditions to allow for the investigation of possible pore pressure effects. The results from phase 11 to 13 are reported by GRÄSLE & PLISCHKE (2007 + 2009).

During phase 12 and 13 the influence of clay microfabric on petrophysical properties was analyzed by KLINKENBERG ET AL. (2008a). In a second step KLINKENBERG ET AL. (2008b) analyzed the mineralogical composition and microfabric of the sandy facies of the Opalinus Clay from Mont Terri, to find differences respectively similarities.

2 DRILLING, SAMPLING, STORING AND PREPARATION

In several phases of the LT-experiment drillholes were realized to obtain core material from the shaly facies of the Opalinus Clay formation from the Mont Terri underground rock laboratory. The drillholes were drilled at the beginning of the LT-experiment by the French company COREIS and from phase 8 on by BGR itself. Both crews used dried air flushing for drilling. For all boreholes a 101 mm inner diameter tungsten carbide bit was used.

The extracted samples were put into aluminium coated plastic foils evacuated from air resulting in a partial vacuum. Thus they were protected against drying and oxidation. Samples from boreholes BLT 9, BLT 10 and BLT 12 were stored in an ANDRA cell, where a silicon tube was slipped over the sample and put into a stiff plastic liner; the space between the liner and the sample was then filled with expanding cement and the ends were closed with plates under pressure of a spring. This is an expensive equipment, where additionally the sample has to be cut to size (300 mm) with parallel heads.

Therefore BGR started to develop a liner system for an easier, quicker and cheaper storage. Beginning in phase 9 the samples were placed inside plastic liners (to reduce effects of further unloading) filled with nitrogen at a pressure of 3 bars (used to avoid the formation of gypsum under contact with oxygen). Prototype liner version A was only used for the samples from BLT 10, but has some problems with pressure tightness. Due to handling and transportation or insufficient welding some plastic tubes lost their vacuum. For this and for storage and handling reasons a stiffer and thicker material was used for liner version B (total length 1.69 cm, max. sample length 152 cm). The ends of the liner were closed with a fixed and a screw cap. Liner version C is shorter than version B (total length 116.5 cm, max. sample length 88.5 cm), so it is possible to handle the liner rig on a euro-palette. Fig. 1 to Fig. 3 show the different liner generations which have been used up to this day.

The time between drilling and packaging the cores into the various liner systems was always minimized in order to reduce drying-out. After transport to BGR the liners were stored at a constant temperature of 22°C.

The location of the boreholes is shown in Fig. 4. Basic information of the boreholes, sample type, type of tests and different storage conditions is presented in Tab. 1 (Appendix A). Sample type denotes the orientation of the bedding to the sample axis: p-samples were drilled parallel to the bedding, s-samples were drilled perpendicular and z-samples inclined (Fig. 5). P-samples can be subdivided whether the borehole orientation was parallel to the strike or the dip of the layer.

Fig. 1 BGR liner version A.

Fig. 2 BGR liner version B.

Fig. 3 BGR liner version C.

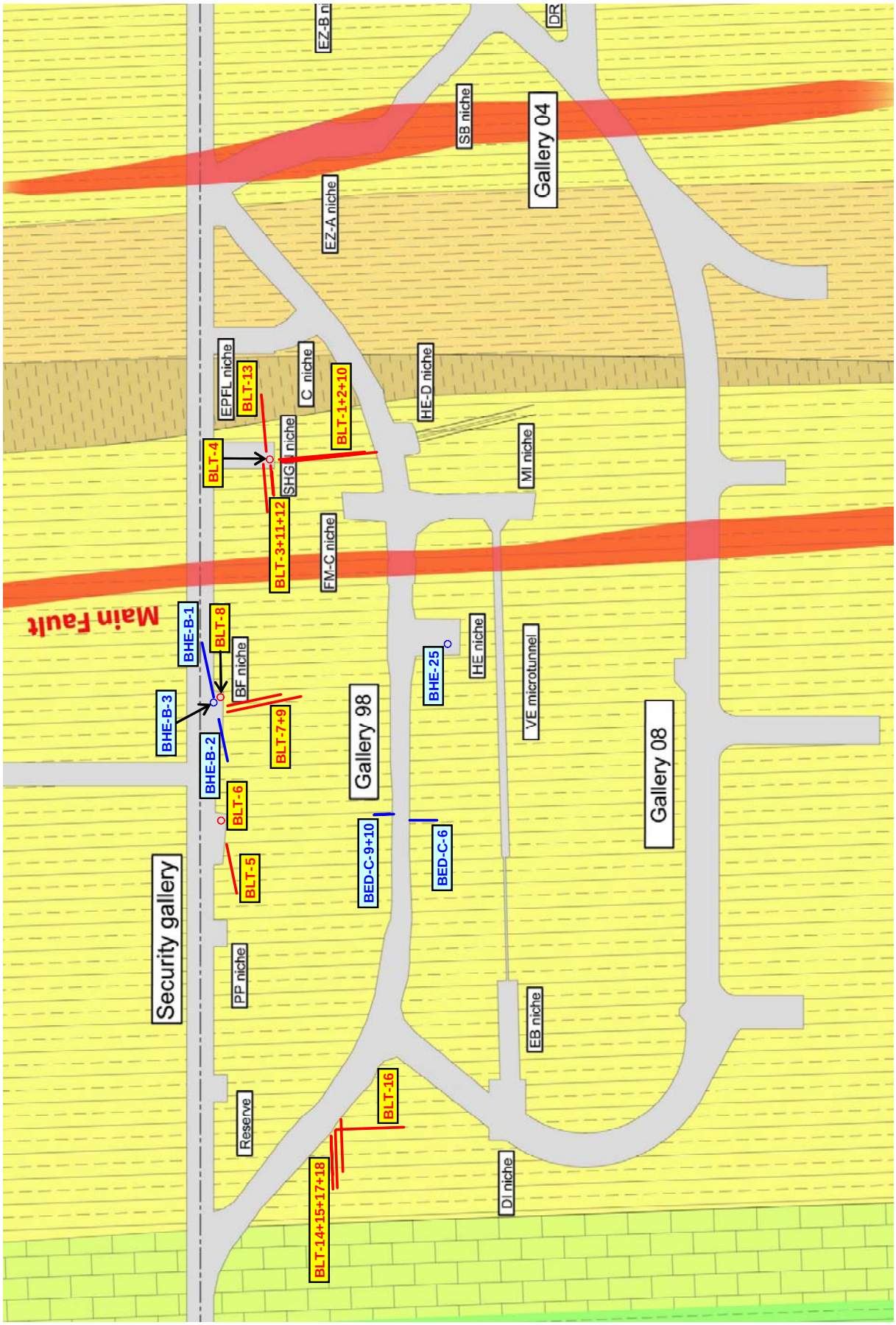

Fig. 4 Location of the BLT-boreholes as well as any other boreholes sampled for tests performed in the LT-experiment.

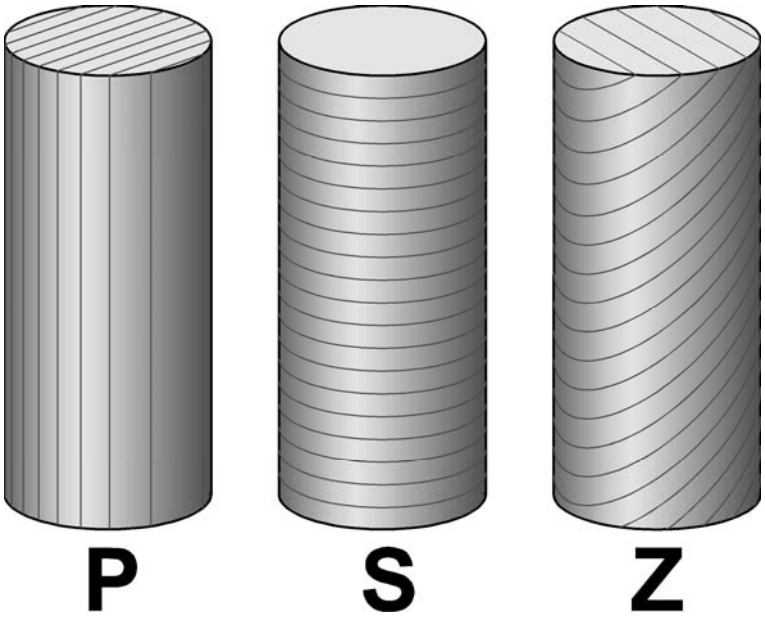

Fig. 5 The alignment of cylindrical samples with respect to bedding for p-, s- and z-geometry.

From phase 9 sample preparation was carried out immediately before the tests. They were cut to length with a band saw. Usually, samples are trimmed to smooth cylindrical shape on lathe. The preparation of the first sample revealed a high risk to generate breakouts at the edges during trimming (see Fig. 6). For s-samples there was also a severe risk of sample disintegration by disking. As the drilled cores already displaced a rather smooth shape the impact of the small deviations from a perfectly cylindrical shape have been considered negligible compared to the impact of possible breakouts. Therefore, the s-samples have been used without trimming on a lathe.

To avoid undesirable friction effects during the tests the samples were covered with a Teflon foil before they were coated in rubber tubes which prevent any contact between the samples and the oil pressuring the Karman cell.

Fig. 6 A breakout at the edge of a specimen generated during trimming on a lathe (p-sample 08018 from BLT 14).

3 GEOLOGICAL AND MINERALOGICAL DESCRIPTION

The general mineralogical properties of the host rocks at the Mont Terri laboratory have been summarized by THURY & BOSSART (1999). Shaly, calcareous-sandy and sandy facies are distinguished. Their main difference in terms of mineralogical composition is the content of clay minerals and quartz. The content of feldspars is similar (PEARSON ET AL., 2003). All samples used for the rock mechanical experiments of the LT-experiment covered by this report belong to the shaly facies.

Properties of the tested samples such as bulk density, water content and ultrasonic velocities are reported in Tab. 2 (Appendix A).

4 ANALYSIS OF MINERAL COMPOSITION AND MICROSTRUCTURE OF SHALY AND SANDY FACIES

The influence of clay microfabric on petrophysical properties was analyzed by KLINKENBERG ET AL. (2008a). It is known that carbonate content significantly affects mechanical strength. The failure strength of Opalinus Clay (shaly facies) from Mont Terri decreases with increasing carbonate content while the failure strength of Callovo-Oxfordian clay-stone from Meuse-Haute-Marne-URL (Bure) increases. This can be explained by the microfabric: Opalinus Clay from Mont Terri contains relatively large carbonate embeddings (mostly shell fragments) surrounded by an argillaceous matrix while Callovo-Oxfordian clay-stones from Bure contain fine-grained homogeneously distributed carbonates.

The most important result of the performed image analysis is, that not only the carbonate (shell) content but also the grain size distribution, shape and spatial distribution of carbonates determine the mechanical behavior of the clay (see also Fig. 7).

KLINKENBERG ET AL. (2008b) also analyzed the mineralogical composition and microfabric of the sandy facies of the Opalinus Clay from Mont Terri, to find differences respectively similarities. In comparison to the shaly facies the sandy facies offered a completely different microfabric. The carbonates of the sandy facies exist cement-like respectively (depending on the percentage) are the matrix itself (see Fig. 8).

One has to keep in mind though that image analysis is not the ideal method for analyzing samples from the sandy facies since the image sections do not reflect the real (larger scale) texture of the rock and therefore are probably not representative.

In summary:

- The image sections of the sandy facies are not representative in relation to the image analysis for the carbonates.
- Extraction of the carbonates in the sandy facies by image analysis is problematical because of the relative big particles.
- Texture attributes of sandy and shaly facies are not comparable directly.
- The carbonates of the sandy facies are existing as cement and there are only marginal big biogenous carbonates like shell fragments.
- There is clustering of the carbonates in the sandy facies. In comparison to this the biogene carbonates (shell fragments) of the shaly facies of the Opalinus Clay respectively the carbonates of the Callovo-Oxfordian from Bure are distributed more homogeneous.

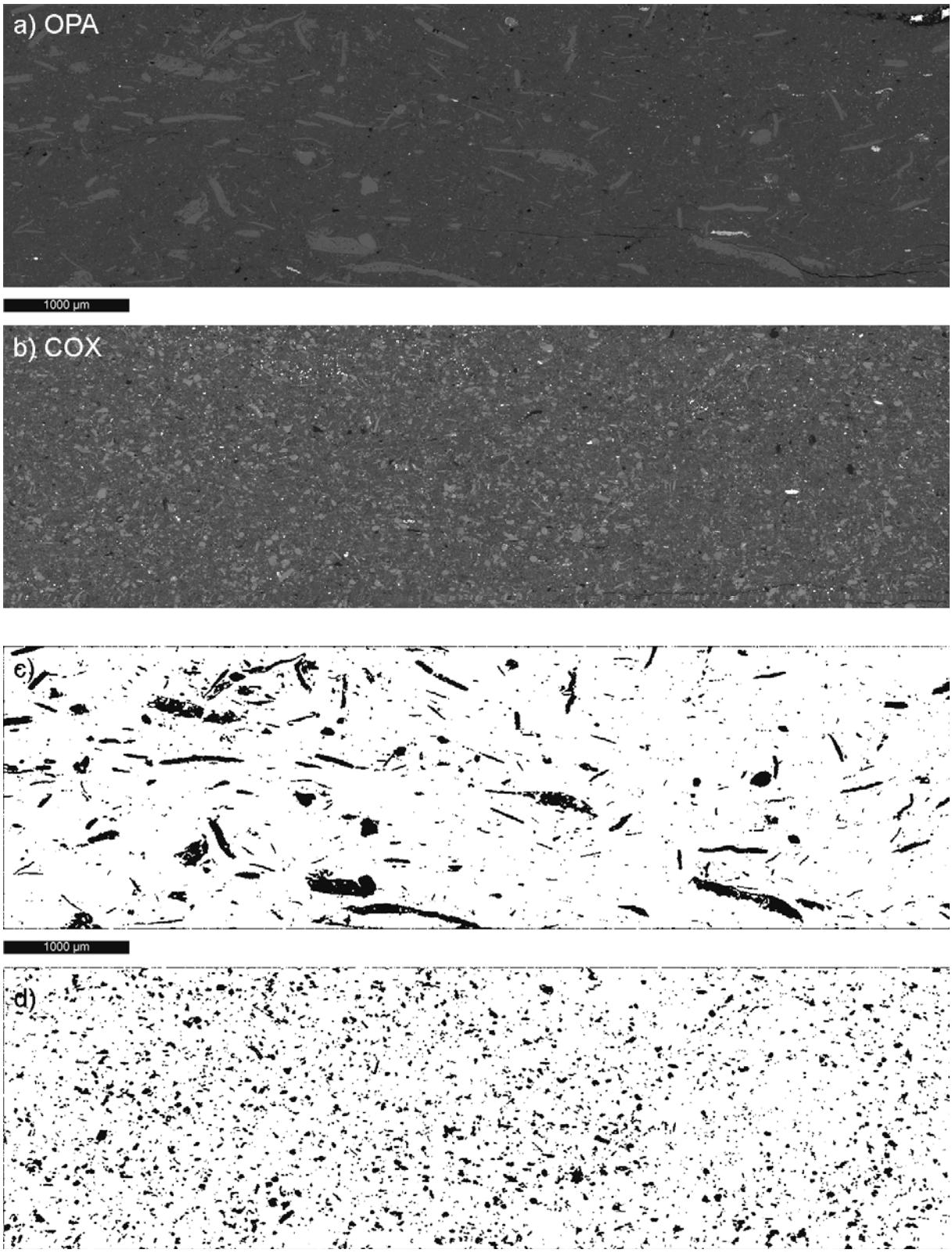

Fig. 7 Comparison of carbonate distribution: a) Opalinus Clay (OPA) BLT 12/10 (BSE-image), b) Callovo-Oxfordian clay-stone (COX) 23_05 (BSE-image), c) extracted carbonates of BLT 12/10, and d) extracted carbonates 23_05 (Figure from KLINKENBERG ET AL., 2008a).

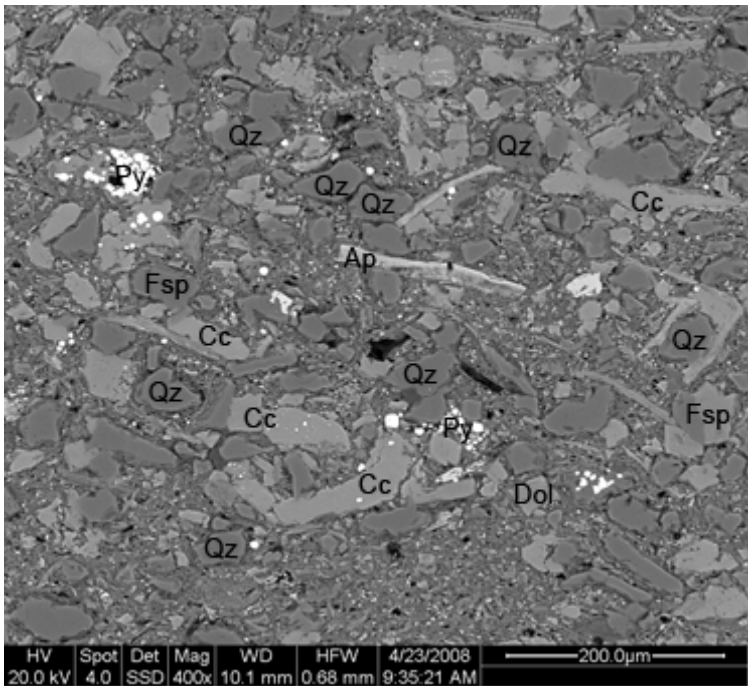

Fig. 8 BSE-image (back scattered electron microscopy) of a polished section of BEZ-G19/1 B from the sandy facies of Mont Terri Opalinus Clay. Qz = quartz, Fsp = feldspar, Cc = calcite, Do = dolomite, Py = pyrite, Ap = apatite (Figure from KLINKENBERG ET AL., 2008b).

5 CREEP TESTS

5.1 EXPERIMENTAL CONCEPT AND DATA ANALYSIS

The long term behavior of rock material under the impact of anisotropic stresses is a key parameter for the evolution of any underground excavation (convergence, reduction of deviatoric stress). Therefore, in the framework of this experiment also creep tests have been carried out on Mont Terri Opalinus Clay samples. The anisotropy of the clay has to be considered in these tests.

The creep tests were carried out in conventional Karman cells. All samples had a diameter of 100 mm and a length of 200 to 250 mm. Altogether, 13 samples (8 in p-orientation and 5 s-samples) have been investigated in triaxial creep tests between 2002 and 2009 (Tab. 3 in Appendix A). All tests have been designed as multistep tests to assess the impact of deviatoric stress σ_{dev}. To allow for the investigation of several other effects, different test layouts have been applied:

- Simple undrained multistep triaxial tests with a confining pressure σ_3 of 10 or 12 MPa (file no. 03035I, 03060, 03061, 03062).
- One test applying extensive variation of confining pressure to analyze its effect on creep behavior (file no. 02009).
- As pore pressure is expected to influence the creep behavior of Opalinus Clay also drained tests have been performed by placing plates of sintered metal at both ends of a sample (file no. 07001 to 07005). Later on, this concept has been enhanced by investigating any sample in two subsequent multistep tests, first in undrained and afterwards in drained mode (file no. 08018/08018A to 08022/08022A). This allows for a comparison of the creep behavior under different hydraulic regimes avoiding the impact of sample variation. Further improvement has been made by preceding any drained loading phase by a consolidation phase (σ_{dev} = 1 MPa) in a way that avoids an increase of the mean stress σ_{oct} at the beginning of any drained loading phase. Otherwise settlement resulting from retarded drainage may superimpose the creep process for a long time (for details see GRÄSLE & PLISCHKE, 2009).

Ideally, the stationary creep rate $\dot{\varepsilon}_\infty$ can be determined as slope of a linear section of the deformation curve ε(t) at the end of a loading phase. It usually takes a long time (several month or even more than a year) until stationary creep is achieved. Therefore, many creep tests terminate while creep is still transient. "Stationary" creep rates are then determined as tangent slope of the deformation curve ε(t) at the end of a loading phase. This leads to a general overestimation of the stationary creep rate.

An extrapolation algorithm has been developed to reduce this problem. Tests revealed that (except for the initial part of a loading phase) the creep rate $\dot{\varepsilon}$ can be described well by

$$\ln(\dot{\varepsilon}(t)) = \ln(\dot{\varepsilon}_\infty) + \exp(a + b\,(t - t_0)) \qquad \text{with fit parameters } \ln(\dot{\varepsilon}_\infty),\ a \text{ and } b \ (\text{where } b < 0)$$

This means, that the logarithm of creep rate $\ln(\dot{\varepsilon})$ exponentially converges towards the logarithm of the stationary creep rate $\ln(\dot{\varepsilon}_\infty)$. For reason of error propagation, fitting the measured strain rates does not work sufficiently for strain rates below $3 \cdot 10^{-6}$ d^{-1}. Performing a weighted fit in the integrated form, i.e. fitting ε instead of $\dot{\varepsilon}$ is an appropriate workaround for this problem:

$$\varepsilon(t) = \varepsilon_0 + \int_{t_0}^{t} \dot{\varepsilon}(t')\,dt' = \varepsilon_0 + \exp(\ln(\dot{\varepsilon}_\infty)) \int_{t_0}^{t} \exp(\exp(a + b\,(t' - t_0)))\,dt'$$

$$\text{with fit parameters } \varepsilon_0 = \varepsilon(t_0),\ \ln(\dot{\varepsilon}_\infty),\ a \text{ and } b \ (\text{where } b < 0)$$

Weighting is performed with $wgt = \dot{\varepsilon}^{-1} = \exp(-\ln(\dot{\varepsilon}_\infty) - \exp(a + b\,(t - t_0)))$ to ensure an error characteristic similar to that of a $\ln(\dot{\varepsilon})$-fit. A detailed description of this method is given in GRÄSLE & PLISCHKE (2009).

This extrapolation method performs well in case of moderate extrapolation and the availability of rather clean data for the still bending section of the deformation curve ε(t) at the end of a loading phase.

5.2 RESULTS

An overview of the creep tests carried out within the LT-experiment is given in Fig. 9 and Tab. 3 (Appendix A). Overall, the data appear to fit well with other published data from Mont Terri Opalinus Clay (NAGRA, 2002, CZAIKOVSKI ET AL., 2006), essentially expanding the covered range of deviatoric stresses towards smaller stresses.

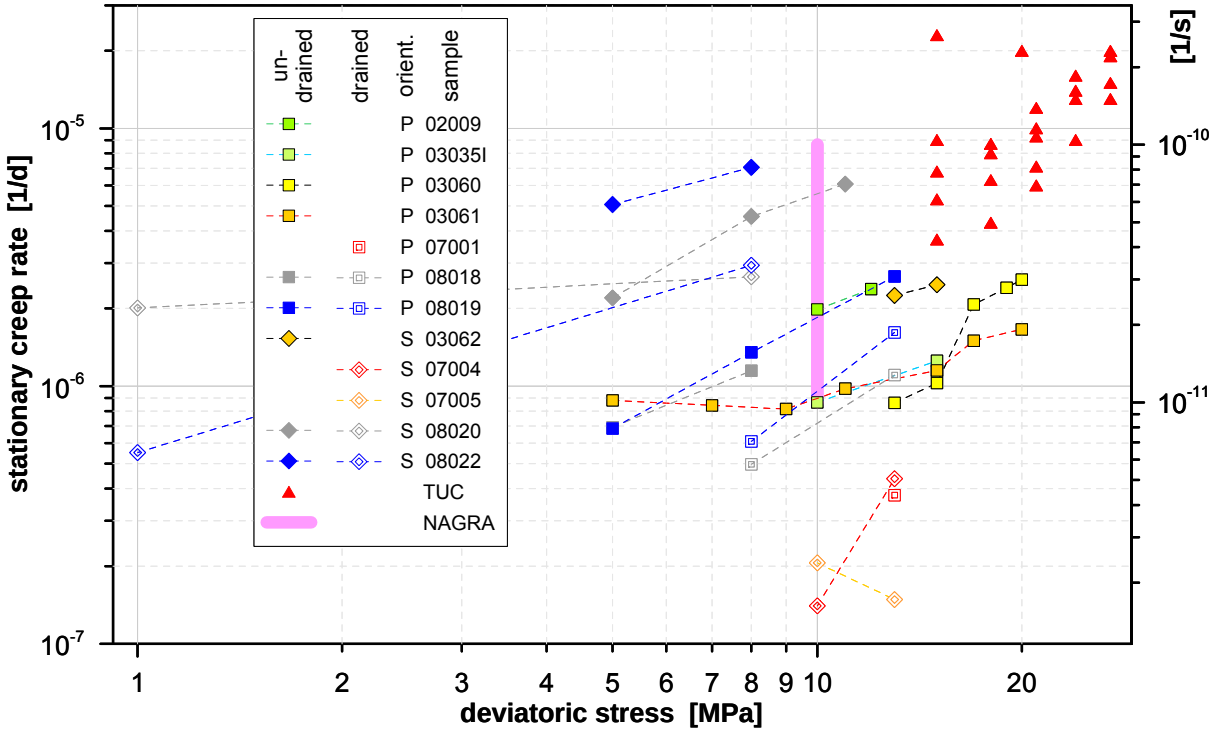

Fig. 9 Results from triaxial creep tests performed in the LT-experiment compared to other published data ("NAGRA" from NAGRA, 2002, "TUC" from CZAIKOVSKI ET AL., 2006). Data measured on the same sample are connected by dashed lines.

It has to be noted that there are a few unusual data that might not be representative for the investigated material:

- These are the samples 07001 to 07005 which have been used in the very first drained tests carried out in phase 12 and 13. They displayed extraordinary small creep rates that are close to the detection limit (therefore, their relative accuracy is assumed to be rather poor). Further-

more, another 9 data points from 0700x-samples at deviatoric stress between 5 MPa and 13 MPa cannot be shown in Fig. 9 because the observed strain rates fall below the detection limit.

- There are some creep rates determined under drained conditions at a deviatoric stress of 1 MPa. It was not expected that any creep would be detectable with an observation time of less than one year at this low deviatoric stress. Nevertheless, the creep rates found can be determined with sufficient reliability (for reliability criteria regarding the extrapolation algorithm see GRÄSLE & PLISCHKE, 2009). Whereas the observed ε(t)-curves for samples 08019A (not shown in Fig. 9 since strain rates is below 10^{-7} d^{-1}) and 08022A do not exhibit any peculiarities, sample 08020A behaves atypically. It reaches an approximately stationary deformation rate within less than 2 weeks (it usually takes several month) and shows almost the same deformation rate at σ_{dev} = 1 MPa and σ_{dev} = 8 MPa. Therefore, the representativeness of this sample is questionable.
- Besides this, the TUC-data shown in Fig. 9 most likely have a biased error. Usually, loading phases in TUC creep tests last approximately 30 d. This is significantly shorter than in creep tests of the LT-experiment (cf. Tab. 3 in Appendix A), and is definitely insufficient to achieve stationary creep. Consequently, TUC-data (representing the strain rate at the end of the loading phase) will overestimate the stationary creep rate $\dot{\varepsilon}_{\infty}$ systematically. Presumably, this overestimation is about half an order of magnitude, as for the undrained creep tests of the LT-experiment the ratio $\dot{\varepsilon}(30\,\mathrm{d}) / \dot{\varepsilon}_{\infty}$ is 3.4 on average (geometric mean).

5.2.1 Anisotropy

The results display a strong anisotropy with significantly higher creep rates under loading perpendicular to the bedding plane (Fig. 10). Except for the atypical 0700x-samples, the creep rates of s-samples surpass those of p-samples by approximately half an order of magnitude, corresponding to a ratio of anisotropy between 3 and 4.

As for any other conclusions from the presented creep test, is has to be stressed that the data basis is still very small, particularly with respect to s-geometry. To enhance reliability, confirmation by an increased data basis is required.

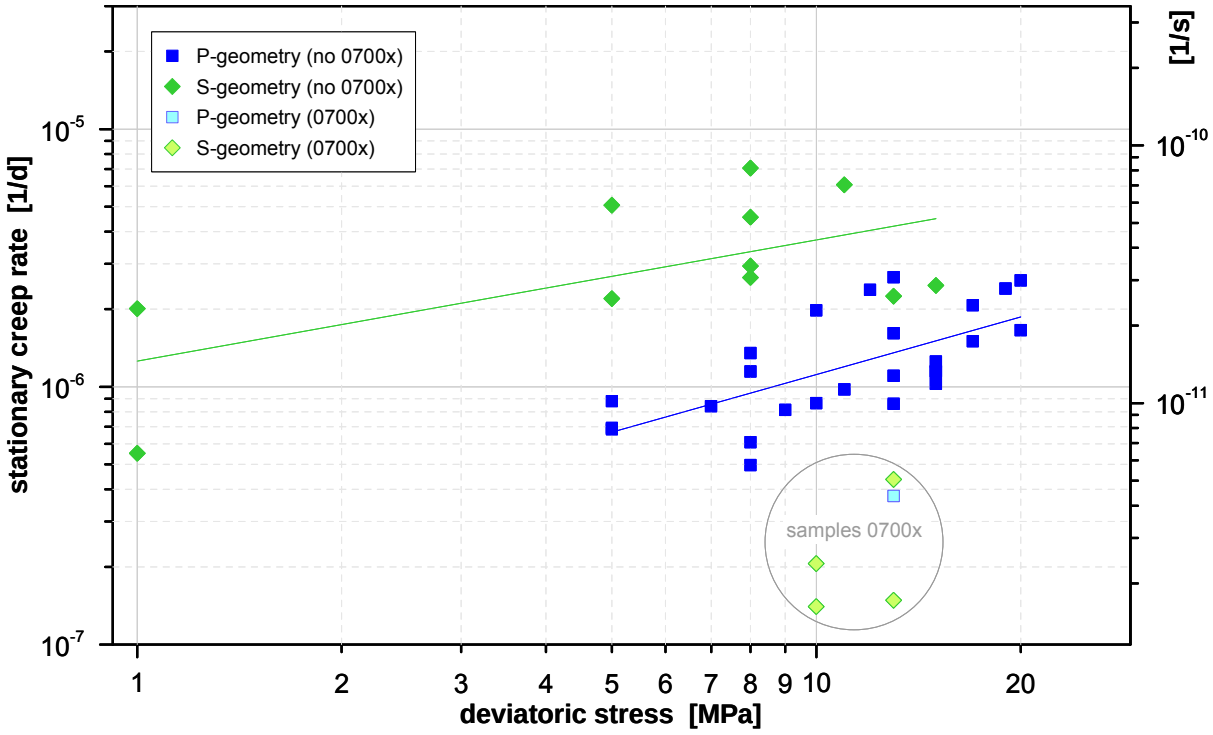

Fig. 10 Except for the data from samples 07001 – 07005 which exhibited extraordinary small creep rates close to or even below the detection limit (data inside the circle), loading in s-direction results in significantly higher creep rates than loading parallel to the bedding. The displayed linear fits for s- respectively p-data are calculated excluding the 0700x-samples.

5.2.2 Influence of deviatoric stress on creep rate

Because the data set for drained tests is too small for a meaningful statistical analysis with respect to deviatoric stress, the following analysis is based on undrained tests only.

When looking at the results of undrained tests from the LT-experiment and from CZAIKOVSKI ET AL. (2006) as a combined data set (of cause, this is somewhat questionable because relevant parameters as sample orientation, mineralogical composition, water content, and details of the test layout may vary systematically between the data sets), the data set is compatible with the assumption of a linear relationship between $\ln(\dot{\varepsilon}_\infty)$ and $\ln(\sigma_{dev})$, corresponding to a power law $\dot{\varepsilon}_\infty \propto \sigma_{dev}^{\ n}$ (Fig. 11).

As any differentiable function can be fitted well by a linear approximation on any sufficiently small interval, and the actual tests cover a rather limited range of $\ln(\sigma_{dev})$, this does not necessarily imply that a linear relationship of $\ln(\dot{\varepsilon}_\infty)$ and $\ln(\sigma_{dev})$ is an appropriate description for an extended range of $\ln(\sigma_{dev})$. As shown in Fig. 11, a superlinear $\ln(\dot{\varepsilon}_\infty)$ vs. $\ln(\sigma_{dev})$ relationship fits the data slightly better (Tab. 4). This would correspond to a $\dot{\varepsilon}_\infty(\sigma_{dev})$-function which is of higher order than any power law, e.g. an exponential relationship (like the LUBBY2 model often used for rock salt). The great discrepancy between both fits at low deviatoric stress highlights the amount of uncertainty inherent to any extrapolation from the available data basis towards deviatoric stress in the order of 1 MPa.

Considering that the TUC data probably overestimate stationary creep rates by half an order of magnitude (cf. p. 12), these fits have also been calculated using TUC data scaled by a factor 0.3 (green curves in Fig. 11). Once again, the exponential fit performs slightly better than the power law (Tab. 4).

The improvement of fit quality for the scaled TUC data which results in a strong reduction of the RMSE (whereas the poorer coefficient of determination simply reflects the dramatic decrease of the population variance) is another indication of the bias in the TUC data.

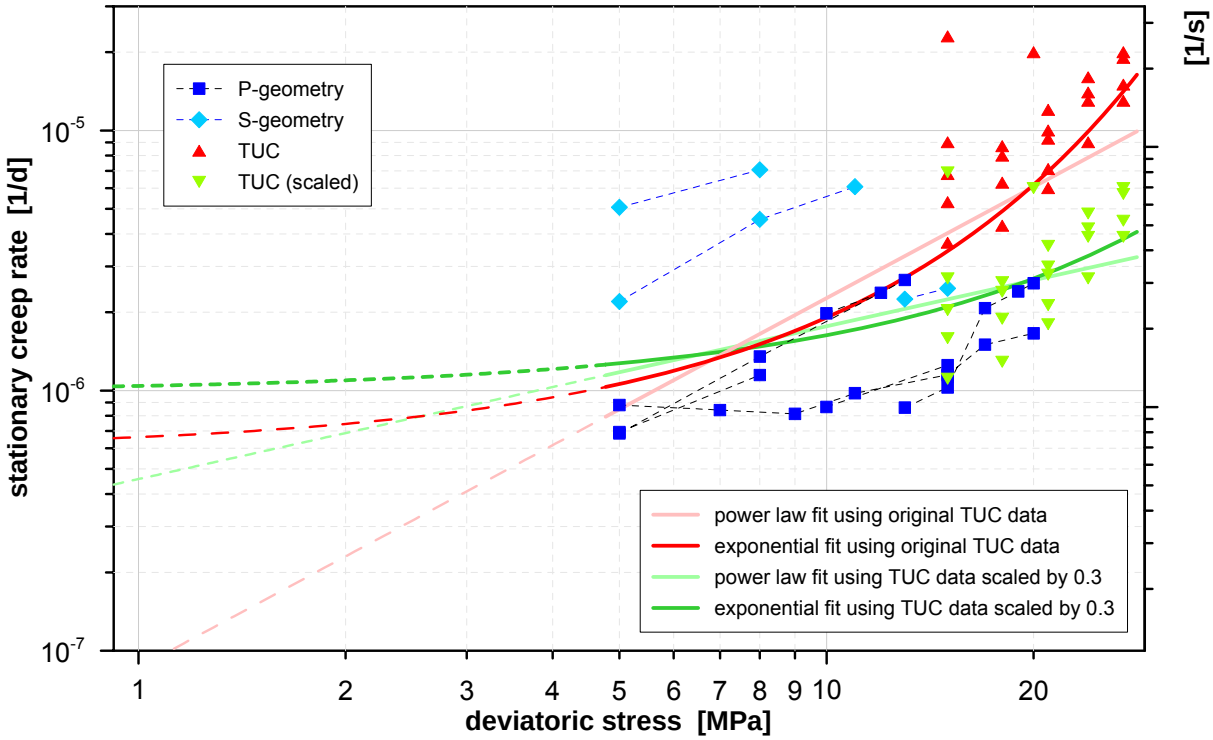

Fig. 11 Undrained stationary creep rates from the LT-experiment (excluding the 0700x-samples) and from TUC (CZAIKOVSKI ET AL., 2006) are slightly better represented by an exponential $\dot{\varepsilon}_\infty(\sigma_{dev})$-function ($R^2 = 0.493$) than by a power law ($R^2 = 0.418$). Nevertheless, the difference between both fits is not statistically significant. Same applies when a data set scaled by factor 0.3 is used instead of the original TUC data.

Tab. 4 Comparison of power law fit respectively exponential fit for the undrained creep test results. Additional fits use TUC data scaled by a factor 0.3 to account for the probable overestimation of stationary creep rates as a consequence of too short test duration. Besides measures of quality of fit, the extrapolated values for $\sigma_{dev} = 1$ MPa are shown to illustrate the uncertainty of such an extrapolation.

with original TUC data		RMSE of $\log_{10}(\dot{\varepsilon}_\infty)$	R^2 of log-log-fit	$\dot{\varepsilon}_\infty(\sigma_{dev}=1\text{MPa})$ [d^{-1}]
power law	$\dot{\varepsilon}_\infty = 8.61\cdot10^{-8}\ d^{-1}\ (\sigma_{dev}/1\text{MPa})^{1.42}$	0.359	0.418	$8.6\cdot10^{-8}$
exponential	$\dot{\varepsilon}_\infty = 5.89\cdot10^{-7}\ d^{-1}\ \exp(0.118\ \text{MPa}^{-1}\ \sigma_{dev})$	0.335	0.493	$6.6\cdot10^{-7}$
TUC data scaled by factor 0.3				
power law	$\dot{\varepsilon}_\infty = 4.57\cdot10^{-7}\ d^{-1}\ (\sigma_{dev}/1\text{MPa})^{0.59}$	0.260	0.190	$4.6\cdot10^{-7}$
exponential	$\dot{\varepsilon}_\infty = 9.91\cdot10^{-7}\ d^{-1}\ \exp(0.050\ \text{MPa}^{-1}\ \sigma_{dev})$	0.252	0.238	$1.0\cdot10^{-6}$

5.2.3 Role of hydraulic regime

In general a lowering of stationary creep rate by application of drained boundary conditions (i.e. the prevention of a permanent buildup of pore pressure) can be observed. Although considerable sample variability and the different structure of the undrained respectively drained data sets hampers the statistical analysis, the difference between undrained and drained tests is statistically significant (Fig. 12). Only in case of a strict reduction of the data set to eliminate any systematic errors (e.g. from atypical samples or from the impact of different σ_{dev}-distribution in both subsets), the data base becomes too small to achieve a 95% level of significance (only 86% are reached).

Conditions for statistical analysis can be improved essentially when sample variability can be eliminated. This applies for results of the latest tests following an enhanced test layout by investigating any sample in two subsequent tests, first in undrained and afterwards in drained mode. There are 5 pairs of measurements (undrained and drained on same sample at equal deviatoric stress) yielded from 4 samples (Fig. 13). In any case drainage reduces stationary creep rate by 0.2 – 0.4 orders of magnitude. The average reduction of $\ln(\dot{\varepsilon}_\infty)$ is -0.67 ± 0.09 ($p < 0.0001$), corresponding to a decrease of 50%. This highlights the prominent role of pore water pressure for the creep behavior of Opalinus Clay.

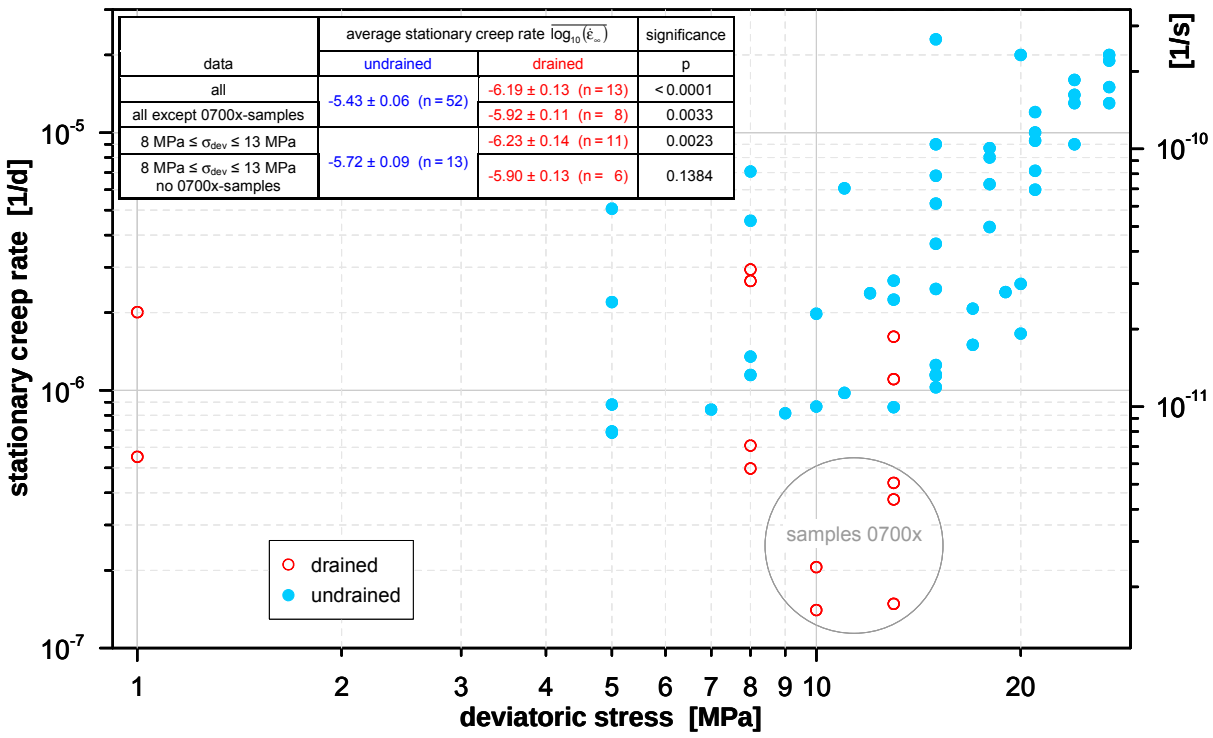

Fig. 12 On average, drained creep tests result in statistically significantly lower stationary creep rates than undrained tests. This applies even when the drained 0700x-samples (the extraordinary low creep rates of which might not be representative) are excluded or the data selection is restricted to $8\,\text{MPa} \le \sigma_{dev} \le 13\,\text{MPa}$ (to eliminate effects from different σ_{dev}-distribution in drained respectively undrained data). When both reductions of data set are applied, the data basis becomes too small to achieve statistical significance (the probability of $\overline{\dot{\varepsilon}_\infty}(\text{drained}) \ge \overline{\dot{\varepsilon}_\infty}(\text{undrained})$ becomes $p = 0.1384$).

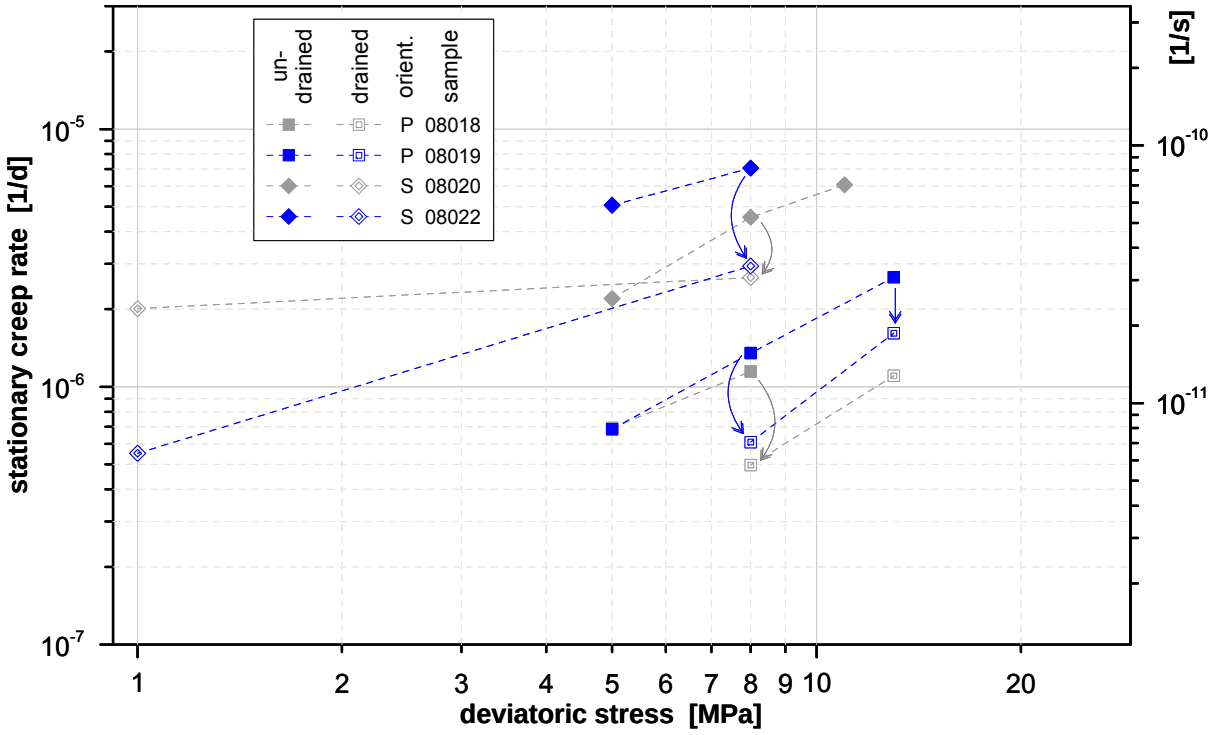

Fig. 13 Results from samples tested in undrained as well as in drained mode. In any case drained data (open markers) fall clearly below the corresponding undrained data (filled markers). For the 5 pairs of undrained/drained data that are measured on one sample at the same deviatoric stress, the reduction of creep rate by excluding the buildup of pore pressure is highlighted by arrows.

5.2.4 Impact of confining pressure

There has been only one test carried out to investigate the influence of confining pressure on creep behavior of Opalinus Clay. A p-sample has been tested at $\sigma_{dev} = 10$ MPa and $\sigma_{dev} = 12$ MPa varying the confining pressure σ_3 in a range from 0.5 to 10 MPa. The results of this test are summarized in Tab. 5 (Appendix A).

As shown in Fig. 14 higher confining pressure appears to reduce stationary creep rate. Similar to the $\ln(\dot{\varepsilon}_\infty)$ vs. $\ln(\sigma_{dev})$ relationship (cf. chap. 5.2.2), a possible (but not necessarily the best or the "true") description of the $\ln(\dot{\varepsilon}_\infty)$ vs. $\ln(\sigma_3)$ relationship is a power law $\dot{\varepsilon}_\infty \propto \sigma_3^{\,n}$. Because of the antagonistic effects of deviatoric stress and confining pressure (destabilizing vs. stabilizing) it has to be expected that their impact on stationary creep rate acts in opposite direction. This expectation is confirmed by the experimental data which result in $n = -0.3$ for $\ln(\dot{\varepsilon}_\infty)$ vs. $\ln(\sigma_3)$, and $n = 1.4$ for $\ln(\dot{\varepsilon}_\infty)$ vs. $\ln(\sigma_{dev})$. Since the impact of σ_3 is much weaker than the impact of σ_{dev}, it might be of little relevance with respect to practical problems.

Although the $\ln(\dot{\varepsilon}_\infty)$ vs. $\ln(\sigma_3)$ relationship shown in Fig. 14 is statistically highly significant for the $\sigma_{dev} = 10$ MPa data set, one has to consider that this determination of the level of significance does not account for the rather limited accuracy and possible systematic errors of the $\dot{\varepsilon}_\infty$-data (some values are based on rather short loading phases lasting less than 1 month; cf. Tab. 5 in Appendix A). Thus, the given levels of significance may essentially overestimate the soundness of the described $\ln(\dot{\varepsilon}_\infty)$ vs.

$\ln(\sigma_3)$ relationship. Furthermore, the findings are based on just one sample and might possibly lack representativeness.

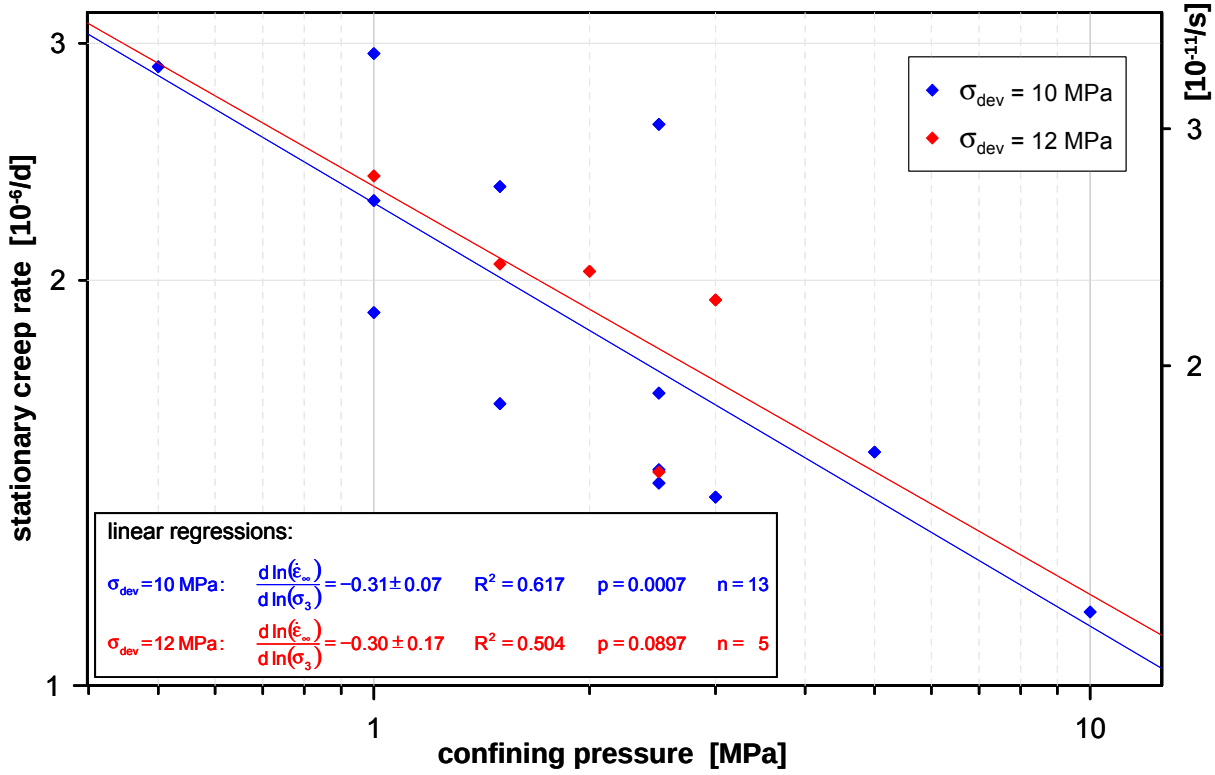

Fig. 14 Results from p-sample 02009 tested at various levels of confining pressure.

6 STRENGTH TESTS

6.1 TESTS EMPLOYED TO INVESTIGATE SHORT TERM MECHANICAL BEHAVIOR

A variety of tests has been used to investigate the mechanical short term behaviour of Mont Terri Opalinus Clay. Particularly, this comprises:

- Brazilian tests to assess tensile strength (3 tests loading normal to bedding, 5 tests loading parallel to the bedding).
- Uniaxial strength tests (3 tests in p-geometry and 3 tests in s-geometry).
- Conventional triaxial strength tests (24 p-, 25 s-, and 16 z-samples).
- Multistep triaxial strength tests (2 p-samples and 1 s-sample).

6.1.1 Indirect tensile tests (Brazilian tests)

In Brazilian tests the specimens are loaded with a line force on opposite sides of the coating. This provokes a tensile stress perpendicular to the loading plane where the load acts, which should result in a crack parallel to the loading direction. There is a great variety of possible stress geometries depending on sample geometry and chosen direction of loading (parallel or perpendicular to bedding) as illustrated in Fig. 15.

The tests were carried out at room temperature on samples measuring 100 mm in diameter as well as in length. Loading was applied with a constant deformation rate of 0.001 mm/s.

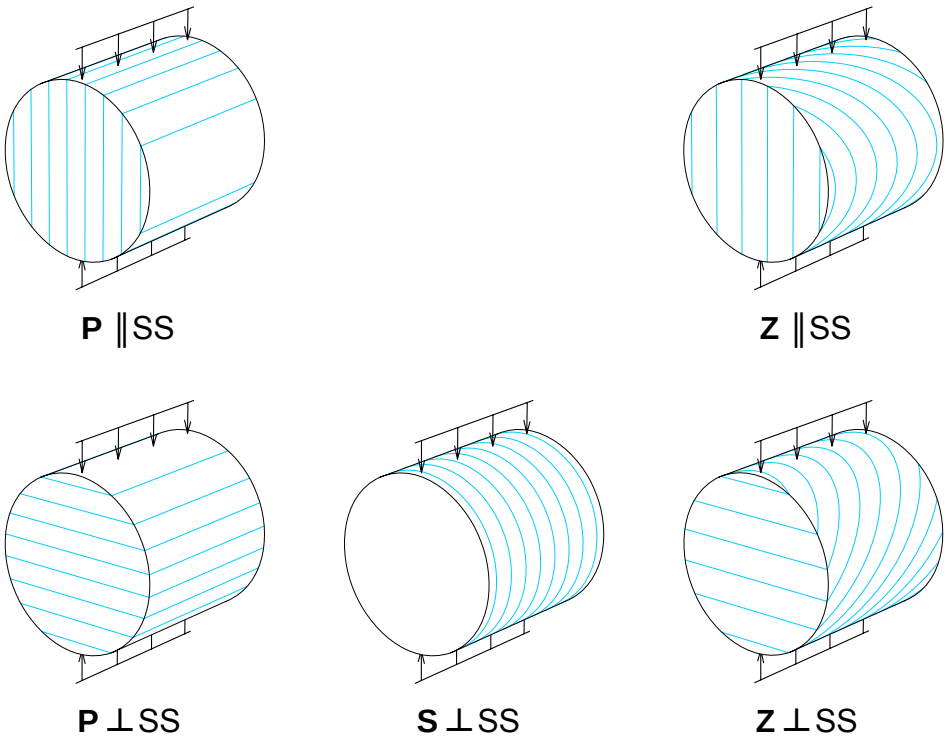

Fig. 15 Main combinations of sample geometry (P, S, and Z) and loading direction with respect to bedding (∥SS and ⊥SS).

6.1.2 Uniaxial and triaxial strength tests

Conventional uniaxial and triaxial strength tests have been employed in the LT-experiment as the most important approach to investigate shear strength $\sigma_{dev,peak}$, residual strength $\sigma_{dev,res}$, Young's modulus E, and residual deformation modulus E_{res} with respect to confining pressure σ_3, anisotropy, and temperature. The impact of moisture (water content or pore water pressure) was not within the focus of the experiment at the beginning. Nevertheless, systematic variation of water content due to the improvement of sample protection methods over the years (cf. chap. 2) resulted in some information concerning the impact of moisture on mechanic behavior.

Altogether, 68 conventional strength tests were performed in the LT-experiment (Tab. 6). A majority of 42 tests was carried out at room temperature (rT), 26 samples were tested at a higher temperature (hT) between 60 and 80°C.

Usually, tests were executed in deformation controlled mode with a deformation rate of $d\varepsilon/dt = 10^{-5}\,s^{-1}$. There are a few exceptions with deformation rates of $5\cdot10^{-5}\,s^{-1}$ (uniaxial tests only) to $10^{-6}\,s^{-1}$, and one uniaxial test (sample 07029) in stress controlled mode ($d\sigma_{dev}/dt$ = 1 MPa/min). Triaxial tests were carried out under undrained condition, and uniaxial tests were also effectively undrained due to the short test duration.

For a presentation of the measured σ(ε)-curves and a detailed description of the samples and the failure geometry see SCHNIER (2005) and SCHNIER & STÜHRENBERG (2007).

Tab. 6 Overview of the number of available strength test data sets.

sample orientation	rT (20 – 35°C)		hT (60 – 80°C)	
	uniaxial	triaxial	uniaxial	triaxial
P	2	13	1	11
S	2	16	0	9
Z	0	9	0	5

6.1.3 Multistep triaxial strength tests

Since sample variability is a major drawback for the identification and quantification of relationships between state variables and material behavior, a complex type of triaxial test was developed. It was the idea of this test to gain as much information as possible about elastic parameters, the onset of damage (irreversible deformation, dilatancy etc.), the shear strength, and the residual strength from a single sample. Furthermore, possible pore pressure effects upon these quantities should be investigated.

A test concept comprising three sections was developed. Section A is focused on the investigation of the limit of linear elastic behavior (which is supposed to be correlated to the onset of damage), section B deals with shear strength, and section C analyses residual strength. In any section investigations are to be done at various minimum principle stresses (i.e. confining pressures).

All loading phases of the complex strength test were carried out under deformation control at a rate of $d\varepsilon/dt = 10^{-7}\ s^{-1}$. Strictly undrained conditions are maintained during the test.

A detailed description of the test procedure, methods of data analysis and tools for evaluation is given in GRÄSLE & PLISCHKE (2007).

Two specimens in p-geometry and one s-sample were investigated in multistep strength tests.

6.2 RESULTS OF STRENGTH TESTS

6.2.1 Tensile strength

Tensile strength of Opalinus Clay has been investigated by a total of 8 Brazilian tests (Fig. 16, Tab. 7 in Appendix A). As expected, tensile strength is lower when loading parallel to the bedding (∥SS) resulting in tensile cracks in the bedding planes compared to loading perpendicular to the bedding (⊥SS):

$$\sigma_{tens}(\parallel SS) = -0.82 \pm 0.15\ MPa \quad (n = 3)$$
$$\sigma_{tens}(\perp SS) = -1.28 \pm 0.07\ MPa \quad (n = 5)$$

Although the data set is very small, notwithstanding the difference is statistically highly significant ($p = 0.0093$).

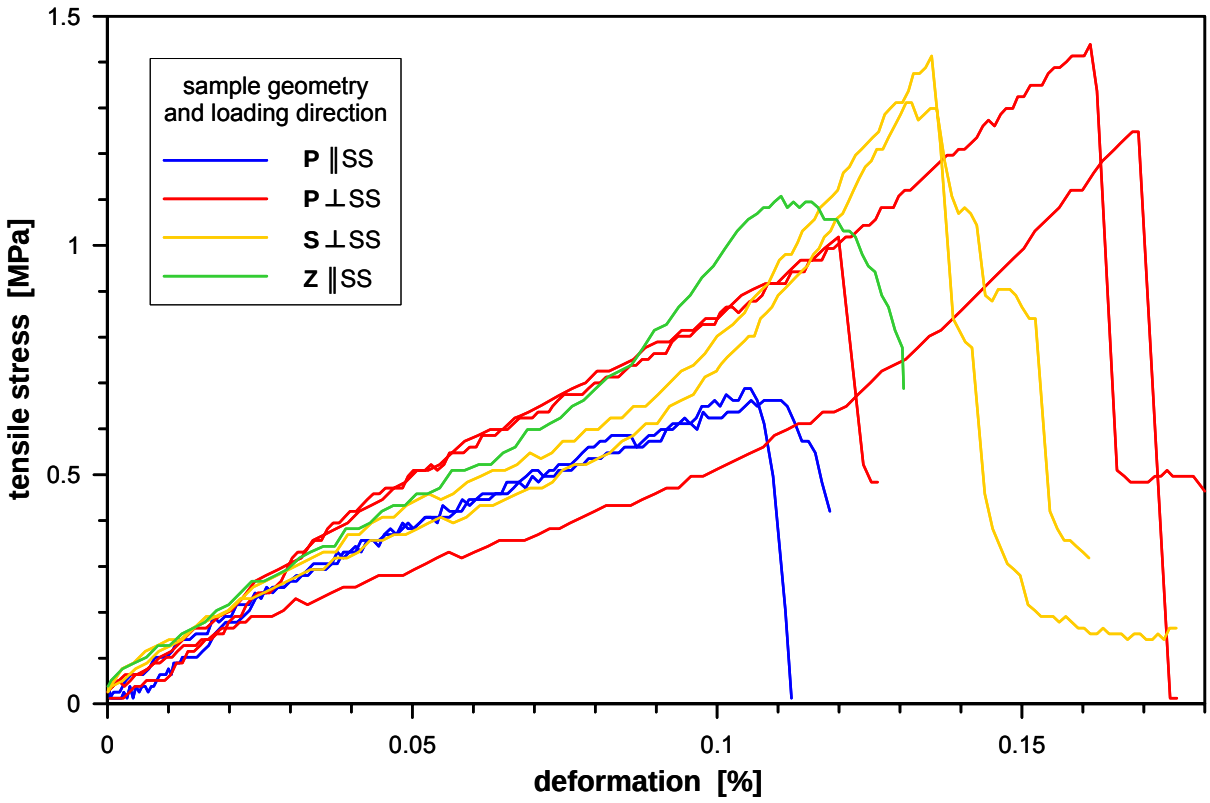

Fig. 16 Stress recordings from the Brazilian tests. On average, loading parallel to the bedding planes (blue and green curves) results in lower tensile strength than loading perpendicular to the bedding (red and orange curves).

6.2.2 Shear strength

Fig. 17 and Tab. 8 (Appendix A) present an overview of all shear strength data. Note that the marker and color scheme shown in Fig. 17 is used throughout the presentation of results from strength test to make understanding easy:

- Colors and markers indicate sample geometry: P = blue diamonds, S = green rectangles, Z = red triangles.
- Brightness of color indicates temperature: room temperature (rT) = darker colors (dark blue, dark green, red), higher temperature (hT) = brighter colors (bright blue, bright green, orange).
- Filling of markers indicates moisture status (for details see p. 22): "dry" samples (water content <6.3% by weight) = open markers, "moist" samples (water content >6.3% by weight) = filled markers.
- Dashed lines connect data points resulting from the same specimen.

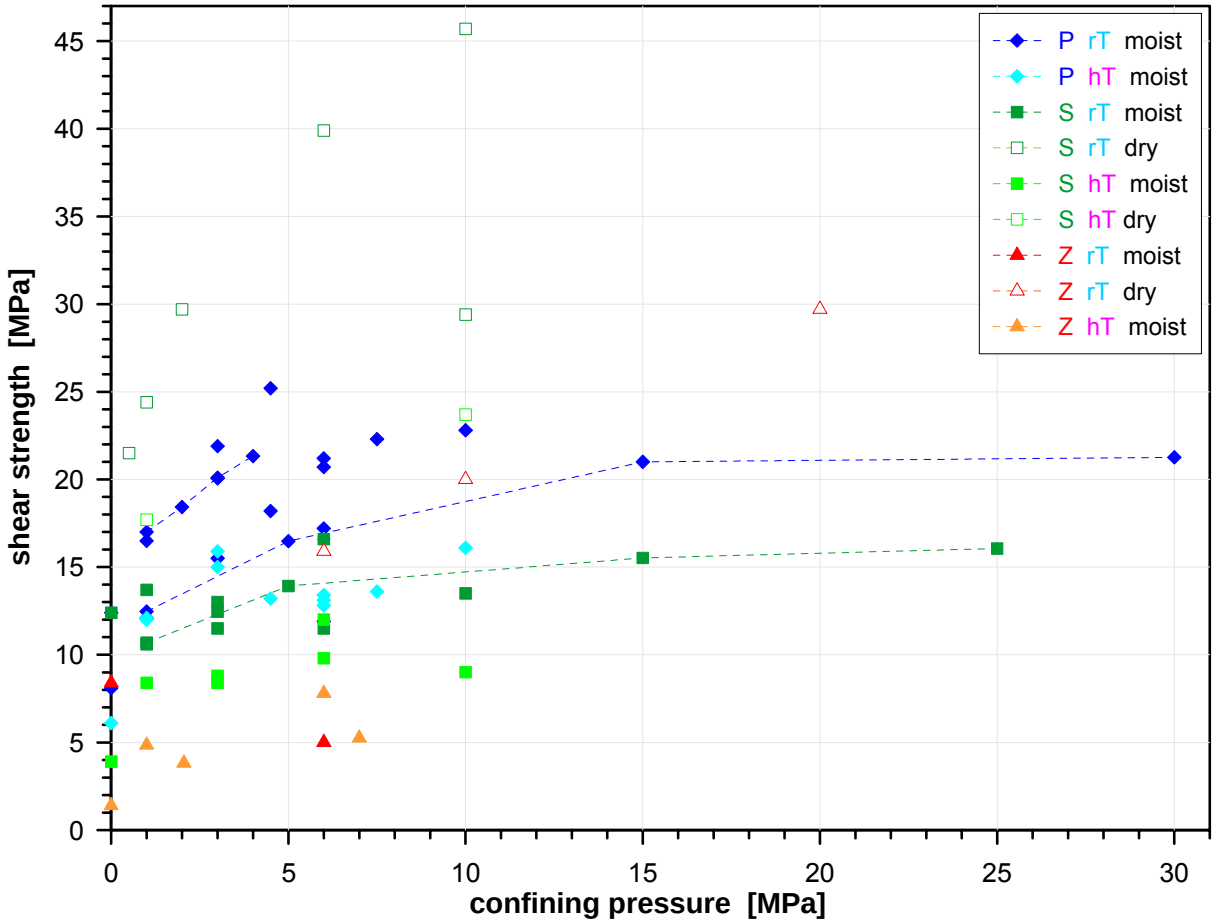

Fig. 17 Results of shear strength $\sigma_{dev.peak}$ determination from uniaxial and triaxial strength tests as well as from multistep triaxial strength tests. Dashed lines connect data points resulting from the same specimen (available from multistep triaxial strength tests only).

Uniaxial strength

Besides 5 uniaxial tests there are another 4 triaxial tests where strength was determined at 0 MPa confining pressure, thus resembling uniaxial tests. Excluding 2 disturbed tests, the uniaxial strength exhibits the expected anisotropy (p-samples > s-samples > z-samples):

$$\sigma_{dev.peak}(P) = 8.9 \pm 1.9 \text{ MPa} \quad (n = 3)$$
$$\sigma_{dev.peak}(S) = 8.2 \pm 4.3 \text{ MPa} \quad (n = 2)$$
$$\sigma_{dev.peak}(Z) = 4.9 \pm 3.5 \text{ MPa} \quad (n = 2)$$

Due to the very small data set the differences are not statistically significant.

The impact of moisture on shear strength

As already mentioned in chap. 6.1.2 the impact of moisture on the short term mechanical behavior of Opalinus Clay was not within the focus of the experiment at the beginning. Later on, when the effects of drying of improperly stored samples had become obvious, successful efforts were made to avoid drying of samples. But there has been no attempt to investigate the role of moisture within strength tests. Therefore, no need was seen to implement pore pressure sensors in the used triaxial cells. Unlike the approach used in creep tests (chap. 5.1), the application of different hydraulic boundary conditions (drained or undrained) is not promising in case of strength tests. Due to the low hydraulic permeability of Opalinus Clay, the draining process would take much longer than the duration of a typical strength test.

As a consequence, the available data set comprises measurements significantly affected by drying of samples (mainly from the early phases of the LT-experiment) but little information to describe the moisture state of the samples. Water content (by weight) is the only measured parameter characterizing the moisture state. Water content has not been determined for the samples from drillhole BED-C9 and BED-C10 investigated in the early stages of the LT-experiment. Nevertheless, from the sample descriptions and regarding the storage conditions there can be no doubt that these samples were desiccated significantly.

For theoretical reasons (e.g. in the framework of theories on effective stress and poro-elasticity, cf. TERZAGHI (1936), BIOT (1941), SKEMPTON (1960), but also in sophisticated concepts involving 7 true degrees of freedom for elastic behavior like FREDLUND & MORGENSTERN, 1977) mechanical behavior will be influenced by pore pressure rather than by water content. There is of cause a correlation between water content and pore pressure, but this correlation is fairly lax and not at all linear for clay.

Data published in BOSSART & THURY (2008) indicate a distinct relationship between shear strength and water content (Fig. 18). Unfortunately, describing shear strength explicitly as a function of water content was not feasible for the available data set. This is due to the fact that water content has not been determined for the very dry BED-C samples, whereas the other samples cover a rather narrow range of water content (5.71% to 8.06%, where 40 out of 51 water content values fall in the narrow interval from 6.3% to 7.3%, cf. Fig. 18). Nevertheless, splitting the data in two subsets according to their water content results in relatively homogeneous subsets, which display a distinctly different mechanical behavior. This finding provides the basis for the separation between "dry" and "moist" samples.

This clustering was performed by placing the BED-C samples and all samples with water content $w < w_{crit}$ into one group (termed "dry"), while any other samples compose the other group (termed "moist"). In doing so, the value of w_{crit} was varied until the intra-group variance was minimized (and thereby the inter-group variance maximized). Regardless whether this was done with respect to shear strength, residual strength or Young's modulus, the optimum value of the critical water content was found to be around $w_{crit} = 6.3\%$ by weight. Note that this is just a rough-and-ready descriptive parameter applicable only for the given data set. This clustering approach should be replaced by an explicit function of water content or pore pressure in the framework of a more generalized description.

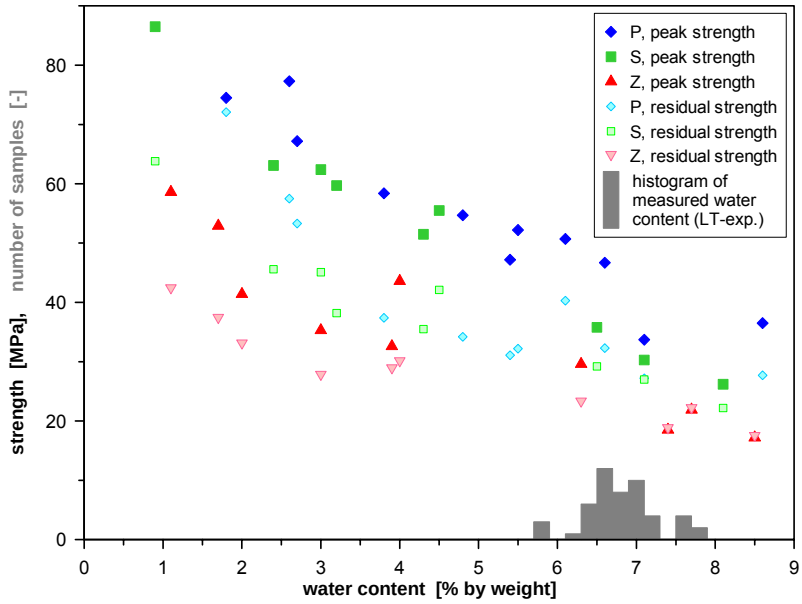

Fig. 18 Strength dependence on water content (modified from Figure AN 4-6 from BOSSART & THURY (2008); $\sigma_3 = 10$ MPa). The added histogram of measured water contents illustrates the narrow range of water content covered in the LT-experiment.

When comparing data sets characterized by homogeneous conditions with respect to sample geometry and temperature (i.e. s-samples at room temperature, s-samples at higher temperature, or z-samples at room temperature), the shear strength of dry samples surpasses that of moist samples by more than 100% on average (Fig. 19). When only data for $0 \le \sigma_3 \le 10$ MPa is considered (to reduce systematical errors from different σ_3-distributions in the compared subsets), the differences between average shear strength of moist respectively dry specimens are statistically significant (Tab. 9). Thus, drying has a tremendous effect on mechanical behavior of Opalinus Clay. This once more emphasizes that proper sample storage and preparation preventing the loss of water is an essential requirement for representative test results.

Tab. 9 Comparison of average shear strength of moist versus dry specimens for data with $0 \le \sigma_3 \le 10$ MPa. Statistical significance, defined by a probability of error $p<0.05$, is indicated by bold type and yellow shading. (Key: rT = room temperature = 20-35°C, hT = higher temperature = 60-80°C)

data set	$\overline{\sigma_{dev.peak}}$ [MPa] moist	dry	significance p (dry>moist)
S rT	12.7 ± 0.5 (n = 11)	31.8 ± 3.8 (n = 6)	**< 0.0001**
S hT	8.6 ± 0.9 (n = 7)	20.7 ± 3.0 (n = 2)	**0.0005**
Z rT	6.7 ± 1.7 (n = 2)	18.0 ± 2.1 (n = 2)	**0.0259**

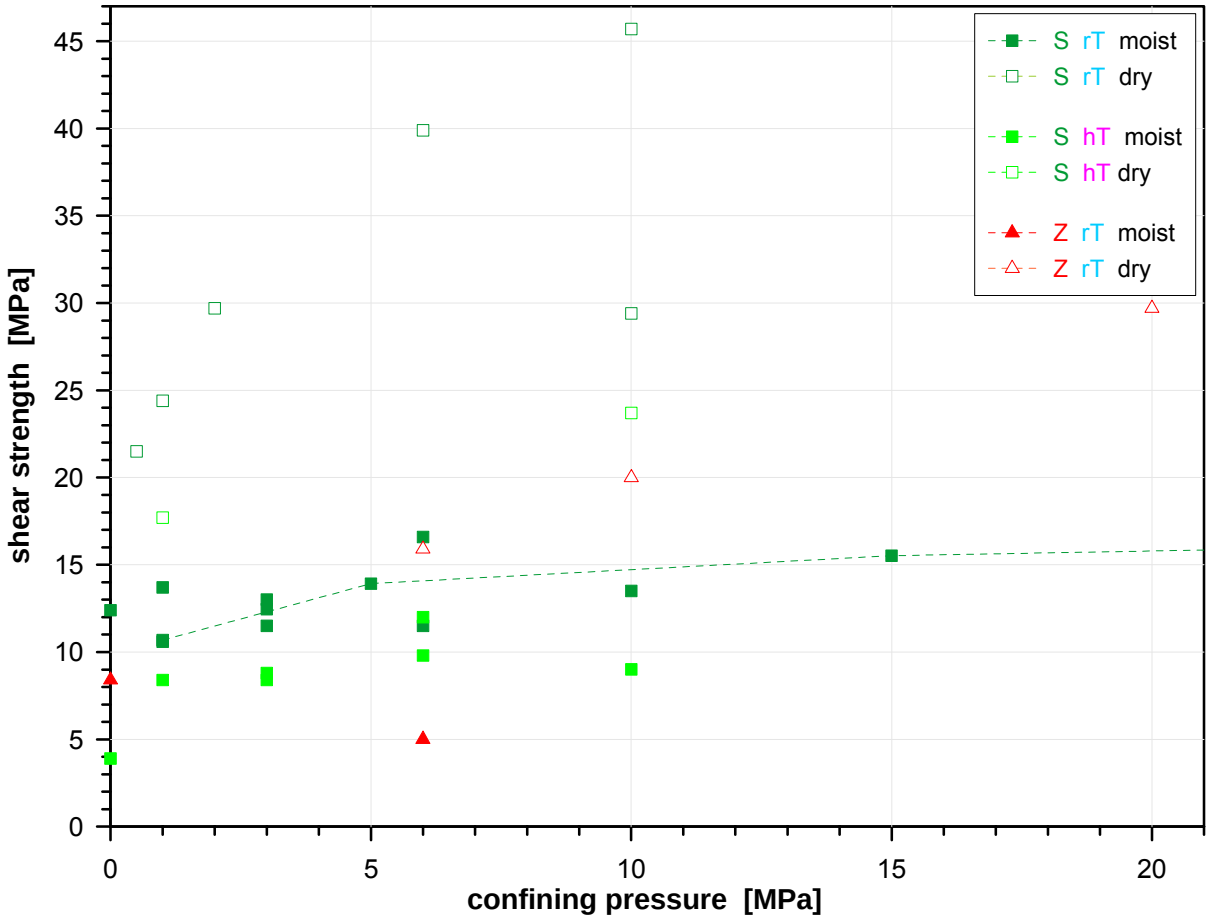

Fig. 19 Within any subset (S hT, S rT, or Z rT) dry specimens (open markers) exhibit considerably higher shear strength than moist ones (filled markers).

Shear strength and temperature

For any sample geometry as well as for any moisture state a lowering of shear strength by heating can be recognized (Fig. 20). Although this effect does not meet statistical significance for dry s-samples and moist z-samples due to very small data basis, an average reduction of shear strength by increasing temperature from rT to hT by approximately ⅓ occurs for any subset of data (Tab. 10).

Tab. 10 Comparison of average shear strength of specimens tested at 20 – 35°C (rT) versus those tested at 60 – 80°C (hT) for data with $0 \leq \sigma_3 \leq 10$ MPa. Yellow shading and bold face indicates statistical significance.

data set	$\overline{\sigma_{dev.peak}}$ [MPa] rT	$\overline{\sigma_{dev.peak}}$ [MPa] hT	significance p (rT>hT)
P moist	17.7 ± 1.0 (n = 21)	13.3 ± 0.8 (n = 12)	**0.0020**
S moist	12.7 ± 0.5 (n = 11)	8.6 ± 0.9 (n = 7)	**0.0003**
S dry	31.8 ± 3.8 (n = 6)	20.7 ± 3.0 (n = 2)	*0.0839*
Z moist	6.7 ± 1.7 (n = 2)	4.6 ± 1.0 (n = 5)	*0.1686*

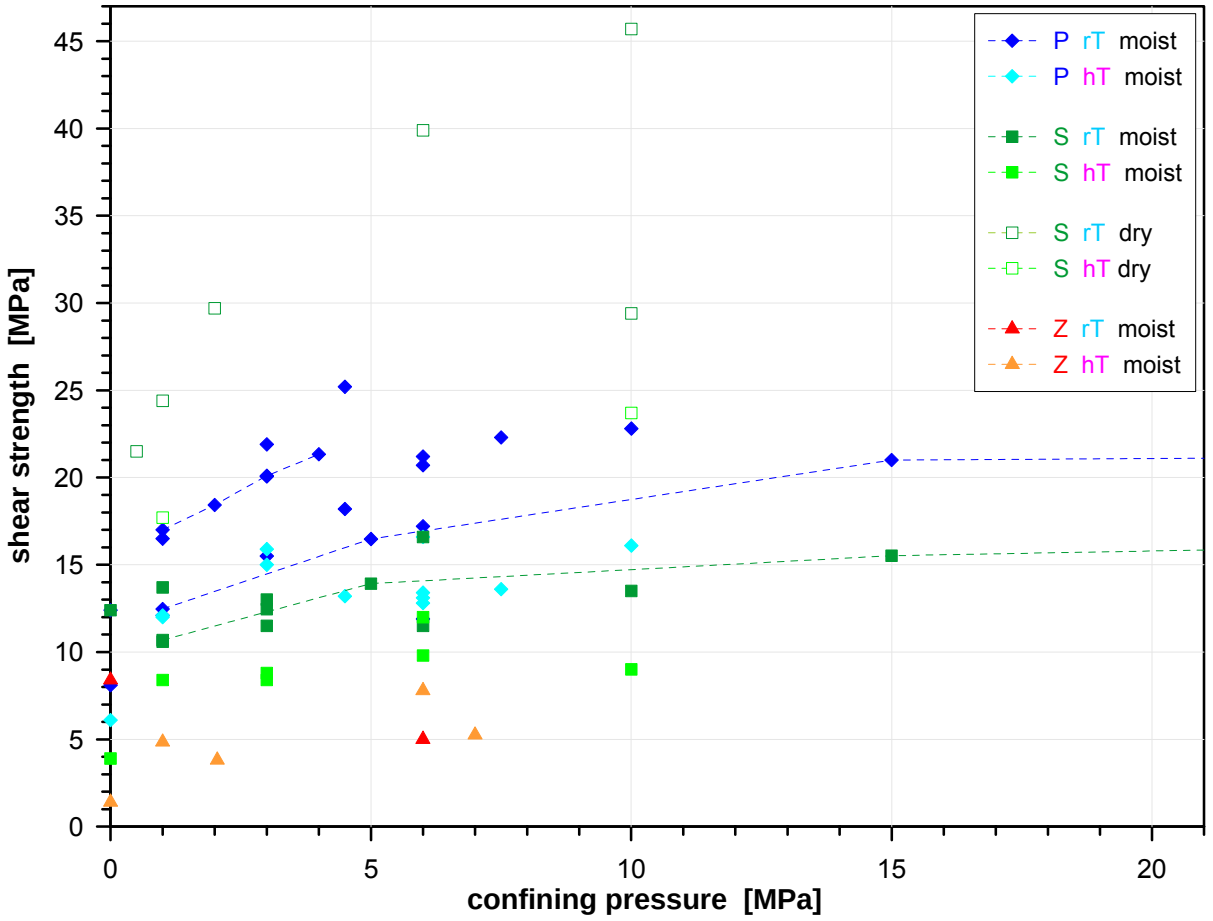

Fig. 20 Within all subsets (P moist, S moist, S dry) shear stress at higher temperature (bright colors) is slightly lower than at room temperature (darker colors).

There are contrary findings reported from true triaxial tests by NAUMANN & PLISCHKE (2006) showing a slight increase of shear strength by heating. As the risk of sample desiccation is strongly increased during tests at higher temperature (particularly in case of true triaxial tests where specimens cannot be sealed completely) a weakening temperature effect most likely will be outbalanced by the strengthening impact of drying in these observations.

Anisotropy of shear strength

As it has to be expected anisotropy of shear strength is a very conspicuous attribute of Opalinus Clay (Fig. 21). Generally, shear strength in p-geometry surpasses that on s-geometry by a factor of approximately 1.4. Shear strength is lowest when loading in z-geometry, reaching less than ½ of the p-sample strength. The differences are statistically significant in any case (Tab. 11).

Tab. 11 Comparison of average shear strength measured on different sample geometry for data with $0 \leq \sigma_3 \leq 10$ MPa. Yellow shading and bold face indicates statistical significance.

	$\overline{\sigma_{dev.peak}}$ [MPa]			significance		
data set	P	S	Z	p (P>S)	p (P>Z)	p (S>Z)
rT moist	17.7 ± 1.0 (n = 21)	12.7 ± 0.5 (n = 11)	6.7 ± 1.7 (n = 2)	**0.0006**	**0.0013**	**0.0006**
hT moist	13.3 ± 0.8 (n = 12)	8.6 ± 0.9 (n = 7)	4.6 ± 1.0 (n = 5)	**0.0008**	**< 0.0001**	**0.0085**
rT dry	–	31.8 ± 3.8 (n = 6)	18.0 ± 2.1 (n = 2)	–	–	**0.0475**

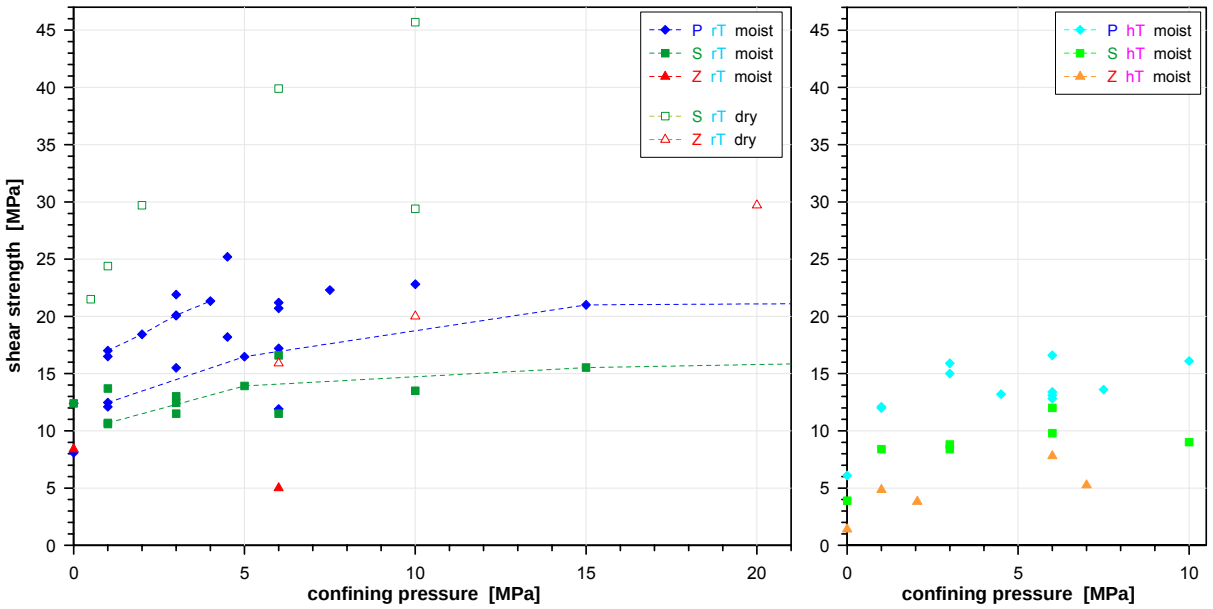

Fig. 21 Within any subset (rT moist, rT dry, hT moist) a distinct anisotropy of shear stress was observed. Shear strength decreases from p- to s- to z-orientation (i.e. red markers below of green ones and blue markers on top).

The relationship of shear strength versus confining pressure

It's a matter of common knowledge that shear strength increases with confining pressure. Of couse this fact also applies to Opalinus Clay (Fig. 17). But since there is a considerable variability between specimens, it is virtually impossible to identify detailed aspects of the $\sigma_{dev.peak}(\sigma_3)$-characteristic. An enormous data set would be required to sufficiently overcome the statistical spread. Particularly, the available data from uniaxial and triaxial strength tests are insufficient to verify the validity of a Mohr-Coulomb-type linear relationship.

Although only 3 tests have been carried out, multistep strength tests offer a workaround for this problem because they avoid sample variability. As it has been demonstrated in the first multistep strength test (sample 02075), 4 values of shear strength at different levels of confining pressure were determined on a single specimen before progressive sample damage led to significantly reduced strength gradually converging towards residual strength (GRÄSLE & PLISCHKE, 2007).

Subsequent tests were modified insofar as they cover a wide range of σ_3 by the 4 sound determinations of shear strength. A distinct deviation from a Mohr-Coulomb-type linear relationship was found, displaying a shape of two linear branches (Fig. 22). Of cause, 4 data points per sample are not enough to justify this detailed conclusion. Nevertheless, as the well-founded results for residual strength yielded from the same tests resemble the two-branched shape perfectly (see Fig. 31 in chap. 6.2.4), there is sufficient confidence in a similar shape of the $\sigma_{dev.peak}(\sigma_3)$-function. Details of the fitted curves are given in GRÄSLE & PLISCHKE (2007+2009).

Effective stress theory offers a reasonable explanation for this finding. A possible buildup of pore pressure due to sample compression at higher confining pressure (and thereby higher mean normal stress) would result in the observed $\sigma_{dev.peak}(\sigma_3)$-function for total stress, when a Mohr-Coulomb-relationship is valid for effective stress. Additional experimental verification of this hypothesis is still lacking since no registration of pore pressure took place in these tests.

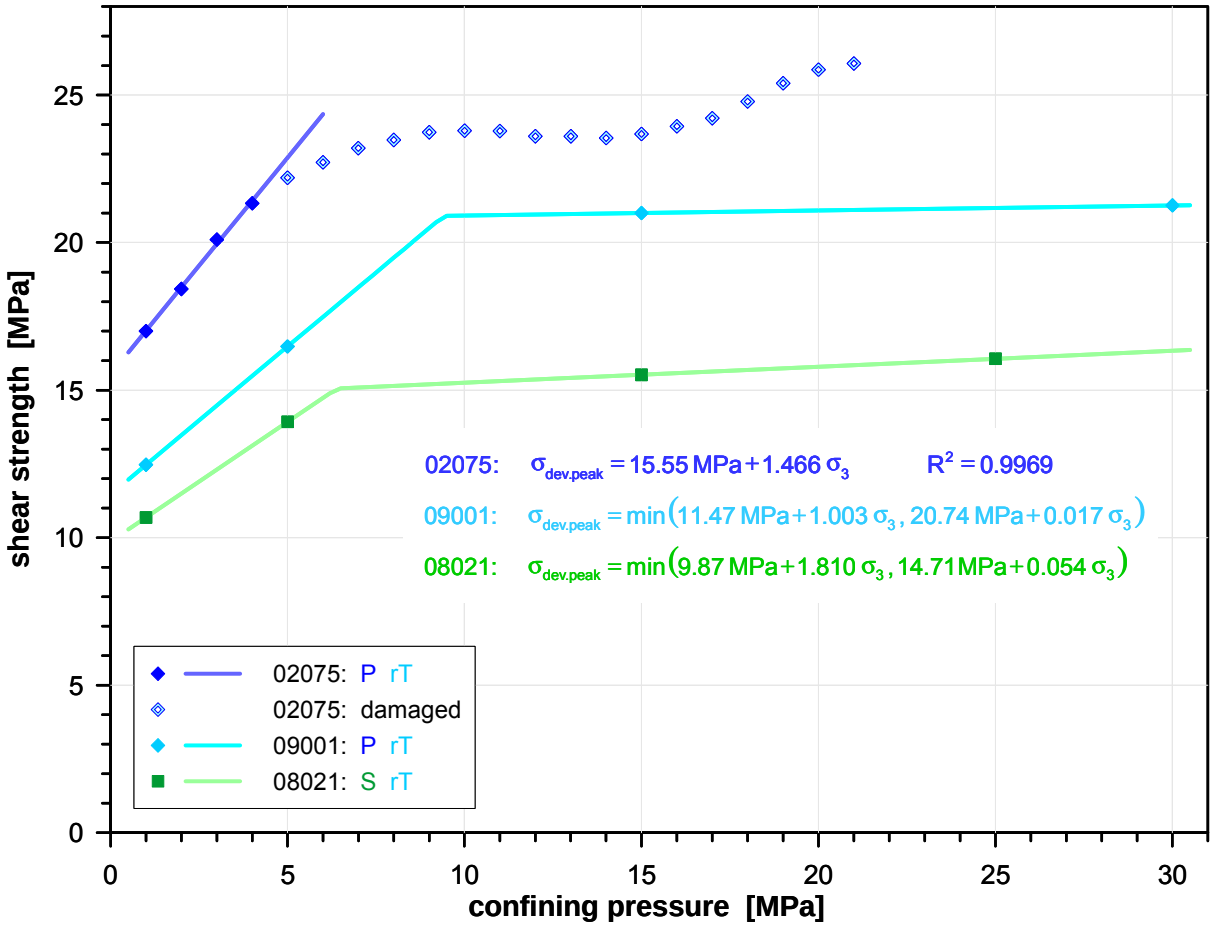

Fig. 22 Shear strength $\sigma_{dev.peak}$ results from multistep triaxial strength tests. The first test (file 02075) executed with σ_3-intervals of 1 MPa showed almost perfect linearity of the $\sigma_{dev.peak}(\sigma_3)$-function for 4 initial measurements before strength was reduced by progressive damage of the specimen. The other tests were carried out with essentially increased σ_3-intervals to cover a wide range of confining pressure by 4 measurements.

Synoptic description

To yield a quantitative characterization of the demonstrated impacts on shear strength, a description linear with respect to any influencing variable (but including products terms between those variables) has been tested as a simple reasonable approach. Because of the two-branch-characteristic of the $\sigma_{dev.peak}(\sigma_3)$-function a linear model can only be reasonable within a σ_3-range limited to on linear branch. Fitting the full two-branch-function would not yield reliable results since there is not a sufficient amount of data available at higher confining pressure to support the second branch (cf. Fig. 17). Therefore, the following fit only uses data with $\sigma_3 \leq 7.5$ MPa which appears to be an appropriate estimation for the inflection point of the two-branch-function (Fig. 22). In doing so, describing shear strength by

$$\sigma_{dev.peak} = (c + a\,\sigma_3)(1 + f_T\,(T - 30°C))\,f_W\,f_A$$

where: c = cohesive shear for moist p-samples at 30°C

$a = \partial\sigma_{dev.peak}/\partial\sigma_3$ for moist p-samples at 30°C

$f_T = \partial \ln \sigma_{dev.peak}/\partial T$ at 30°C

f_W = moisture coefficient $= \begin{cases} f_{W.m} = 1 & \text{for moist samples} \\ f_{W.d} & \text{for dry samples} \end{cases}$

f_A = anisotropy coefficient $= \begin{cases} f_{A.p} = 1 & \text{for p-geometry} \\ f_{A.s} & \text{for s-geometry} \\ f_{A.z} & \text{for z-geometry} \end{cases}$

results in a fairly good fit ($R^2 = 0.8373$, RMSE = 2.6 MPa). The determined parameter values are listed in Tab. 12.

Tab. 12 Parameters describing shear strength of Opalinus Clay. Parameters are determined by fitting $\sigma_{dev.peak} = (c + a\,\sigma_3)(1 + f_T\,(T - 30°C))\,f_W\,f_A$ to the available data for $\sigma_3 \leq 7.5$ MPa.

c [MPa]	cohesive shear for moist p-samples at 30°C	15.7
a	$\partial\sigma_{dev.peak}/\partial\sigma_3$ for moist p-samples at 30°C	1.374
φ [°]	corresponding friction angle $\varphi = \arctan\left(\frac{\sqrt{2}\,a}{3 + a}\right)$	24.0
f_T [K^{-1}]	$\partial \ln \sigma_{dev.peak}/\partial T$ at 30°C	-0.0050
$f_{W.d}$	ratio of dry versus moist shear strength	2.30
$f_{A.s}$	ratio of anisotropy for s-geometry versus p-geometry	0.76
$f_{A.z}$	ratio of anisotropy for z-geometry versus p-geometry	0.35
n	number of data points	62
R^2	coefficient of determination	0.8373
RMSE [MPa]	root mean squared error	2.6

6.2.3 Failure strain

Fig. 23 and Tab. 8 (Appendix A) present an overview of all data for failure strain ε_{fail}. Note that for multistep triaxial strength tests only the first incidence of a failure condition is shown in Fig. 23, because the strain path preceding later incidences of a failure condition is not comparable to a standard strength test.

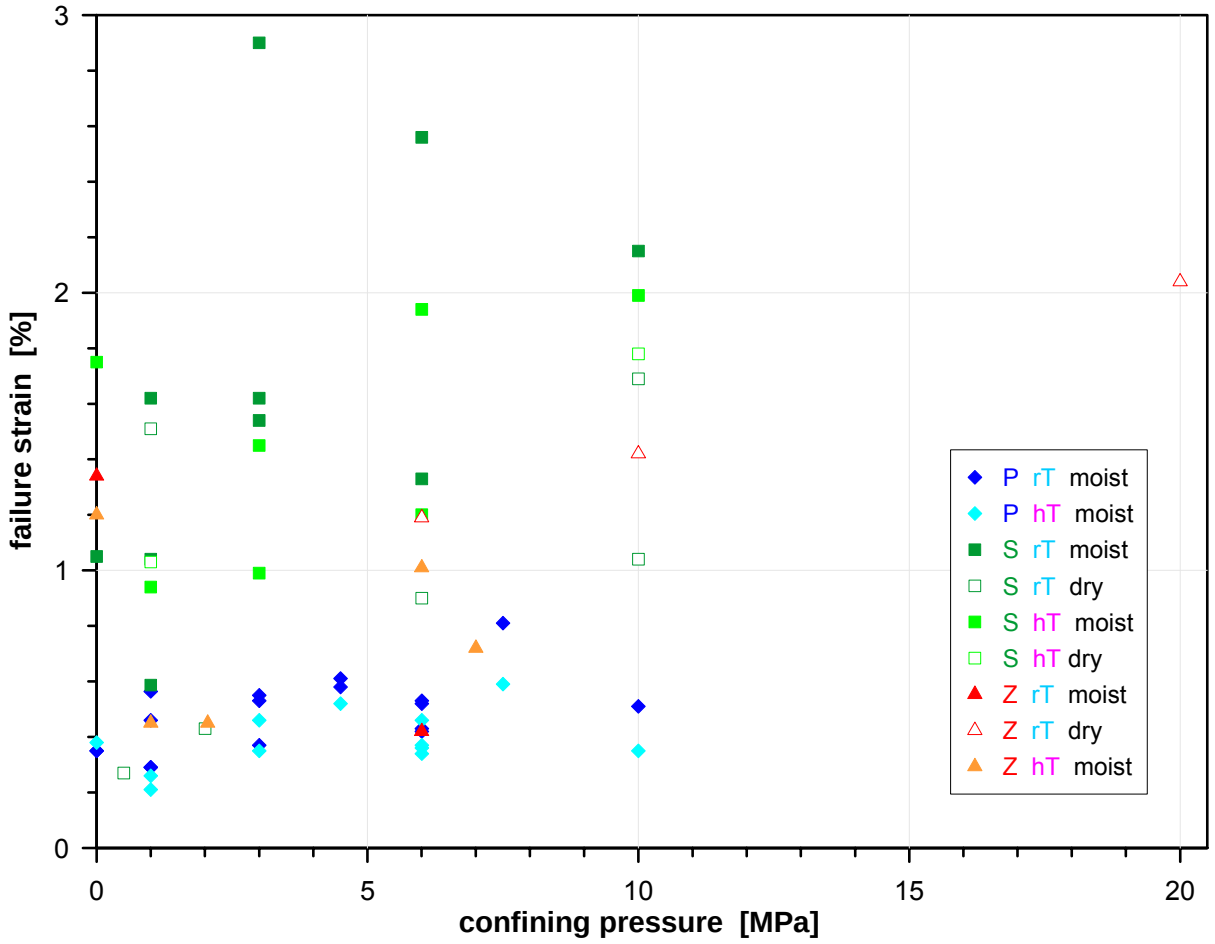

Fig. 23 Results of strain at the first occurrence of the failure condition from uniaxial and triaxial strength tests as well as from multistep triaxial strength tests.

The impact of moisture on failure strain

Although drying results in a considerable increase of shear strength, shear failure usually occurs at lower deformation for dry samples compared to moist ones. However, this impact of moisture state is less distinct than in case of shear strength. It is obvious only for s-geometry at room temperature (Fig. 24) and even then hardly meets statistical significance (Tab. 13). Considerably high sample variability (eye-catching in case of “S rT moist” data) hampers the identification of relationships between test conditions and failure strain. Note that one data point (for $\sigma_3 = 20$ MPa, see Fig. 23) has been excluded from this and any subsequent analysis to avoid a non representative impact of this outlier.

Tab. 13 Comparison of average failure strain of moist versus dry specimens for data with $0 \le \sigma_3 \le 10$ MPa. Statistical significance is indicated by bold face and yellow shading.

	$\overline{\varepsilon_{fail}}$ [%]		significance
data set	moist	dry	p (dry<moist)
S rT	1.56 ± 0.20 (n = 12)	0.97 ± 0.23 (n = 6)	**0.0445**
S hT	1.47 ± 0.17 (n = 7)	1.41 ± 0.38 (n = 2)	*0.4360*
Z rT	0.88 ± 0.46 (n = 2)	1.31 ± 0.12 (n = 2)	*0.7677*

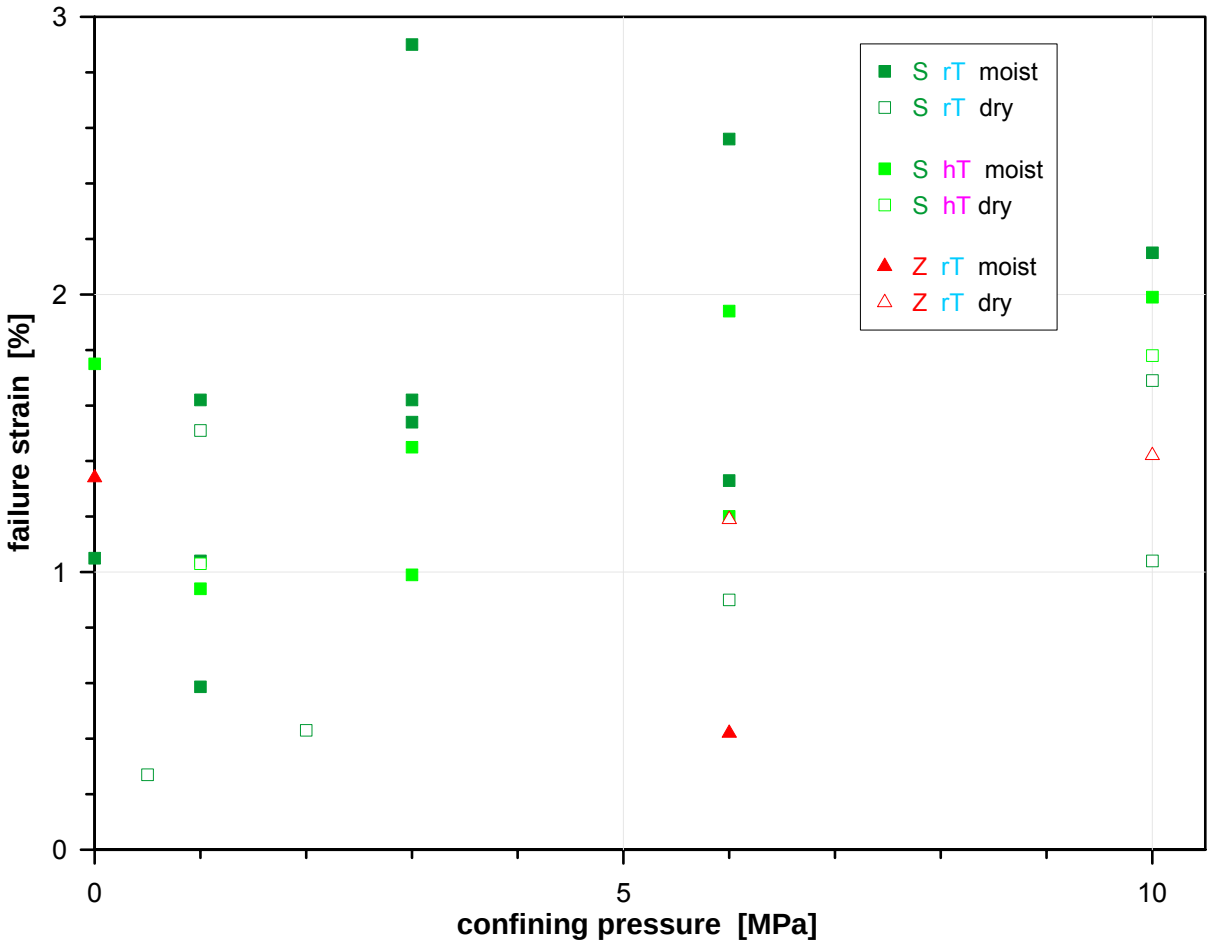

Fig. 24 Only for s-samples at room temperature (S rT) dry specimens (open markers) obviously meet failure at lower strain than moist ones (filled markers).

Failure strain and temperature

Only in case of p-specimens (which exhibit by far the smallest sample variability) a significant reduction of failure strain at higher temperature can be recognized (Tab. 14 and Fig. 25).

Tab. 14 Comparison of average failure strain of specimens tested at 20 – 35°C (rT) versus those tested at 60 – 80°C (hT) for data with $0 \le \sigma_3 \le 10$ MPa. Statistical significance is indicated by bold face and yellow shading.

data set	$\overline{\varepsilon_{fail}}$ [%] rT	hT	significance p (rT>hT)
P moist	0.48 ± 0.03 (n = 17)	0.39 ± 0.03 (n = 12)	**0.0271**
S moist	1.56 ± 0.20 (n = 12)	1.47 ± 0.17 (n = 7)	*0.3779*
S dry	0.97 ± 0.23 (n = 6)	1.41 ± 0.38 (n = 2)	*0.8092*
Z moist	0.88 ± 0.46 (n = 2)	0.77 ± 0.15 (n = 5)	*0.3788*

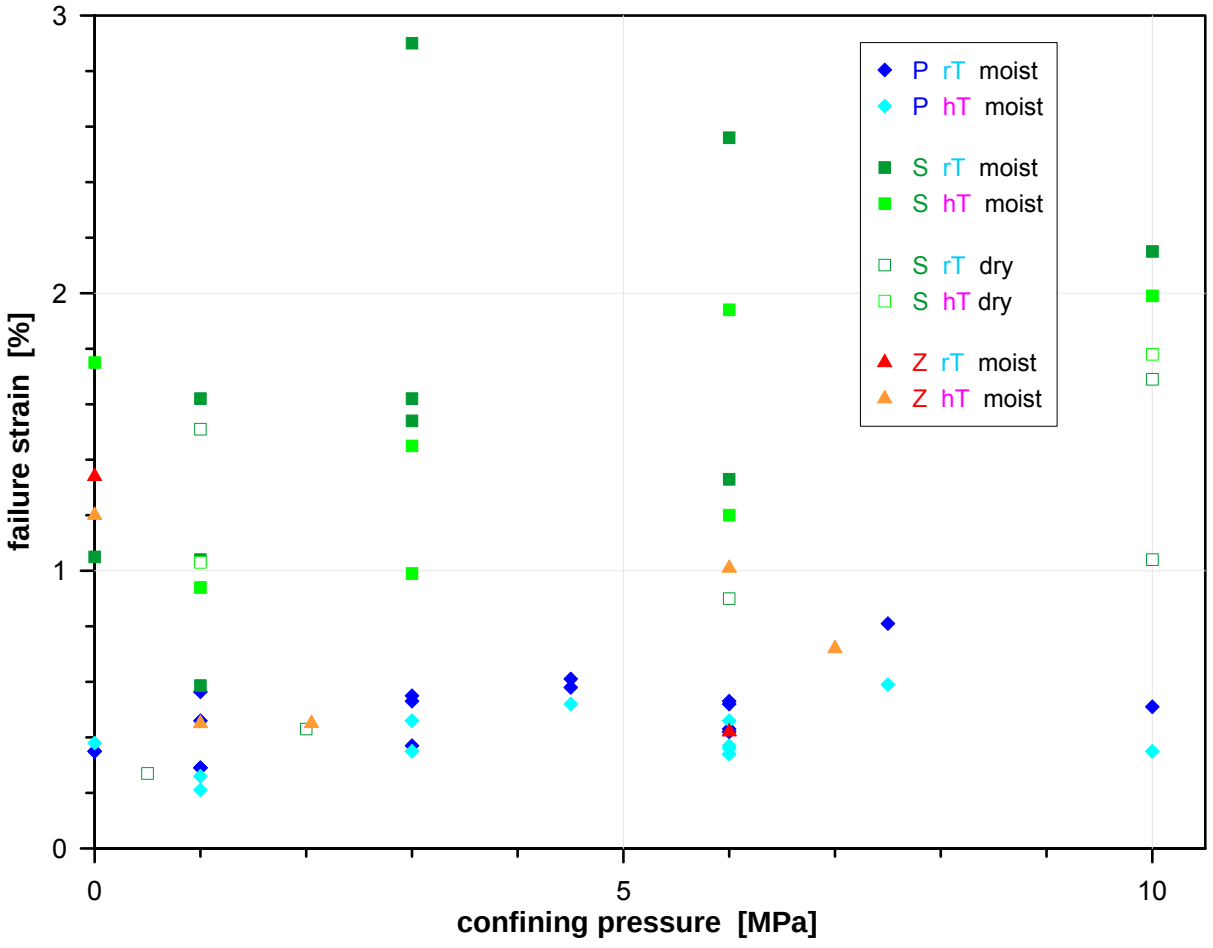

Fig. 25 Only for p-samples a significant decrease of failure strain by heating was found.

Anisotropy of failure strain

The anisotropy of failure strain is very distinct for Opalinus Clay (Tab. 15). Unsurprising, deformations normal to the bedding planes clearly surpass deformations parallel to the bedding more than threefold (Fig. 26). Failure strain in z-geometry is in between and still twice as high as in p-geometry.

Tab. 15 Comparison of average failure strain measured on different sample geometry for data with $0 \leq \sigma_3 \leq 10$ MPa. Statistical significance is indicated by yellow shading.

	$\overline{\varepsilon_{fail}}$ [%]			significance		
data set	P	S	Z	p (P<S)	p (P<Z)	p (S>Z)
rT moist	0.48 ± 0.03 (n = 17)	1.56 ± 0.20 (n = 12)	0.88 ± 0.46 (n = 2)	< 0.0001	0.0088	*0.1068*
hT moist	0.39 ± 0.03 (n = 12)	1.47 ± 0.17 (n = 7)	0.77 ± 0.15 (n = 5)	< 0.0001	0.0012	0.0069
rT dry	–	0.97 ± 0.23 (n = 6)	1.31 ± 0.12 (n = 2)	–	–	*0.7674*

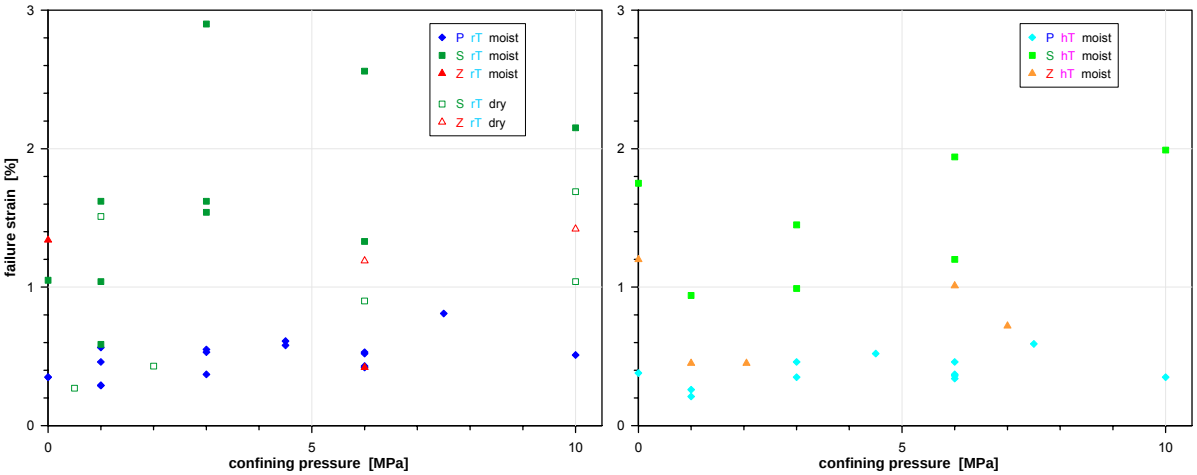

Fig. 26 Within most subsets (rT moist, rT dry, hT moist) a distinct anisotropy of failure strain was observed. Except for dry samples, failure strain increases from p- to z- to s-orientation (i.e. blue markers below of red ones and green markers on top).

The relationship of shear strength versus confining pressure

Due to sample variability the available data do not allow for any detailed investigation of a $\varepsilon_{fail}(\sigma_3)$-relationship. Overall, there appears to be the expected positive correlation of failure strain and confining pressure (cf. Fig. 23). But there is no basis to decide whether this relationship is linear or whatsoever.

Synoptic description

As there are indications for a relevant impact of moisture, temperature, confining pressure, and loading geometry on failure strain, a synoptic description similar to that demonstrated for shear strength is an appropriate approach. Once again, the simplest type of fitting function has been chosen:

$$\varepsilon_{fail} = (\varepsilon_0 + a\,\sigma_3)(1 + f_T\,(T - 30°C))\,f_W\,f_A$$

where: ε_0 = failure strain for moist p-samples at 30°C in uniaxial test

a = $\partial\varepsilon_{fail}/\partial\sigma_3$ for moist p-samples at 30°C

f_T = $\partial \ln\varepsilon_{fail}/\partial T$ at 30°C

f_W = moisture coefficient = $\begin{cases} f_{W.m} = 1 & \text{for moist samples} \\ f_{W.d} & \text{for dry samples} \end{cases}$

f_A = anisotropy coefficient = $\begin{cases} f_{A.p} = 1 & \text{for p-geometry} \\ f_{A.s} & \text{for s-geometry} \\ f_{A.z} & \text{for z-geometry} \end{cases}$

As in any case, where the simplicity of a model is legitimated only by the absence of sufficient experimental evidence for a more complex model (particularly, when this results from considerable data variability), the model is just an empirical description. In the first instance, it does not imply any physically based description, and any extrapolation beyond the range of the underlying data deserves little confidence.

The resulting parameters are reported in Tab. 16. The rather poor coefficient of determination of the fit ($R^2 = 0.6572$) reflects the high sample variability. Presumably, this variability results from a pronounced susceptibility of failure strain to the conditions during drilling, sample storage and specimen preparation. Whereas other investigated parameters like shear strength, residual strength and Young's modulus are absolute quantities, failure strain is defined relative to the initial state of the test. Of cause, this initial state can be affected significantly by the history of the specimen.

Tab. 16 Parameters describing failure strain of Opalinus Clay. Parameters are determined by fitting $\varepsilon_{fail} = (\varepsilon_0 + a\,\sigma_3)(1 + f_T\,(T - 30°C))\,f_W\,f_A$ to the available data for $\sigma_3 \le 10$ MPa.

ε_0 [-]	Failure strain for moist p-samples at 30°C in uniaxial test	0.0037
a [MPa^{-1}]	$\partial\varepsilon_{fail}/\partial\sigma_3$ for moist p-samples at 30°C	0.0288
f_T [K^{-1}]	$\partial \ln\varepsilon_{fail}/\partial T$ at 30°C	-0.0019
$f_{W.d}$	ratio of dry versus moist shear strength	0.68
$f_{A.s}$	ratio of anisotropy for s-geometry versus p-geometry	3.6
$f_{A.z}$	ratio of anisotropy for z-geometry versus p-geometry	2.2
n	number of data points	65
R^2	coefficient of determination	0.6572
RMSE [MPa]	root mean squared error	0.0035

6.2.4 Residual strength

Two methods of measuring residual strength $\sigma_{dev.res}$ have been employed in the LT-experiment. When a specimen is loaded in post-failure state at constant confining pressure with a constant strain rate until the deviatoric stress becomes stationary, the measurement is termed "stationary" and yields just one data point $\sigma_{dev.res}(\sigma_3)$. A complete $\sigma_{dev.res}(\sigma_3)$-function is registered in a so called "dynamic" measurement, where confining pressure is reduced continuously while applying a constant strain rate. A dynamic measurement can only be performed subsequent to a stationary measurement. As equilibration of stresses always requires some time, even in case of reaching the residual strength curve, results of dynamic measurements may slightly deviate from those of stationary measurements. Systematical deviations are expected to arise from a retarded equilibration of pore pressure during the reduction of σ_3. Therefore, pore pressure at a given σ_3 will be slightly higher in a dynamic measurement than in a stationary one, resulting in a lower effective confining pressure and thereby in a lower residual strength.

Stationary data are listed in Tab. 8 (Appendix A), and all data are shown in Fig. 27.

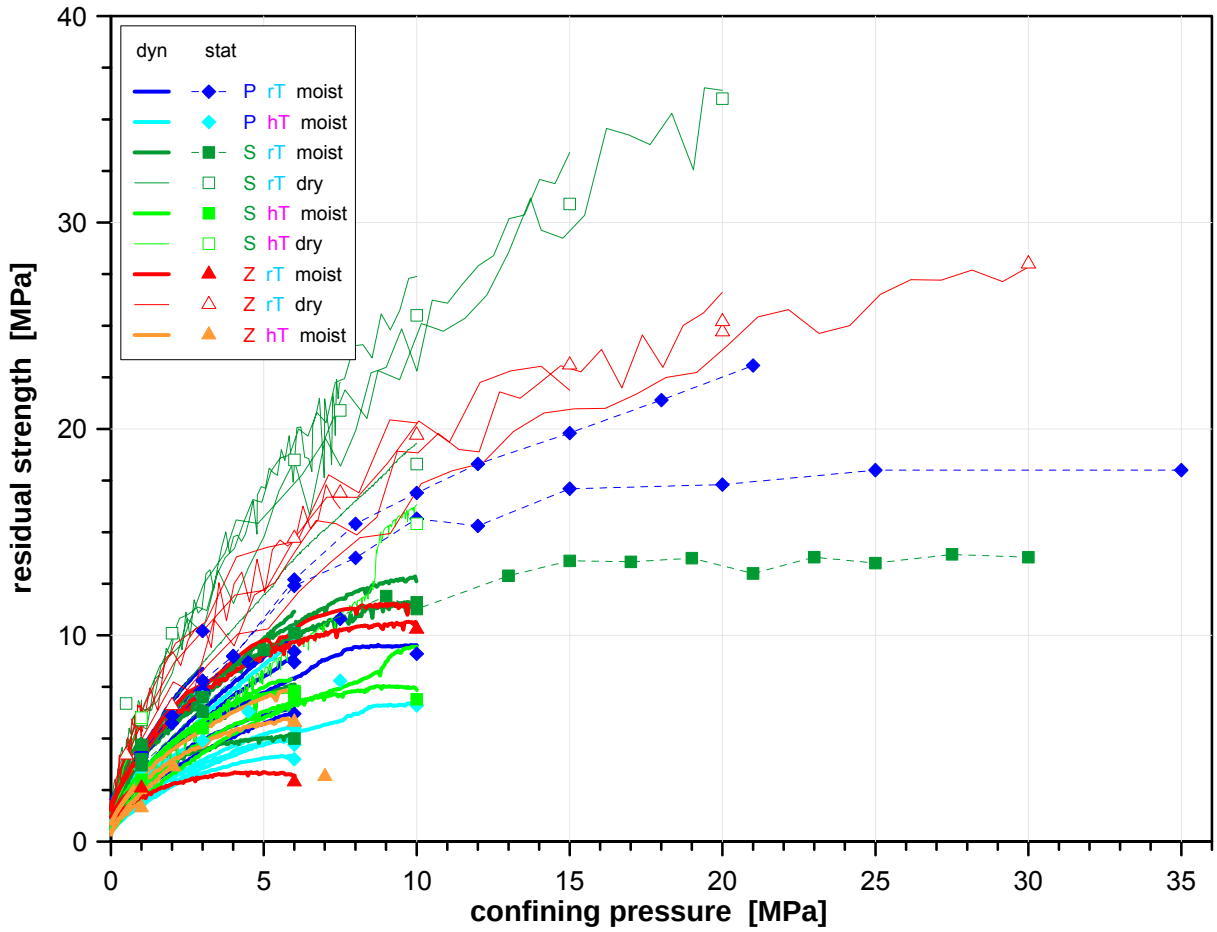

Fig. 27 Results of residual strength $\sigma_{dev.res}$ determination from uniaxial and triaxial strength tests as well as from multistep triaxial strength tests. Markers represent stationary measurements, solid lines show dynamic measurements. Dashed lines connect stationary data resulting from the same specimen. The noisy curves for the BED-C specimens (S rT dry and Z rT dry) originate from lower resolution sensors employed in the early phases of the LT-experiment.

The impact of moisture on residual strength

Similar to the findings for shear strength, a significant increase of residual strength occurs when Opalinus Clay is desiccated (Fig. 28). On average, the residual strength of dry samples surpasses that of moist samples by 50% – 100%.

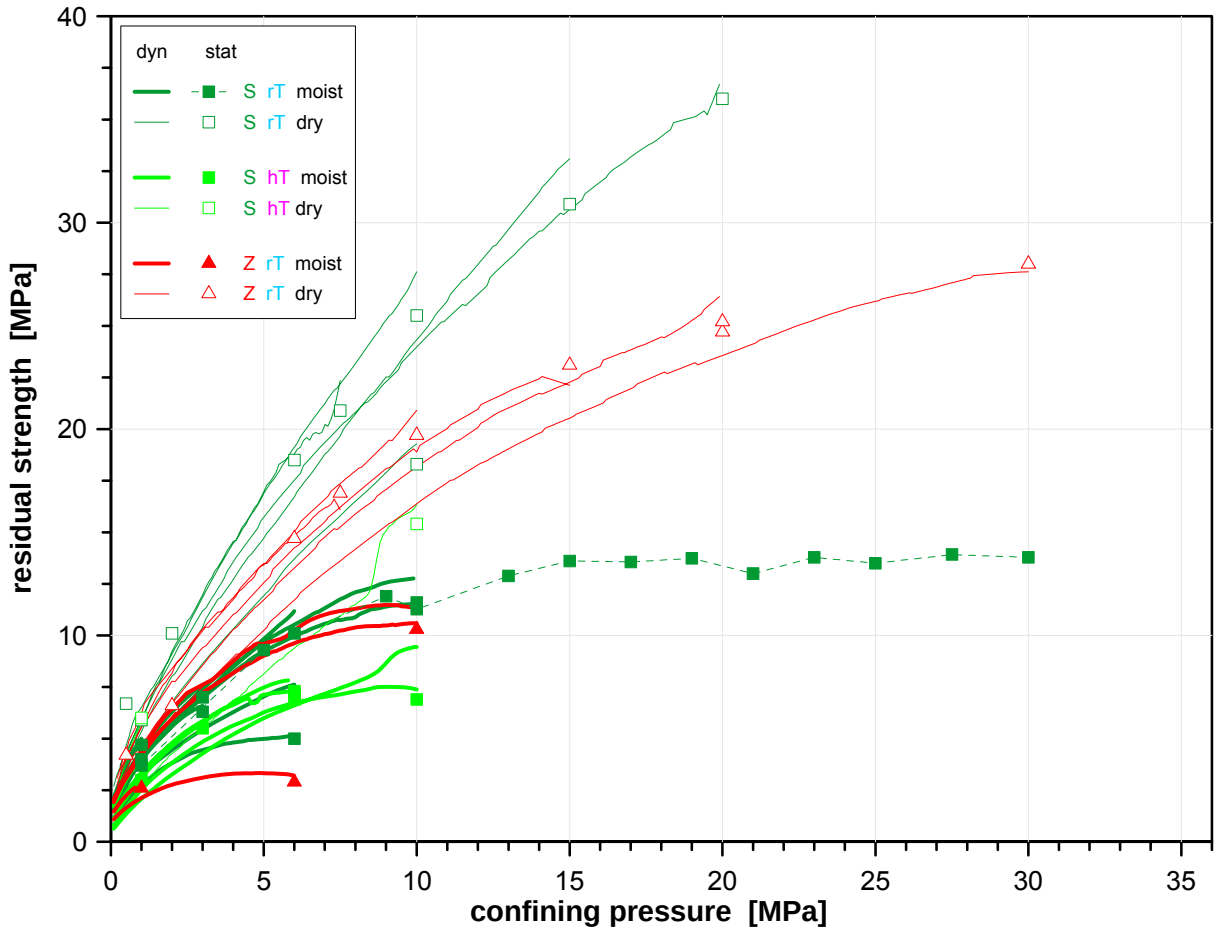

Fig. 28 Within any subset (S hT, S rT, or Z rT) dry specimens (open markers / thin lines) exhibit considerably higher residual strength than moist ones (filled markers / broad lines). Note that for the sake of clarity dynamic data in this and the following plots are smoothed.

Residual strength and temperature

A reduction of residual strength by heating can be recognized in the data (Fig. 29). The effect is less distinct than the impact of drying. Nevertheless, an average reduction of residual strength by increasing temperature from rT to hT by approximately ⅓ occurs can be found.

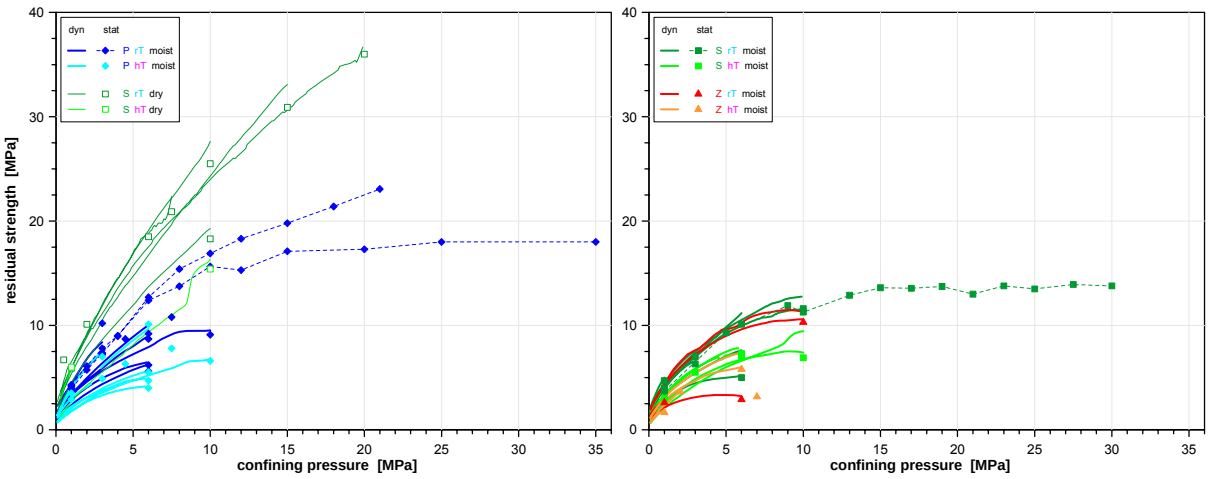

Fig. 29 Within most subsets (P moist, S moist, S dry) residual stress at higher temperature (bright colors) is slightly lower than at room temperature (darker colors). Only for moist z-samples considerable sample variability obscures any impact of temperature.

Anisotropy of residual strength

In contrast to shear strength anisotropy is not very distinct for residual strength (Fig. 30). Considering that residual strength does no longer represent the strength of the undisturbed, laminated and thereby significantly anisotropic material, but is essentially a property of the fully developed shear plane, this finding is quite plausible. It will be shown later that some weak anisotropy can still be identified by statistical analysis, whereas it can be hardly verified from a data plot (except for dry samples).

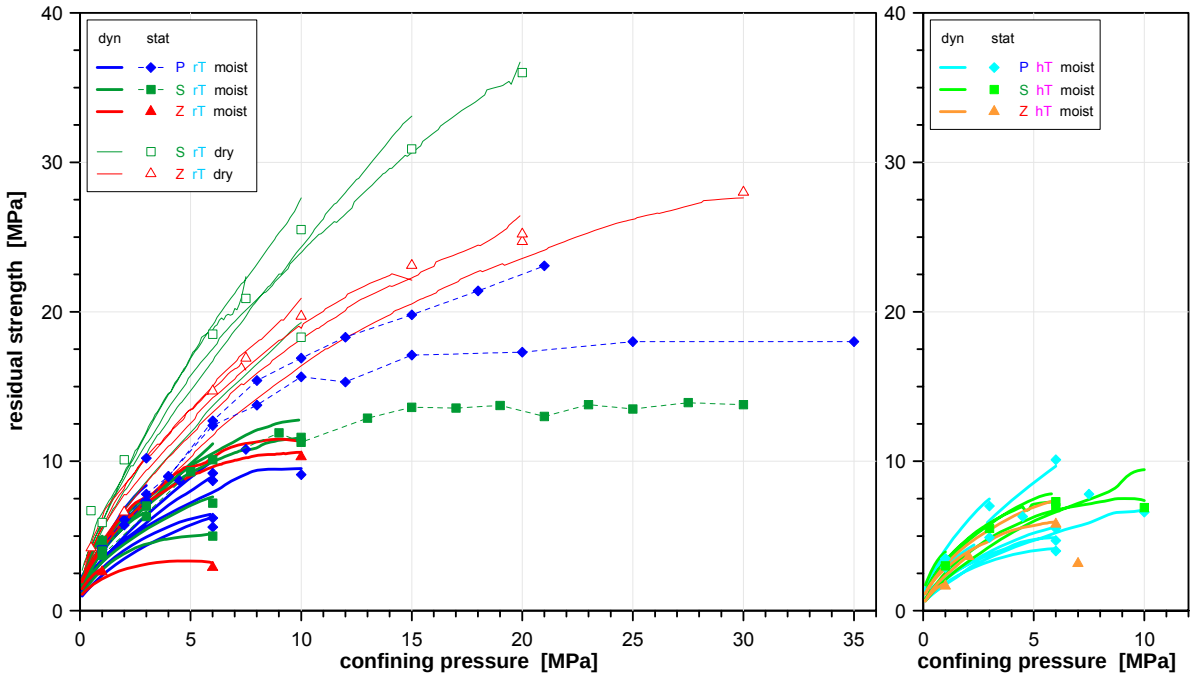

Fig. 30 For residual strength anisotropy is difficult to be seen from these plots, except for dry specimens. Although there is some anisotropy, it is far less distinct than for shear strength.

The relationship of residual strength versus confining pressure

Whereas it is very difficult to get more than one measurement of shear strength from a single sample, doing so is easy in case of residual strength. Therefore, there is a more comprehensive data basis available.

Unfortunately, most data result from dynamic measurements which are expected to exhibit some minor but systematic underestimation of residual strength. These systematic deviations might lead to some changes of the shape of the $\sigma_{dev.res}(\sigma_3)$-function. Considering this, the analysis of the $\sigma_{dev.res}(\sigma_3)$-characteristic has been based on stationary data from multistep strength tests that comprise numerous determinations of residual strength from a single sample. These data sets exhibit a characteristical shape of two linear branches (Fig. 31). As in case of shear strength (cf. chap. 6.2.2), the reduction of effective confining pressure due to a buildup of pore pressure at higher mean normal stress σ_{oct} offers a plausible explanation of this finding.

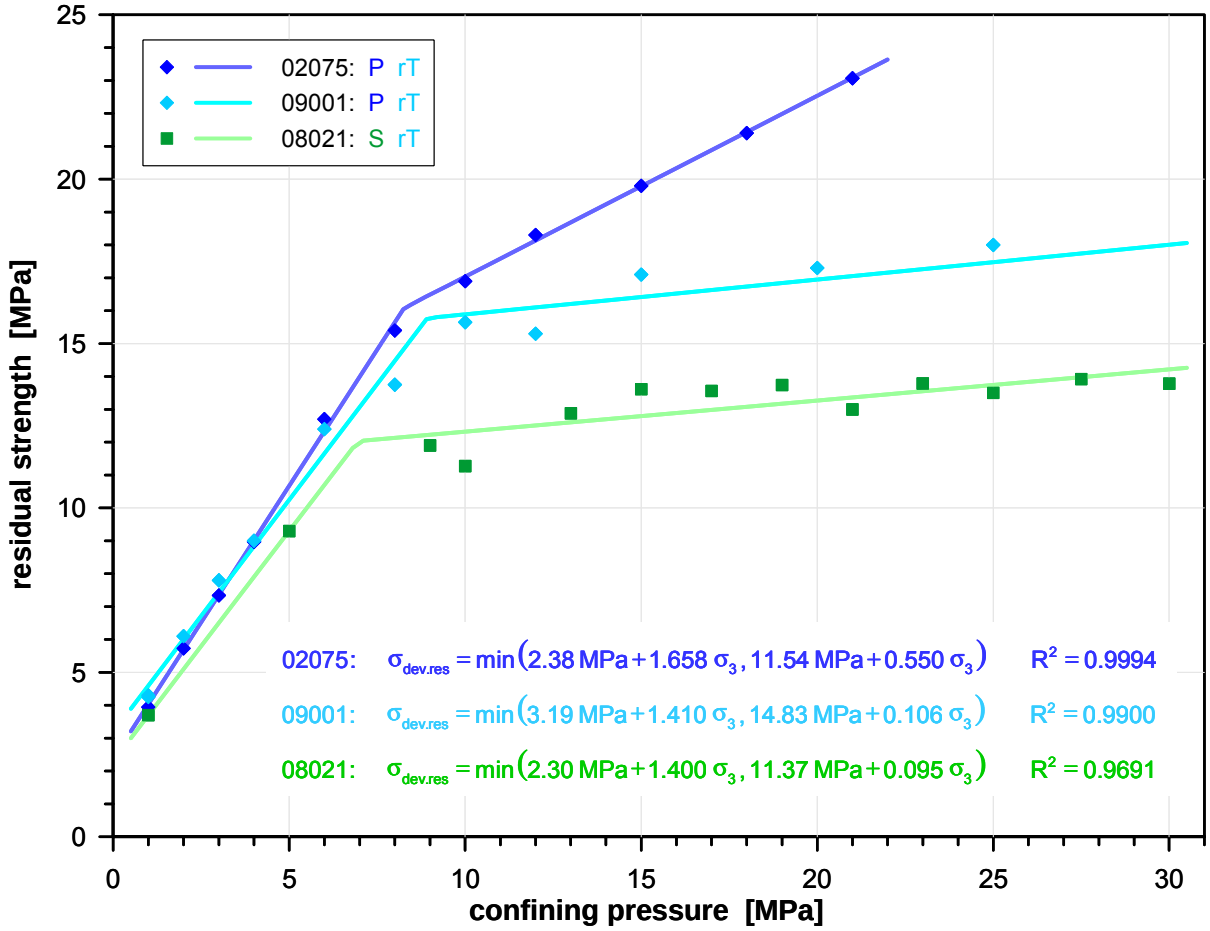

Fig. 31 Residual strength $\sigma_{dev.res}$ results from multistep triaxial strength tests. In any case a curve build from two linear branches represents the data almost perfectly.

On the contrary to the stationary data, dynamic measurements display a gradually bending $\sigma_{dev.res}(\sigma_3)$-function instead of two linear branches (Fig. 27). Assuming a systematic deviation of dynamic data due to a retarded equilibration of pore pressure, this is exactly what one would expect. As

any dynamic measurement starts subsequent to a stationary measurement (thus starting almost without a systematic error), and it passes through a more or less extended period of low σ_{oct} where pore pressure fades away (thus ending almost without a systematic error), the corresponding stationary two-branch-curve will be an asymptote of the curved dynamic $\sigma_{dev.res}(\sigma_3)$-relationship.

Synoptic description

Considering the similarities in the behavior of shear strength and residual strength it is a self-evident approach to perform a synoptic description of the various impacts on residual strength in a similar way as it has been shown in case of shear strength. There are three facts that require a somewhat more sophisticated approach:

- First, the data set for residual strength compared to shear strength is more comprehensive. Particularly, there is also sufficient data coverage in the range of higher confining pressure ($\sigma_3 > 10$ MPa). This allows for fitting the full two-branch-function. It is parameterized by a simple extension of the type of fit used for shear strength (cf. p. 28):

$$\sigma_{dev.res} = \min\left(c_1 + a_1\,\sigma_3\,,\, c_2 + a_2\,\sigma_3\right)\,\left(1 + f_T\,(T - 30°C)\right)\,f_W\,f_A$$

- Secondly, the systematic deviation of dynamic data requires the introduction of a smoothing parameter into the model (this parameter is applied to dynamic data only). The smoothing parameter describes something like a radius of curvature in the transition of the two branches. The smoothing parameter can be introduced similar to a catenary by

$$\sigma_{dev.res} = -r\,\ln\left[\exp\left(\frac{c_1 + a_1\,\sigma_3}{-r}\right) + \exp\left(\frac{c_2 + a_2\,\sigma_3}{-r}\right)\right]\,\left(1 + f_T\,(T - 30°C)\right)\,f_W\,f_A$$

where:
c_1 = inter sec t of 1st linear branch for moist p-samples at 30°C
= residual cohesion
a_1 = slope of 1st linear branch for moist p-samples at 30°C
c_2 = inter sec t of 2nd linear branch for moist p-samples at 30°C
a_2 = slope of 2nd linear branch for moist p-samples at 30°C
f_T = $\partial \ln \sigma_{dev.res} / \partial T$ at 30°C
f_W = moisture coefficient = $\begin{cases} f_{W.m} = 1 & \text{for moist samples} \\ f_{W.d} & \text{for dry samples} \end{cases}$
f_A = anisotropy coefficient = $\begin{cases} f_{A.p} = 1 & \text{for p-geometry} \\ f_{A.s} & \text{for s-geometry} \\ f_{A.z} & \text{for z-geometry} \end{cases}$
r = smoothing parameter

- Thirdly, fitting a function to a data set comprising subsets of essentially different structure requires the introduction of arbitrary weighting factors to balance the impact of the subsets in an appropriate way. This inevitably introduces an element of subjectiveness to the fit.

Whereas for stationary data any specimen is represented by one or even a few data points, dynamic measurements result in a huge number of registrations per specimen displaying a complete $\sigma_{dev.res}(\sigma_3)$-curve (of cause including considerable noise). Therefore, applying higher weights to stationary data is required, because otherwise dynamic data will completely dominate the fitting

result simply by their overwhelming number of data points. Since stationary data are assumed to own higher reliability, and the number of specimens represented by stationary respectively dynamic data is in the same order, weighting was performed in a way that results in an equal sum of weights for both subsets.

As the rate of data registration during dynamic measurements was subject to considerable variation, dynamic data exhibit significant variation of data density along the registered curves. Thus, weighting data within the subset of dynamic data is also a nontrivial task. It was intended to realize a uniform weight per σ_3-interval for any specimen. The chosen solution is to generate an interpolated data set evenly spaced with respect to σ_3. Separately for any specimen, interpolation was done by linear regression based on all data within a given σ_3-interval centered around the interpolation point. This does not only solve the problem of weighting but also reduces high-frequency noise in the data similar to the effect of a running average (compare the dynamic raw data shown in Fig. 27 with the smoothly interpolated data displayed in Fig. 28 to Fig. 31).

This approach results in a fairly good fit ($R^2 = 0.9392$, RMSE = 1.9 MPa). The determined parameter values are listed in Tab. 17. To check whether there are systematic differences between stationary and dynamic data which are not covered by the smoothing parameter, the fit was also carried out for stationary respectively dynamic data only.

Obviously, there are systematic differences, leading to considerable differences in the parameter sets, particularly for φ_1, $f_{W.d}$, $f_{A.s}$ and $f_{A.z}$. Adding the observation of a striking similarity of the parameter set for stationary measurements only to those parameters calculated for shear strength (cf. values from Tab. 12 included in Tab. 17), particularly for a_1, $f_{W.d}$ and $f_{A.s}$, this rises some doubt concerning the reliability of the dynamic data.

It does not necessarily imply problems attributable to the method of dynamic measurements. It is also a plausible possibility that there are some dynamic data sets from samples not fitting well in the moist/dry-scheme established on the basis of shear strength data (cf. p. 22 in chap. 6.2.2). For instance, a specimen "behaving moist" until failure might "behave dry" in the residual state (or vice versa), due to changes caused by excessive deformation. There are at least two specimen (02016.102 and 03006.053) which possibly show a transition towards "moister behavior" during the post failure phase of the test (Fig. 32). Of cause, a few inappropriate attributions of samples regarding their moisture state would explain a reduction of the fitted $f_{W.d}$ parameter for the dynamic data. In the likely case that the frequency of such miss-attributions varies with sample orientation, disturbed values of anisotropy parameters $f_{A.s}$ and $f_{A.z}$ would be a consequence.

Based on these considerations we regard the parameter set resulting from a fit to stationary data only (shaded green in Tab. 17) to be the most reliable description of residual strength.

Tab. 17 Parameters characterizing residual strength of Opalinus Clay in the framework of the synoptic description. Besides the characterization resulting from all available data (shaded blue) results for dynamic respectively stationary data are also shown to depict the systematic differences between these subsets. The analogous parameters determined for shear stress show a remarkable similarity to those of the stationary residual strength data (shaded green) with respect to a_1 , $f_{W.d}$ and $f_{A.s}$.

	residual strength			shear strength
	dynamic data only	equal sum of weights	stationary data only	$\sigma_3 \leq 7.5$ MPa only
c_1 [MPa]	8.5	3.4	4.5	15.7
a_1	2.220	1.461	1.229	1.374
φ_1 [°]	31.0	24.9	22.3	24.0
c_2 [MPa]	22.1	14.1	21.0	?
a_2	0.000	0.328	0.047	?
φ_2 [°]	0.0	7.9	1.3	
f_T [K^{-1}]	-0.0056	-0.0056	-0.0054	-0.0050
$f_{W.d}$	1.60	2.06	2.17	2.30
$f_{A.s}$	1.22	0.84	0.76	0.76
$f_{A.z}$	0.92	0.66	0.61	0.35
r [MPa]	16.8	2.4	–	–
n	52 curves	104 stat. points + 52 dyn. curves	104	62
R^2	0.9658	0.9392	0.9446	0.8373
RMSE [MPa]	1.4	1.9	1.8	2.6

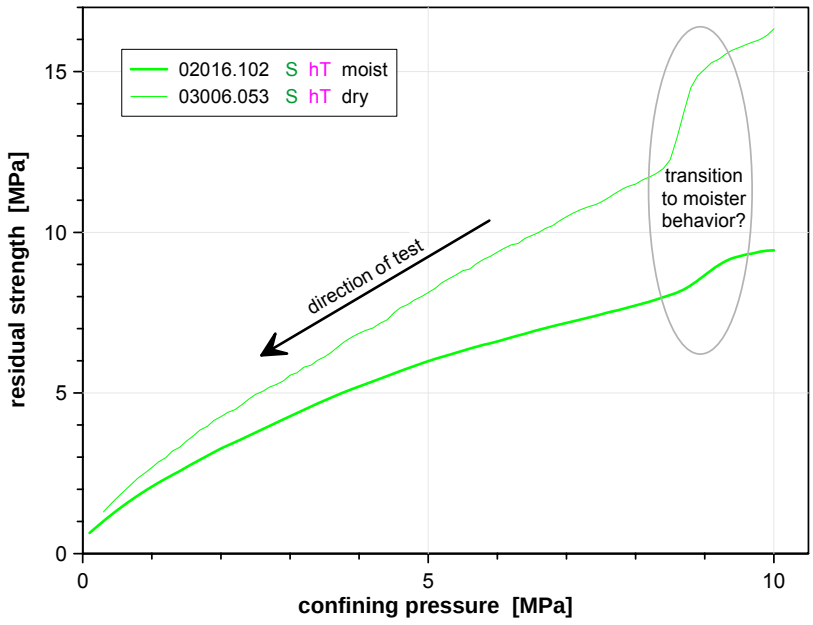

Fig. 32 Dynamic data from two samples possibly showing a transition towards a "moister behavior".

6.2.5 Linear elastic limit

The linear elastic limit $\sigma_{dev.lin}$ was investigated in multistep triaxial strength tests. In fact, the applied experimental approach (for details see GRÄSLE & PLISCHKE, 2007) determines the limit of linearity of the $\sigma_{dev}(\varepsilon)$-relationship in an overconsolidated regime. The limit of linearity and the limit of elasticity (full reversibility) coincide for many materials, but this does not necessarily apply to Opalinus Clay. Therefore, the limit of linear elasticity is possibly far below any level of relevant material damage (such as measurable dilatancy or even failure). It nevertheless characterizes the transition to another deformation regime, either to a non-linear elastic behavior or to an irreversible alteration of material properties.

Overall, 3 multistep triaxial strength tests have been carried out in the LT-experiment. Therefore, the results provide just a first qualitative characterization of the linear elastic limit and there is no basis for a statistical analysis. Similar to the findings for shear strength and residual strength the $\sigma_{dev.lin}(\sigma_3)$-relationship exhibits a two-branch shape (Fig. 33). As the transition between the branches appears to occur at rather high confining pressure (24 MPa for sample 09001, 17.1 MPa for sample 08021), the covered σ_3-range for specimen 02075 does not allow for a determination of the second branch. Once again, the bending of the $\sigma_{dev.lin}(\sigma_3)$-function is assumed to result from pore pressure effects at higher confining pressure.

A significantly higher variability of the data compared to residual strength (see Fig. 31 and Fig. 33) reflects the complicated way of $\sigma_{dev.lin}$-determination which is more susceptible to disturbances in the data. Consequently, $\sigma_{dev.lin}$ is described by the fits with lower coefficients of determination and the fit parameters bear a higher degree of uncertainty.

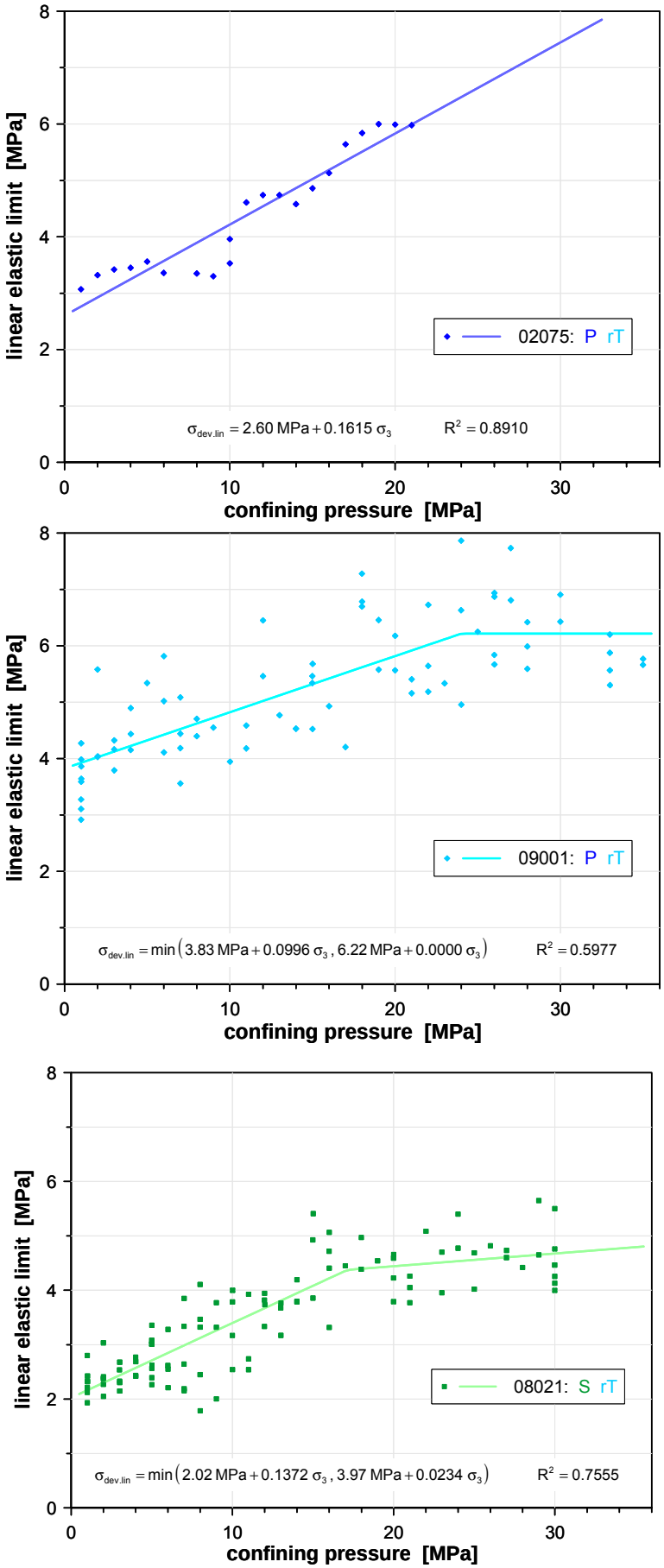

Fig. 33 Results for linear elastic limit collected in three multistep triaxial strength tests.

6.2.6 Elastic moduli

Three types of elastic moduli have been determined on samples of Opalinus Clay:

- Young's modulus E is determined as a secant modulus in an unloading cycle of the stress strain curve before failure. The secant is supported by the points at $⅓\cdot\sigma_{dev.peak}$ and $⅔\cdot\sigma_{dev.peak}$. Young's modulus describes the fully elastic behavior in an overconsolidated state.
- The tangent modulus E_v determined as the slope of the initial loading curve at $½\cdot\sigma_{dev.peak}$. Therefore, the tangent modulus usually represents a superposition of fully elastic behavior and irreversible compaction in a normal consolidated material.
- The residual deformation modulus E_{res} is calculated from an unloading and reloading cycle in the post failure phase. The resulting stress strain curve in this cycle is nonlinear. E_{res} is calculated similar to Young's modulus using the minimum point and the point of intersection of unloading and reloading.

These moduli are virtually independent from confining pressure. Thus, analysis is focused on the impact of moisture, temperature and loading geometry (anisotropy).

The impact of moisture on elastic moduli

The moisture state does not only affect strength parameters, it also exhibits significant impact on elastic moduli. For E and E_v as well as for E_{res} drying increases stiffness considerably (Tab. 18 and Fig. 34 to Fig. 36). Although the amount of available data is rather limited, the effect meets statistical significance in almost any case (except in case of E and E_{res} for s-geometry at higher temperature, where only one respectively two data points from dry samples are available).

Tab. 18 Comparison of average elastic moduli of moist versus dry specimens. Statistical significance is indicated by bold face and yellow shading.

	data set	moist	dry	p (dry>moist)
E [GPa]	S rT	2.72 ± 0.36 (n = 9)	9.57 ± 2.01 (n = 5)	**0.0004**
	S hT	1.88 ± 0.14 (n = 6)	4.90 ± ∞ (n = 1)	*0.5000*
	Z rT	2.50 ± 0.65 (n = 2)	7.33 ± 0.93 (n = 3)	**0.0169**
E_v [GPa]	S rT	1.19 ± 0.17 (n = 8)	6.27 ± 1.33 (n = 6)	**0.0004**
	S hT	0.96 ± 0.21 (n = 7)	1.85 ± 0.10 (n = 2)	**0.0337**
	Z rT	1.23 ± 0.08 (n = 2)	3.52 ± 0.47 (n = 3)	**0.0164**
E_{res} [GPa]	S rT	0.94 ± 0.09 (n = 9)	8.16 ± 1.38 (n = 9)	**< 0.0001**
	S hT	1.04 ± 0.09 (n = 6)	1.35 ± 0.20 (n = 2)	*0.0742*
	Z rT	1.87 ± 0.31 (n = 5)	3.82 ± 0.42 (n = 9)	**0.0038**

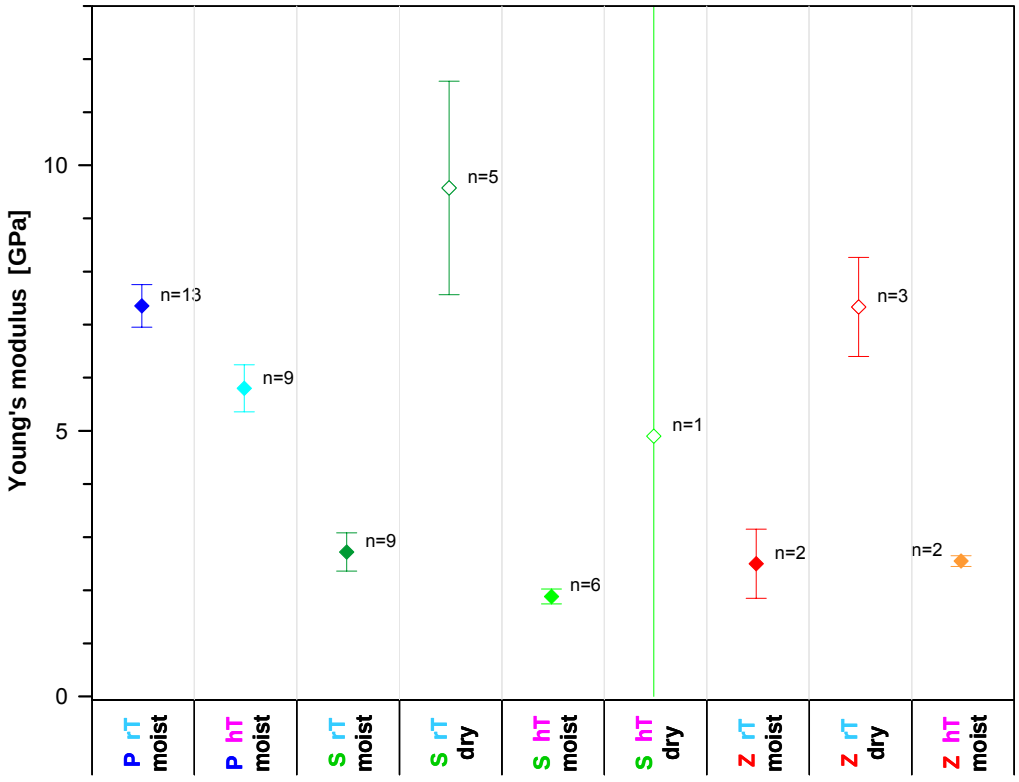

Fig. 34 Average Young's modulus for various combinations of test conditions. Error bars indicate standard errors of mean.

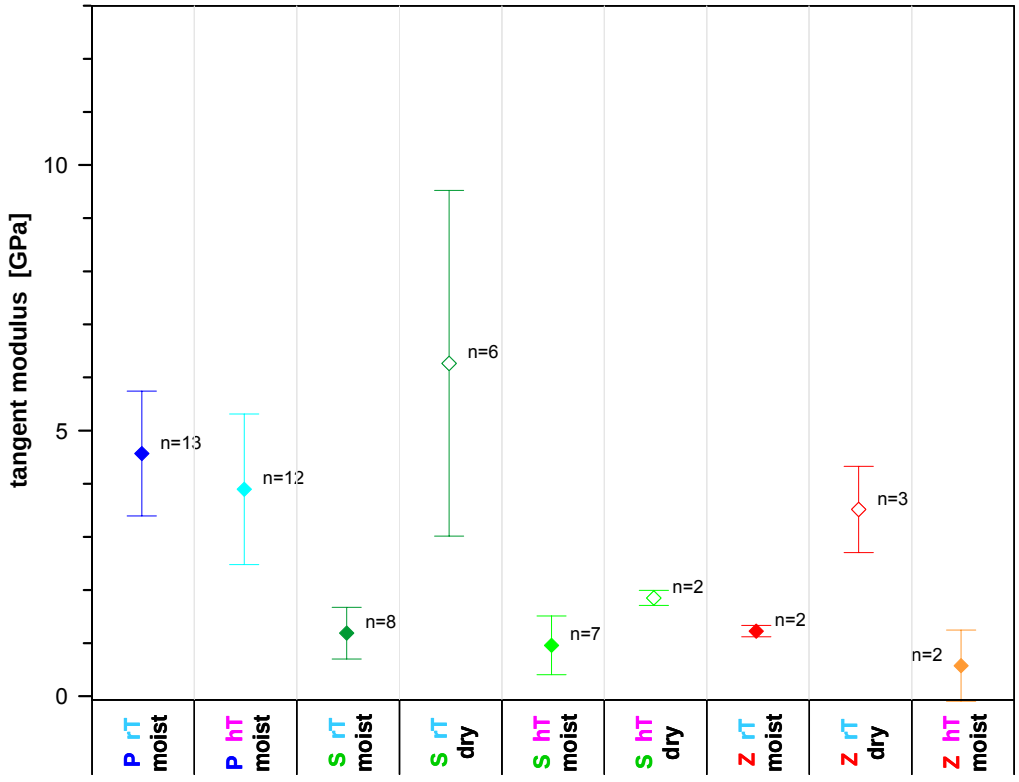

Fig. 35 Average tangent modulus for various combinations of test conditions. Error bars indicate standard errors of mean.

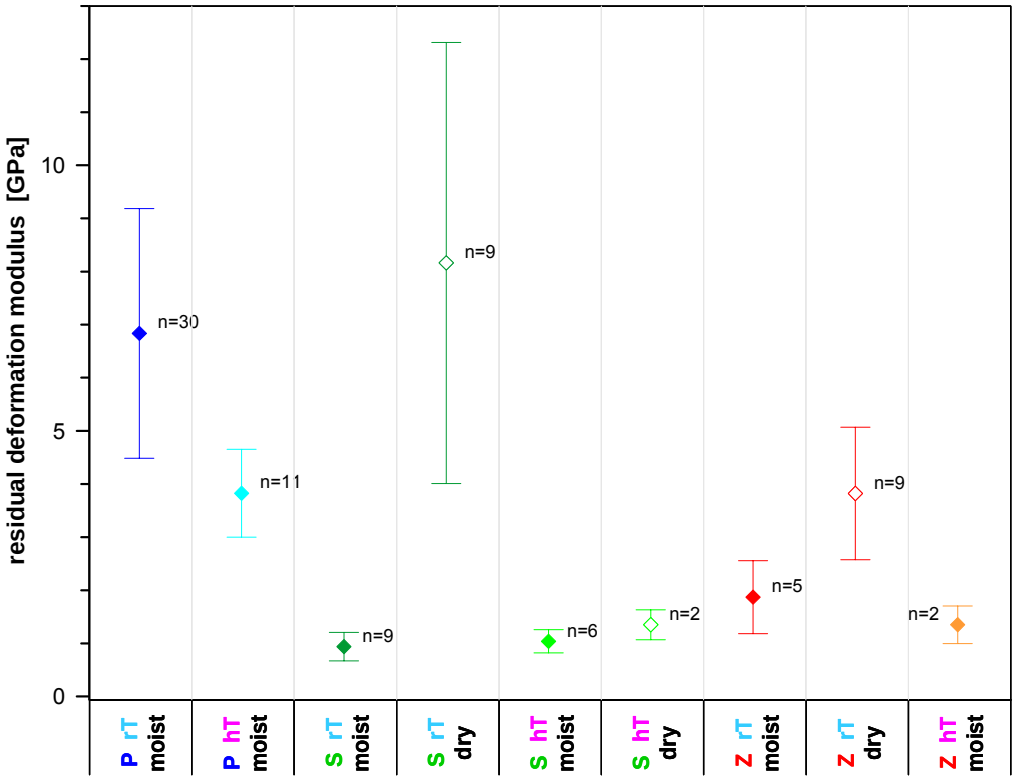

Fig. 36 Average residual deformation modulus for various combinations of test conditions. Error bars indicate standard errors of mean.

Elastic moduli and temperature

Similar to the findings for strength parameters, increased temperature also results in a decrease of elastic moduli (see Tab. 19 and Fig. 34 to Fig. 36). However, the impact of temperature in the data set is much smaller than the moisture effect. Due to the relatively small data set and considerable variation within each subset (Fig. 34 to Fig. 36), the impact of temperature meets statistical significance only in a minority of pairs of matchable subsets (Tab. 19).

Tab. 19 Comparison of average elastic moduli of specimens tested at 20 – 35°C (rT) versus those tested at 60 – 80°C (hT). Yellow shading and bold face indicates statistical significance.

	data set	rT	hT	p (rT>hT)
E [GPa]	P moist	7.35 ± 0.40 (n = 13)	5.80 ± 0.44 (n = 9)	**0.0095**
	S moist	2.72 ± 0.36 (n = 9)	1.88 ± 0.14 (n = 6)	**0.0453**
	S dry	9.57 ± 2.01 (n = 5)	4.90 ± ∞ (n = 1)	*0.5000*
	Z moist	2.50 ± 0.65 (n = 2)	2.51 ± 0.15 (n = 5)	*0.5090*
E_v [GPa]	P moist	4.57 ± 0.33 (n = 13)	3.90 ± 0.41 (n = 12)	*0.1039*
	S moist	1.19 ± 0.17 (n = 8)	0.96 ± 0.21 (n = 7)	*0.2030*
	S dry	6.27 ± 1.33 (n = 6)	1.85 ± 0.10 (n = 2)	*0.0593*
	Z moist	1.23 ± 0.08 (n = 2)	0.98 ± 0.23 (n = 5)	*0.2803*
E_{res} [GPa]	P moist	6.84 ± 0.43 (n = 30)	3.83 ± 0.25 (n = 11)	**< 0.0001**
	S moist	0.94 ± 0.09 (n = 9)	1.04 ± 0.09 (n = 6)	*0.7681*
	S dry	8.16 ± 1.38 (n = 9)	1.35 ± 0.20 (n = 2)	**0.0265**
	Z moist	1.87 ± 0.31 (n = 5)	1.46 ± 0.14 (n = 5)	*0.1284*

Anisotropy of elastic moduli

Any elastic modulus displays a distinct anisotropy insofar as stiffness for p-geometry surpasses stiffness for s- respectively z-geometry by a factor of 3 on average (Tab. 20 and Fig. 34 to Fig. 36). In contrast to strength parameters, elastic moduli do not show a homogeneous decrease from s-samples to z-samples.

This finding is plausible, when one considers the different mode of impact that loading geometry takes on strength respectively stiffness of a laminated material. Bedding planes will generally be the features most susceptible to shear failure and shear deformation as well as to perpendicular deformation:

- Shear failure always occurs inclined with respect to the direction of loading (the angle between loading direction and the normal on the failure plane is $\frac{1}{2}(\pi+\varphi)$ in isotropic materials). Therefore, the inclined loading direction termed z-geometry favors a failure plane virtually coinciding with the direction of bedding, thus resulting in the lowest possible shear strength.
- Stiffness describes axial deformation in the direction of loading. This deformation partly results from compression (since loading increases σ_{oct}) and from shear deformation (since loading increases σ_{dev}). In laminated material, the maximum contribution of shearing to the axial deformation will occur in z-geometry where the plane of highest shear stress approximately coincides with the bedding planes. In contrast, maximum compressive deformation will always occur normal to the bedding planes. Whereas the first effect reduces stiffness in z-geometry, the second one reduces stiffness in s-geometry. Consequently, both loading geometries will be less stiff than p-geometry, but there might be little difference between s- and z-geometry.

Tab. 20 Comparison of average elastic moduli measured on different sample geometry. Yellow shading indicates statistical significance for the expected anisotropy P > S > Z, orange shading highlights statistical significance contrary to this expectation.

	data set	P	S	Z	p (P>S)	p (P>Z)	p (S>Z)
E [GPa]	rT moist	7.35 ± 0.40 (n = 13)	2.72 ± 0.36 (n = 9)	2.50 ± 0.65 (n = 2)	**< 0.0001**	**0.0003**	*0.3981*
	hT moist	5.80 ± 0.44 (n = 9)	1.88 ± 0.14 (n = 6)	2.51 ± 0.15 (n = 5)	**< 0.0001**	**< 0.0001**	**0.9934**
	rT dry	–	9.57 ± 2.01 (n = 5)	7.33 ± 0.93 (n = 3)	–	–	*0.2243*
E_v [GPa]	rT moist	4.57 ± 0.33 (n = 13)	1.19 ± 0.17 (n = 8)	1.23 ± 0.08 (n = 2)	**< 0.0001**	**0.0009**	*0.5401*
	hT moist	3.90 ± 0.41 (n = 12)	0.96 ± 0.21 (n = 7)	0.98 ± 0.23 (n = 5)	**< 0.0001**	**0.0003**	*0.5280*
	rT dry	–	6.27 ± 1.33 (n = 6)	3.52 ± 0.47 (n = 3)	–	–	*0.1026*
E_{res} [GPa]	rT moist	6.84 ± 0.43 (n = 30)	0.94 ± 0.09 (n = 9)	1.87 ± 0.31 (n = 5)	**< 0.0001**	**< 0.0001**	**0.9984**
	hT moist	3.83 ± 0.25 (n = 11)	1.04 ± 0.09 (n = 6)	1.46 ± 0.14 (n = 5)	**< 0.0001**	**< 0.0001**	**0.9875**
	rT dry	–	8.16 ± 1.38 (n = 9)	3.82 ± 0.42 (n = 9)	–	–	**0.0042**

Synoptic description

As elastic moduli can be regarded as independent from confining pressure, a synoptic description will be simpler than those used for $\sigma_{dev.peak}$ and $\sigma_{dev.res}$. Once again, a description linear with respect to any influencing variable (but including products terms between those variables) has been tested:

$$E = E_0 \left(1 + f_T \left(T - 30°C\right)\right) f_W \, f_A$$

where: E_0 = modulus for moist p-samples at 30°C

f_T = $\partial \ln E / \partial T$ at 30°C

f_W = moisture coefficient = $\begin{cases} f_{W.m} = 1 & \text{for moist samples} \\ f_{W.d} & \text{for dry samples} \end{cases}$

f_A = anisotropy coefficient = $\begin{cases} f_{A.p} = 1 & \text{for p-geometry} \\ f_{A.s} & \text{for s-geometry} \\ f_{A.z} & \text{for z-geometry} \end{cases}$

Analogous fits were used for E_v and E_{res}.

With coefficients of determination around 0.6 to 0.7 (Tab. 21) the quality of these fits appear to be moderate at first glance. However, this appraisal changes when the general conditions of the fits are analyzed in detail.

When a group of data (like "P rT moist", "S hT dry" and so on) is defined by homogeneous test conditions with respect to loading geometry, moisture and temperature regime, the variability within a group cannot be explained by any model solely based on loading geometry, moisture and temperature regime as independent variables. Therefore, the intra-group variance of the data set is essentially inexplicable by the model. When p_{intra} denotes the fraction of intra-group variance relative to the total variance of the data set, $R^2_{expl} = R^2 / (1 - p_{intra})$ describes the coefficient of determination with respect to the maximum fraction of variance which is in principle explicable by this type of model. $R^2_{expl} = 1$ would characterize the best model possible without introducing additional independent variables.

With $0.97 \leq R^2_{expl} \leq 0.98$ (Tab. 21) the fits for E and E_{res} show a very good quality. The somewhat lower but still satisfactory coefficient of determination for E_v ($R^2_{expl} = 0.90$) might result from a higher susceptibility of E_v to the conditions during drilling, sample storage and specimen preparation, similar to the situation described for failure strain (p. 33 in chap. 6.2.3).

Further analysis has been performed to check whether any impact of confining pressure is detectable in the data. As the amount of explained variance (i.e. R^2) can be improved by the introduction of a term linear in σ_3 (analogous to the synoptic models presented for shear strength and residual strength) by less than 1% for E and E_v and by 3.5% for E_{res}, the benefit of this type of extension of the model is negligible. This confirms the assumption that confining pressure does not affect the elastic moduli.

Tab. 21 Parameters characterizing elastic moduli of Opalinus Clay in the framework of the synoptic description. For comparison some information is included concerning alternative models: The "$\Delta R^2(\sigma_3)$"-row shows the benefit the introduction of an additional σ_3-dependency into the model would yield with respect to the coefficient of determination.

	Young's modulus E	tangent modulus E_v	residual deformation modulus E_{res}
E_1 [GPa]	8.44	5.51	8.90
f_T [K^{-1}]	-0.0042	-0.0045	-0.0080
$f_{W.d}$	3.10	4.11	4.85
$f_{A.s}$	0.39	0.28	0.22
$f_{A.z}$	0.32	0.18	0.11
n	53	58	86
R^2	0.6966	0.5980	0.6307
RMSE [GPa]	1.66	1.41	1.97
p_{intra}	0.2833	0.3390	0.3558
R^2_{expl}	0.9720	0.9047	0.9790
$\Delta R^2(\sigma_3)$	0.0055	0.0021	0.0352

p_{intra} = fraction of intra-group variance
R^2_{expl} = coefficient of determination with respect to the inter-group variance
$\Delta R^2(\sigma_3)$ = increase of R^2 by introducing a linear dependency from σ_3 into the model

7 TRUE TRIAXIAL TESTS ON CUBIC SPECIMENS

BGR's laboratory program focuses on investigations of deformation processes and distortion-dilatation relations to find a reliable base for the development of constitutive equations for Opalinus Clay. In phases 9 and 10 true triaxial experiments were conducted with respect to the deformation behavior under isostatic and shear loading and anisotropies of strength and dilatancy of Opalinus Clay.

7.1 EXPERIMENTAL SETUP

The true triaxial test apparatus for cubic samples from the laboratory of BGR was used to observe strains in the three normal directions, volumetric deformation, and the development of stress up to failure of the specimens (see Fig. 37 and Fig. 38). During the tests, the applied principal stresses can be controlled independently for each of the three orthogonal axes. The normal strains of the specimens were gathered from two displacement sensors per axes (see Fig. 37). Technical specifications of the machine and test procedures are given by NAUMANN & PLISCHKE (2006).

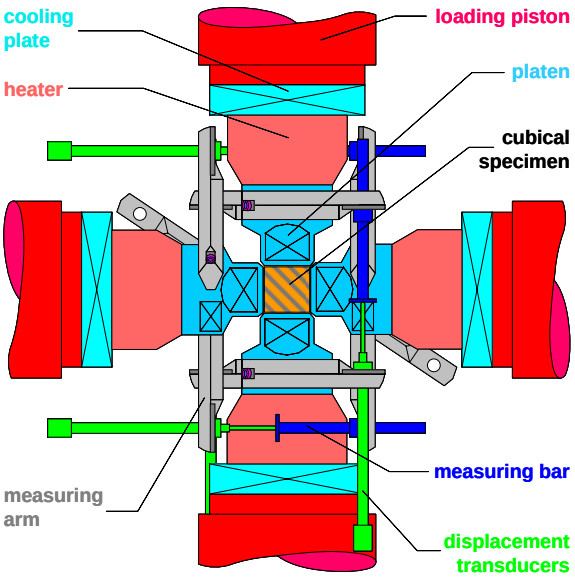

Fig. 37 Loading and measuring principle of the true triaxial apparatus.

Fig. 38 Cubic Opalinus Clay specimen after true triaxial compression test.

7.2 EXPERIMENTAL PROGRAMME

In total 15 true triaxial experiments were performed at room temperature. They provide information on the deformation behavior (compaction and elasticity), strength, and dilatancy. Two differently oriented types of cubic samples were used in order to assess the presumably anisotropic properties. The orientation of the maximum principal stress to the bedding plane of the rock was parallel for p-samples but perpendicular for s-samples (see Fig. 39). Experimental conditions deformation behavior under isostatic loading (compaction), elasticity, strength, and dilatancy are described at NAUMANN & PLISCHKE (2006).

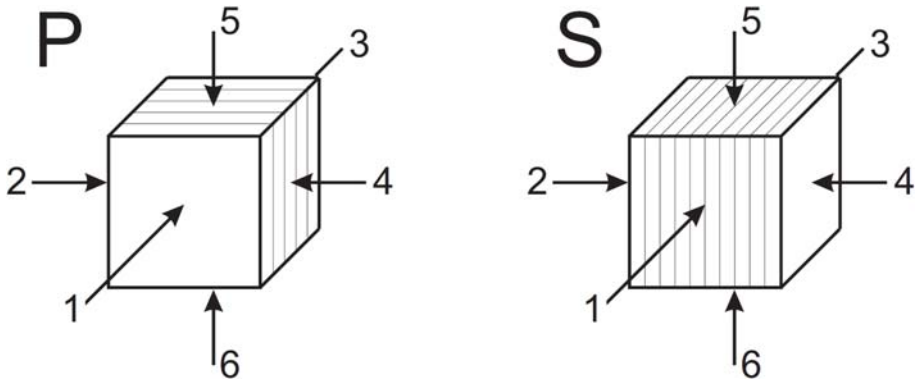

Fig. 39 Orientation of cubic specimens within the true triaxial machine, Numbers define axes directions and associated normal stresses (e.g. normal stress σ_{13} acts in direction 1-3). Left hand side: p-sample (bedding parallel σ_{24} – maximum principal stress), right hand side: s-sample (bedding normal σ_{24}). Note: Do not confuse subscripts of stresses with the common denotation for shear stresses.

7.3 RESULTS

It can be summarized for isostatic loading that pronounced anisotropic deformation behavior of the Opalinus Clay is manifested in higher deformation normal to the bedding than parallel to the bedding under identical loads. The ratio between the strains normal and parallel to the bedding shows considerable variations from one sample to another due to a different origin and pre-existing damage, but the difference is in no case negligible. The intermediate and minimum principle strain which always occurs parallel to the bedding are in most cases almost identical under isostatic loading conditions (Fig. 40). An apparent deformability decrease (stiffening) of the samples has been observed under increasing isostatic load. The initial transitional phase with increasing stiffness is followed by a phase where the sample shows approximately constant stiffness independent of further stress increase in each loaded direction (Fig. 41). Onset of constant stiffness in direction normal to the bedding occurs at higher stress levels (or time-delayed) and was more difficult to identify than in directions parallel to the bedding. Isostatic load of the onsets of the nearly linear phase of the stress-strain curves is on the order of 9±3 MPa within the bedding planes and of 15±3 MPa perpendicular to them.

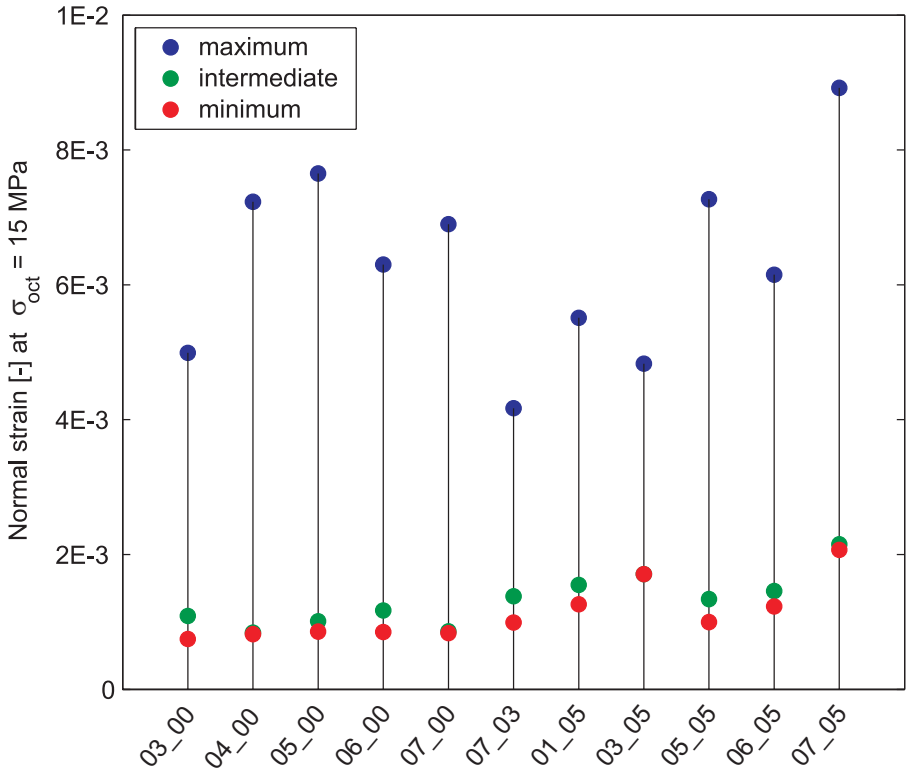

Fig. 40 Evolution of normal strains of cubic Opalinus Clay samples subjected to an isostatic load of 15 MPa. Bedding planes are parallel to cube faces. Test-ID given on the x-axis. Blue markers depict strain normal to the bedding. Green and red markers represent strain parallel to the bedding.

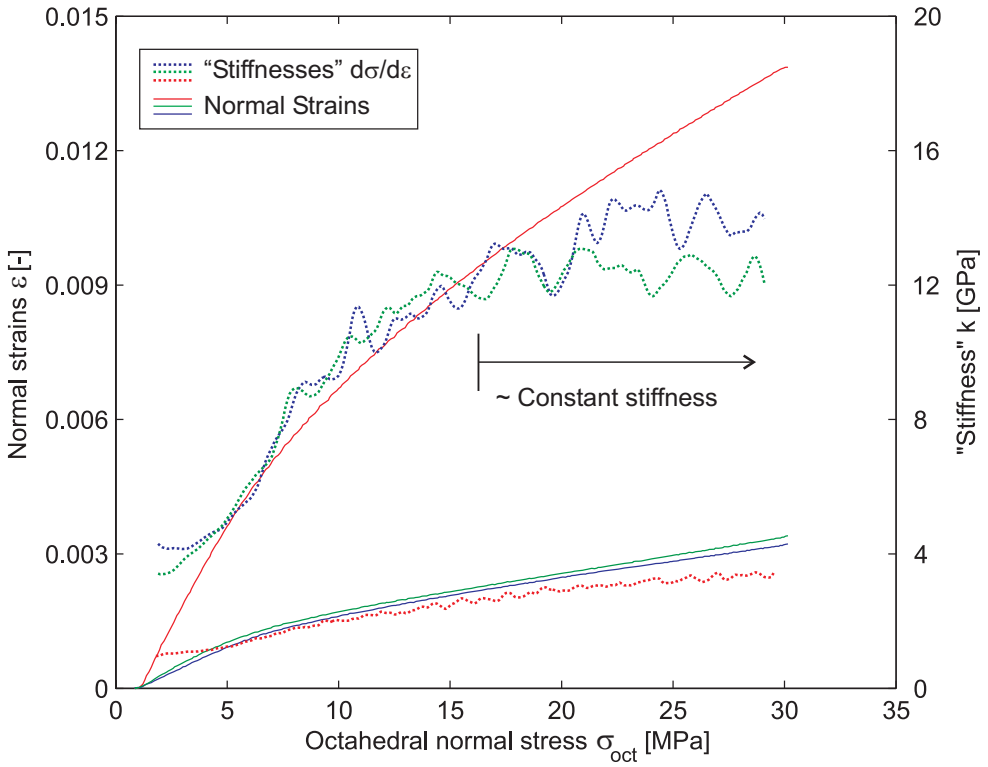

Fig. 41 Evolution of normal strains of cubic Opalinus Clay sample (Test-ID: 06_05) subjected to isostatic loading conditions. Bedding planes are parallel to cube faces. Strain and stiffness: parallel to bedding (blue and green lines), normal to bedding (red lines).

The investigations with regard to elasticity show following results. The parameters E_2 and ν_2 contained in the transversely isotropic elastic tensor are obtained from shear loading of cubic specimens in true triaxial tests. The deduced parameters are strongly influenced by the loading. The essentially undrained modulus perpendicular to the bedding planes E_2 takes values of about 6 to 8 GPa at the beginning of the shear loading. It reduces to rather low values of 1 to 2 GPa at the ending of the loading stage. The modulus seems to be influenced by time-dependent processes. Poisson's ratio ν_2 is also very inconstant during the loading of the specimen. It takes values from 0.1 in the beginning to more than 0.4 at the end of a loading phase. The applied experimental methodology is not as favorable for a reliable determination of elastic properties as for example the execution of cyclic tests.

For the determination of strength it can be assumed as followed. Failure strength increases with mean stresses. A distinct strength anisotropy has been observed. Specimens loaded parallel to the bedding plane show higher failure strengths than samples loading perpendicular to the bedding. The strength anisotropy increases with higher mean stresses. Specimens from drillhole BED-C6 show higher failure strengths than the investigated specimens from BLT drillholes. Maybe that depends on the storage conditions of this specimens. It is likely that some desiccation caused higher strength according to the findings from triaxial strength tests (cf. chap. 6.2.2). Strengths from the BLT drillholes are slightly higher than the comprehensive values presented by BOCK (2001) derived from Kármán tests. The results agree well with the findings of RUMMEL ET AL. (1998) obtained by conventional Kármán tests also (Fig. 42). Failure strengths of specimens from BED boreholes correspond very well with the values given for the Benken site (NAGRA, 2002).

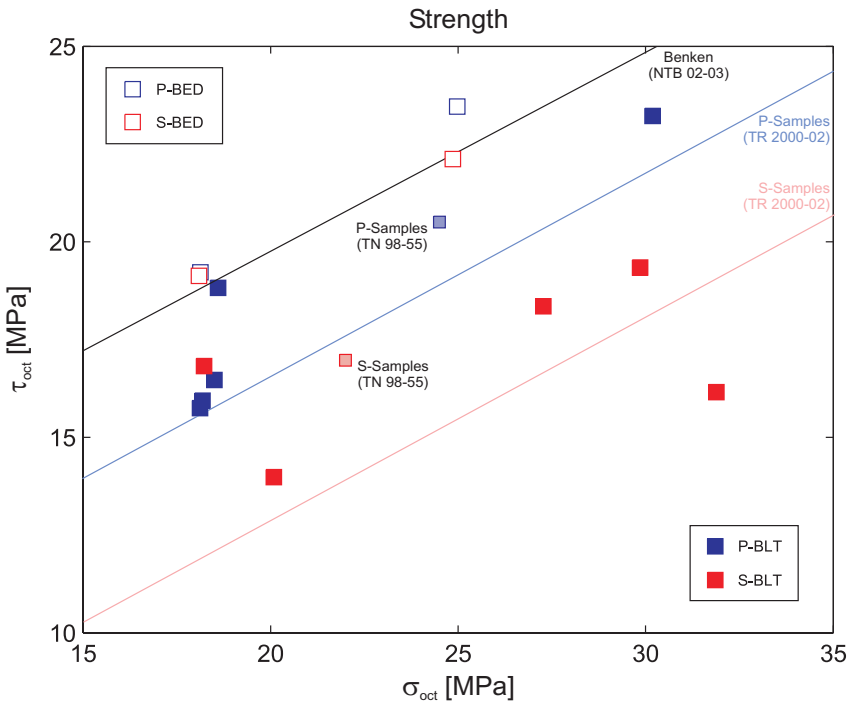

Fig. 42 Failure strength of Opalinus Clay as function of the mean stress (σ_{oct}) and orientation of the maximum principal stress (p-/s-sample). Open squares represent true triaxial tests on samples from the BED drillhole, filled squares stand for BLT material. Failure envelopes from the comprehensive reports from BOCK (2001) (TR 2000-02), NAGRA (2002) (NTB 02-03) and RUMMEL ET AL. (1998) (TN 98-55) are plotted for comparison.

The dilatancy boundary has been determined from the evolution of volumetric strain during shear loading at constant mean stress. Dilatancy strength increases with mean stresses and exhibits just like failure strength a non negligible degree of anisotropy. Onset of dilatancy detected is lower for p- than for s-specimen (opposite of the failure strength observations) as shown in Fig. 43. For p-specimen the onset of dilatancy was on average at 67±4 % of the appertaining failure strength, contrary to s-specimen, here the onset was detected at 85±5 %.

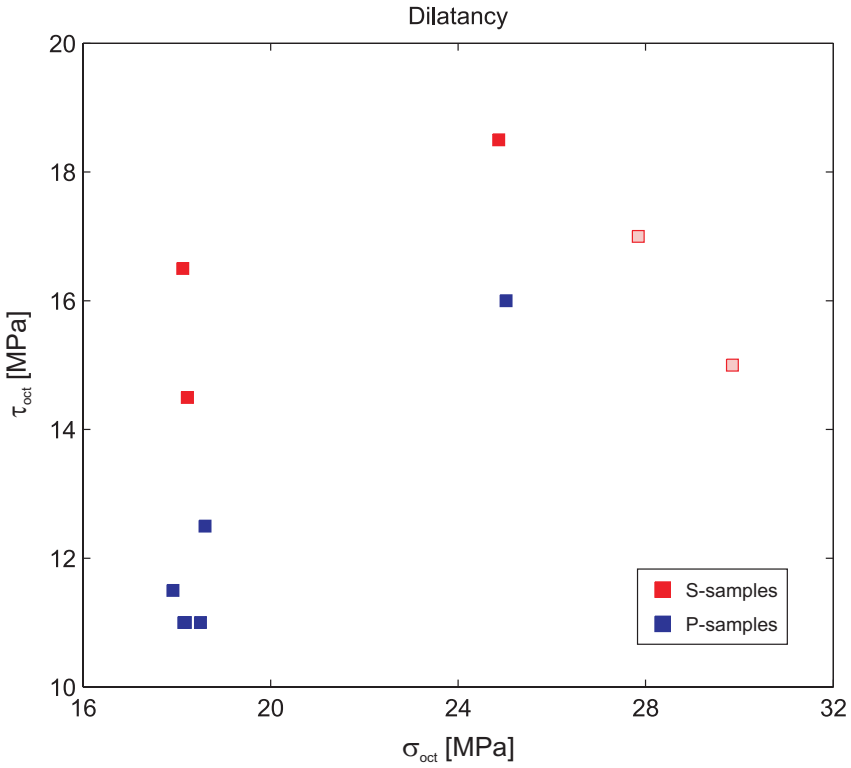

Fig. 43 Onset of dilatancy of Opalinus Clay as function of the mean stress (σ_{oct}) for specimens loaded normal (S) and parallel (P) to the bedding planes. Experiments 07_03 and 14_03 depicted in pale color show a differing behavior presumably due to their different origin and problems with proper parallel alignment of cube faces and bedding planes.

8 SUMMARY

Drilling, sampling, storing and preparation

- The drilling-, sampling- and storing-system was optimized with regard to gentle handling of the specimen before testing.
- Sample preparation was reduced to absolutely essential manipulations.

Analysis of mineral composition and microstructure of shaly and sandy facies

- For microfabric analysis, appropriate methods for optical representation show that BSE images of polished sections provide optimum images for subsequent image analysis aiming at the quantification of parameters of coarse particles like carbonate shell fragments in clay-stones.
- The most important result of this analysis is that not only the carbonate content but also the grain size distribution, shape and distribution of carbonates determine the mechanical behavior of the clay.
- In case of the Opalinus Clay, cracks are mostly connected to coarse shell fragments. In Callovo-Oxfordian clay-stones, carbonates are supposed to play a completely different role. Here carbonate content has a positive correlation for failure strength, because a pronounced dovetail connection with the clayey matrix was found, which seems to play an important role with respect to the relation of failure strength and carbonate content.

Creep behavior

- The common problem that test duration usually is to short to allow for a valid determination of stationary creep rate $\dot{\varepsilon}_\infty$ can be mitigated to some extend by an extrapolation algorithm performing a weighted fit of the observed ε(t)-curve with

$$\varepsilon_0 + \exp(\ln(\dot{\varepsilon}_\infty)) \int_{t_0}^{t} \exp(\exp(a + b\,(t' - t_0)))\,dt'$$

- On average, creep rate in s-geometry is 3 to 4 times higher than in p-geometry, thus showing a distinct anisotropy of Opalinus Clay.
- Creep rates are significantly affected by the hydraulic regime. Generally, avoiding a permanent buildup of pore pressure by application of drained boundary conditions reduces stationary creep rate by 50% compared to undrained tests.
- Concerning the $\dot{\varepsilon}_\infty(\sigma_{dev})$-function, experimental results slightly favor an exponential relationship $\dot{\varepsilon}_\infty = 5.89 \cdot 10^{-7} \exp(0.118\ \sigma_{dev})$ compared to a power law $\dot{\varepsilon}_\infty = 8.61 \cdot 10^{-8}\ \sigma_{dev}^{\ 1.42}$, but the difference is not statistically significant.

Strength and stiffness

- Concerning the detailed investigation of σ_3-dependencies of strength parameters, multistep triaxial strength tests proved to be a suitable tool to overcome the problem of sample variability.
- Shear strength $\sigma_{dev.peak}$ and residual strength $\sigma_{dev.res}$ as well as Young's modulus E, tangent modulus E_v, and residual deformation modulus E_{res} display a moderate decrease at increasing temperature. Strain at shear failure ε_{fail} only slightly decreases at higher temperature.
- Although not investigated systematically, the impact of moisture state on strength and stiffness of Opalinus Clay turned out to be prominent. Drying samples to a water content less than 6.3% by weight results in an increase of $\sigma_{dev.peak}$ and $\sigma_{dev.res}$ of >100%. The moduli E, E_v, and E_{res} even increase by a factor 3 to 5. At the same time failure strain is reduced by ⅓. There is a serious need for an improved description of moisture effects based on data that comprise registration of pore pressure respectively suction.
- The anisotropy of Opalinus Clay is a dominant feature with respect to strength and stiffness. Strength and moduli considerably decrease from p- to s- to z-geometry. On average, the ratio is 1 : ¾ : ⅓ for $\sigma_{dev.peak}$, and 1 : ¾ : ⅗ for $\sigma_{dev.res}$. For the moduli the relative reduction in s- and z-geometry is even stronger. Failure strain decreases from s- to z- to p-geometry with a ratio of 3.6 : 2.2 : 1.
- Whereas moduli are independent from minimum normal stress σ_3, $\sigma_{dev.peak}$ and $\sigma_{dev.res}$ exhibit a characteristic shape of the $\sigma_{dev}(\sigma_3)$-curve composed of two linear branches. Assuming the occurrence of saturated conditions, a buildup of pore pressure and a corresponding reduction of effective confining pressure at higher σ_3, this would be consistent with a Mohr-Coulomb-type linear relationship in effective stress space.
- A synoptic description including the impact of moisture state, temperature, anisotropy and minimum normal stress on strength and stiffness parameters of Opalinus Clay has been developed. For the tested range of σ_3 an approach with two linear branches with respect to σ_3 and linear in all other independent variables appears to be sufficient for any investigated parameter. Due to sample variability, the data basis is insufficient to justify any model of higher complexity. Thus, any parameter Y can be described by $Y = \min(c_1 + a_1\sigma_3, c_2 + a_2\sigma_3)\ (1 + f_T(T - 30°C))\, f_W\, f_A$. The fitting coefficients yielded from the available data are summarized in Tab. 22.

Tab. 22 Coefficients of the synoptic description for the investigated strength and stiffness parameters.

parameter Y	shear strength $\sigma_{dev.peak}$	residual strength [1] $\sigma_{dev.res}$	failure strain ε_{fail}	Young's modulus E	tangent modulus E_v	residual deformation modulus E_{res}
Units	[MPa]	[MPa]	[-]	[GPa]	[GPa]	[GPa]
c_1 intersect of 1st branch [units]	15.7	4.5	0.0037	8.44	5.51	8.90
a_1 slope of 1st branch [units / MPa]	1.374	1.229	0.0288	0	0	0
$\varphi_1 = \arctan\left(\sqrt{2}\ a_1/(3+a_1)\right)$ friction angle of 1st branch [°]	24.0	22.3	–	–	–	–
c_2 intersect of 2nd branch [units]	?	21.0	–	–	–	–
a_2 slope of 2nd branch [units / MPa]	?	0.047	–	–	–	–
$\varphi_2 = \arctan\left(\sqrt{2}\ a_2/(3+a_2)\right)$ appar. frict. angle of 2nd branch [°]	?	1.3	–	–	–	–
f_T $\partial \ln Y/\partial T$ at 30°C [K^{-1}]	-0.0050	-0.0054	-0.0019	-0.0042	-0.0045	-0.0080
$f_{W.d}$ ratio dry vs. moist	2.30	2.17	0.68	3.10	4.11	4.85
$f_{A.s}$ ratio of anisotropy s vs. p	0.76	0.76	3.6	0.39	0.28	0.22
$f_{A.z}$ ratio of anisotropy z vs. p	0.35	0.61	2.2	0.32	0.18	0.11
n	62	104	65	53	58	86
R^2 coefficient of determination	0.8373	0.9446	0.6572	0.6966	0.5980	0.6307
R^2_{expl} ditto for explainable variance				0.9720	0.9047	0.9790
RMSE [units]	2.6	1.8	0.0035	1.66	1.41	1.97
range of validity [MPa]	$0 \le \sigma_3 \le 7.5$	$0 \le \sigma_3 \le 30$	$0 \le \sigma_3 \le 10$	$0 \le \sigma_3 \le 30$	$0 \le \sigma_3 \le 30$	$0 \le \sigma_3 \le 30$

[1] Coefficients derived from stationary measurements only.

Dilatancy

- Dilatancy strength increases with mean stresses and exhibits a distinct anisotropy. Whereas p-samples show higher shear strength than s-samples, it is the opposite way around for dilatancy strength. Hence, the ratio of dilatancy strength versus shear strength is 0.67±0.04 for p-geometry and 0.85±0.05 for s-geometry

9 REFERENCES

BIOT, M. (1941): General theory of three-dimensional consolidation. – J. Appl. Phys. 12,155-164.

BOCK, H. (2001): RA Experiment, Rock Mechanics Analyses and Synthesis: Data Report on Rock Mechanics. – Technical Report TR 2000-02, Federal Office of Water and Geology, Berne, 52 p.

BOSSART, P. AND THURY, M. (eds.) (2008): Mont Terri Rock Laboratory. Project, Programme 1996 to 2007 and Results. Reports of the Swiss Geological Servey No.3. Swiss Geological Survey, Wabern, Switzerland.

CZAIKOVSKI, O., WOLTERS, R., DÜSTERLOH, U. AND LUX, K.-H. (2006): Abschlussbericht zum BMWi-Forschungsvorhaben Laborative und numerische Grundlagenuntersuchungen zur Übertragbarkeit von Stoffmodellansätzen und EDV-Software für Endlager im Salzgestein auf Endlager im Tongestein. – Lehrstuhl für Deponietechnik und Geomechanik, Technische Universität Clausthal, Germany, 270 p.

FREDLUND, D.G. AND MORGENSTERN, N.R. (1977): Stress state variables for unsaturated soils. – ASCE J. Geotech. Eng. Div. GT5, 103,447-466.

GRÄSLE, W. AND PLISCHKE, I. (2007): LT Experiment: Strength and Deformation of Opalinus Clay. – Technical Report TR 2007-05, 28 p, Federal Institute for Geosciences and Natural Resources (BGR), Hannover.

GRÄSLE, W. AND PLISCHKE, I. (2009): Laboratory Testing of Opalinus Clay (LT) Experiment: Strength and Deformation of Opalinus Clay: Data report from Phase 13. – Technical Note TN 2008-81, 47 p, Federal Institute for Geosciences and Natural Resources (BGR), Hannover.

KLINKENBERG, M., DOHRMANN, R., KAUFHOLD, S. AND SIEGESMUND, S. (2008a): Mont Terri Project – Comparison of Opalinus Clay and Callovo-Oxfordian clay-stone with respect to mechanical strength and carbonate microfabric. – LT-Experiment, Technical Report TR 2008-03, 59 p, Federal Institute for Geosciences and Natural Resources (BGR), Hannover.

KLINKENBERG, M., DOHRMANN, R. AND KAUFHOLD, S. (2008b): Quantitativer Mineralbestand und Microgefüge der sandigen Fazies des Opalinustons (Mont Terri, Schweiz) – Bundesanstalt für Geowissenschaften und Rohstoffe (BGR), Hannover (preliminary unreleased Report).

NAGRA (2002): Projekt Opalinuston – Synthese der geowissenmschaftlichen Untersuchungsergebnisse. – Technischer Bericht 02-03, 659 p.

NAUMANN, M. AND PLISCHKE, I. (2006): Laboratory Temperature Testing (LT) Experiment: Phases 9 and 10 – True Triaxial Experiments on Cubic Specimens. – Technical Note TN 2005-71, 70 p, Federal Institute for Geosciences and Natural Resources (BGR), Hannover.

PEARSON, F.J., ARCOS, D., BATH, A., BOISSON, J.-Y., FERNANDEZ, A., GAEBLER, H.-E., GAUCHER, E., GAUTSCHI, A., GRIFFAULT, L., HERNAN, P. AND WABER, H.N. (2003): Geochemistry of Water in the Opalinus Clay Formation at the Mont Terri Rock Laboratory - Synthesis Report. – Geological Report No. 5. Swiss National Hydrological and Geological Survey, Ittigen-Berne, 319 p.

RUMMEL, F., HETTKAMP, T. AND WEBER, U. (1998): DM experiment: Laboratory Experiments for the Determination of Deformation Mechanisms and a Constitutive Law for Time Dependent Deformation Behaviour of the Opalinus Clay (Phase 3), Technical Note TN 98-55, 17 p.

SCHNIER, H. (2005): LT Experiment: Strength tests on cylindrical specimens, documentation and evaluation, (Phases 6 & 7). – Technical Note TN 2002-50, 27 p, 3 appendices, Federal Institute for Geosciences and Natural Resources (BGR), Hannover.

SCHNIER, H. AND STÜHRENBERG, D. (2007): LT Experiment: Strength tests on cylindrical specimens, documentation and evaluation, (Phases 8 & 9). – Technical Note TR 2003-04, 124 p, 3 appendices, Federal Institute for Geosciences and Natural Resources (BGR), Hannover.

SKEMPTON, A.W. (1960). Effective stress in soils, concrete and rocks. – Proc. Conf. Pore Pressure and Suction in Soils, 4–16, Butterworth, London.

TERZAGHI, K. (1936): The shearing resistance of saturated soils and the angle between the planes of shear. – In: CASAGRANDE, A., RUTLEDGE, P.C. AND WATSON, J.D. (Eds.): Proc. 1st Int. Conf. Soil Mech. Found. Eng. Vol.1,54-56.

THURY, M. AND BOSSART, P. (1999): Results of hydrogeological, chemical and geotechnical experiments performed in 1996-1997. – Mont Terri Project. Rapport géologique n°23, Bern, 191 p.

10 LIST OF TABLES

11 LIST OF FIGURES

APPENDIX A: SAMPLE AND DATA DOCUMENTATION

Tab. 1 Basic information about drillings and samples used for laboratory tests.

Drilling	drilling company	date of drilling	sample type	type of tests	storage conditions
BLT 1	COREIS	phase 6	p-sample	true triaxial	Al-tube, pa ev
BLT 2	COREIS	phase 6	p-sample	true triaxial	Al-tube, pa ev
BLT 3	COREIS	phase 6	s-sample	strength	Al-tube, pa ev
BLT 4	COREIS	phase 6	z-sample	strength	Al-tube, pa ev
BLT 5	COREIS	phase 7	s-sample	strength	Al-tube, pa ev
BLT 6	COREIS	phase 7	z-sample	strength	Al-tube, pa ev
BLT 9	COREIS	phase 8	p-sample ‖ strike	strength	Al-tube, pa ev / ANDRA cell
BLT 10	BGR	phase 8	p-sample ‖ strike	strength / true triaxial	Al-tube, pa ev / ANDRA cell / air press. 2.5 bar / BGR liner version B
BLT 12	BGR	phase 8	s-sample	strength / true triaxial	Al-tube, pa ev / ANDRA cell / air press. 2.5 bar / BGR liner version B
BLT 13	BGR	phase 11	p-sample	true triaxial	BGR liner version B
BLT 14	BGR	phase 11	p-sample	creep	BGR liner version C
BLT 15	BGR	phase 11	s-sample	creep / multistep strength	BGR liner version C
BLT 16	BGR	phase 11	p-sample	creep	BGR liner version C
BLT 17	BGR	phase 12	z-sample 60°	creep	BGR liner version C
BLT 18	BGR	phase 12	z-sample 30°	creep	BGR liner version C
BLT 19	BGR	phase 13	s-sample	strength	BGR liner version C
BED-C 6	COREIS	phase 5	s-sample	true triaxial	Al-tube, pa ev
BED-C 9	COREIS	phase 5	s-sample	strength	Al-tube, pa ev
BED-C 10	COREIS	phase 5	z-sample	strength	Al-tube, pa ev

Al-tube, pa ev = aluminium coated tube, partly evacuated

Tab. 2 Properties of the tested samples of Opalinus Clay.

core specification	unique specimen identifier	depth [m]	dimension		orien-tation	type of test	bulk density ρ [g/cm³]	water content [%]	ultrasonic velocities [m/s]					dynamic parameters			
									P-wave			S-wave		E_{dyn} [MPa]		ν_{dyn}	
			length [mm]	diameter [mm]					axial	radial ∥SS	radial ⊥SS	radial ∥SS	radial ⊥SS	radial ∥SS	radial ⊥SS	radial ∥SS	radial ⊥SS
BLT 1/02/01/02	01017.120	0.51 - 0.61	100.0	99.9	P	braz	2.43	7.01	3100	3150							
BLT 1/05/01/02	01017.112	2.49 - 2.59	100.0	99.9	P	braz	2.45	6.64	3000								
BLT 2/05/01/01	02003.006	2.59 - 2.69	100.0	99.9	P	braz	2.45	6.60	3350	3400		1950		23300		0.25	
BLT 1/08/01/02	01017.117	3.90 - 4.00	100.00	99.93	P	braz	2.45	6.04	3500	3450	2600						
BLT 2/13/01/01	02003.005	6.05 - 6.15	100.20	99.95	P	braz	2.44	6.06	3400	3400							
BLT 3/03/01/01	02009.040	1.18 - 1.28	101.0	100.9	S	braz	2.41	6.90									
BLT 3/17/01/01	02009.042	4.51 - 4.61	99.8	100.7	S	braz	2.42	7.11									
BLT 4/07/02	02009.047	2.75 - 2.85	99.2	100.8	Z	braz	2.43	6.89									
BHE-B 1/01/10/01	02073	6.26 - 6.46	200.02	99.44	P	uni	2.442										
BLT 1/04/01/01	01017.113	2.10 - 2.35	250.0	98.9	P	uni	2.44	7.00		3150							
BLT 13/08/01	05001		199.98	99.64	P	tri	2.451		3365								
BLT 1/05/01/01	01017.111	2.60 - 2.85	250.0	99.9	P	tri	2.45	6.51		3350		1800		20600		0.30	
BLT 1/08/01/03	01017.118	3.64 - 3.89	250.0	99.9	P	tri	2.45	6.49	3350	3450	2500	1900		22700		0.28	
BLT 2/08/01/01	01017.124	4.17 - 4.32	250.0	99.95	P	tri	2.45	6.50	3300	3450	2700	1750		19900		0.33	
BLT 2/16/01/01	01017.126	6.81 - 7.06	250.0	99.95	P	tri	2.43	6.72	3100	3350	2450						
BLT 2/24/01/01	02007.025	9.80 - 10.05	250.0	98.9	P	tri	2.42	7.19	3200	3250	2300						
BLT 2/35/01/01	02009.039	13.60 - 13.85	248.8	102.4	P	tri	2.34	6.99									
BLT 9/03/01/01	03005.040	2.00 - 2.25	246.8	92.7	P	tri	2.42	7.55		3150							
BLT 9/07/01/01	03005.038	3.18 - 3.43	248.9	92.5	P	tri	2.41	7.57	3000	3150	2000						
BLT 9/10/01/01	03005.039	4.07 - 4.32	247.7	92.6	P	tri	2.42	7.88	2850	2100	2500						
BLT 10/02/01/01	03006.045	2.62 - 2.87	248.65	101.30	P	tri	2.45	6.48	3400	2700	3450		1800		20850		0.31
BLT 10/12/01/01	03006.043	10.77 - 11.02	249.55	101.60	P	tri	2.44	7.00									

unique specimen identifier: any specimen is identified by a combination of laboratory no. + specimen no. (xxxxx.xxx) in old BGR laboratory code, respectively by a file no. (xxxxx) in new BGR laboratory code, or by a test-ID (xx_xx) in case of true triaxial tests.

type of test: braz = Brazilian test, uni = uniaxial strength test, tri = triaxial strength test, mult = multistep triaxial strength test, cr_u = undrained creep test, cr_d = drained creep test, tr_tri = true triaxial test

ultrasonic velocities and dynamic parameters: axial = along sample axis, radial ∥SS = radial parallel to bedding, radial ⊥.SS = radial normal to bedding
Due to strong absorption there are no axial S-wave velocities available and therefore no axial dynamic parameters.

Tab. 2 (continued)

core specification	unique specimen identifier	depth [m]	dimension		orien-tation	type of test	bulk density ρ [g/cm³]	water content [%]	ultrasonic velocities [m/s]						dynamic parameters			
			length [mm]	diameter [mm]					P-wave			S-wave			E_{dyn} [MPa]		ν_{dyn}	
									axial	radial ∥SS	radial ⊥SS	radial ∥SS	radial ⊥SS		radial ∥SS	radial ⊥SS	radial ∥SS	radial ⊥SS
BLT 10/13/01/01	03006.044	11.15 – 11.40	250.15	101.67	P	tri	2.43	6.94	3150	3100	1600							
BHE-B 1/01/15/01	02075	7.82 – 8.02	200.01	99.57	P	mult	2.392		2909									
BLT 16/09/01	09001		201.60	100.26	P	mult	2.471		3363									
BLT 1/02/01/01	01017.119	0.26 – 0.51	250.22	100	P	uni	2.43	7.26		3100								
BLT 2/01/01/01	02003.007	0.34 – 0.59	250.0	99.55	P	tri	2.43	6.91		3350								
BLT 2/05/01/01	02003.008	2.34 – 2.59	250.0	98.9	P	tri	2.44	6.88		3150								
BLT 2/10/01/01	01017.122	4.95 – 5.20	250.2	99.95	P	tri	2.45	6.55	3400	3450	2650	1800			20850		0.31	
BLT 2/11/01/01	01017.121	5.21 – 5.46	250.0	99.95	P	tri	2.45	6.58	3350	3450	2600							
BLT 2/14/01/01	01017.125	6.15 – 6.40	250.0	99.95	P	tri	2.44	6.70	3300	3300	2550							
BLT 2/25/01/01	02007.026	10.15 – 10.40	250.00	99.93	P	tri	2.43	7.28	3150	3200	2100							
BLT 9/08/01/01	03005.041	3.63 – 3.88	249.6	92.6	P	tri	2.40	8.06	2950	3100	2150							
BLT 9/13/01/01	03005.042	4.95 – 5.20	249.2	92.5	P	tri	2.41		3000	3150	2400							
BLT 10/03/01/01	03006.046	2.98 – 3.23	249.23	101.30	P	tri	2.45	6.39	3450	3500	2700	1850			21900		0.31	
BLT 10/04/01/01	03006.047	3.30 – 3.55	250.8	100.7	P	tri	2.50	6.52	3400	2650	3400							
BLT 10/06/01/01	03006.048	3.94 – 4.19	249.71	101.62	P	tri	2.45		2450	3100	2450	1600			16550		0.32	
BLT 15/25/01	07029		167.57	101.58	S	uni	2.457											
BLT 19/06/01	08064		181.82	101.68	S	uni												
BLT 12/06/01	04179	4.55 – 4.75	198.88	100.82	S	tri	2.442											
BLT 3/23/01/01	02016.100	5.80 – 6.03	225.75	100.80	S	tri	2.40	7.85										
BLT 5/03/01/01	02016.096	2.88 – 3.10	215.6	100.3	S	tri	2.43	7.01										
BLT 5/05/01/01	02016.098	3.52 – 3.77	243.5	100.6	S	tri	2.39	6.83										
BLT 5/15/01/01	02016.089	6.54 – 6.79	248.30	100.17	S	tri	2.45	6.92										
BLT 5/19/01/01	02016.091	7.53 – 7.73	196.3	100.4	S	tri	2.44	6.57										
BLT 5/22/01/01	02016.103	9.00 – 9.20	199.9	101.5	S	tri	2.38	6.50										
BLT 5/27/01/01	02016.101	10.28 – 10.51	231.0	100.3	S	tri	2.46	6.85										
BLT 12/03/01/01	03006.054	3.13 – 3.38	250.7	100.9	S	tri	2.44	7.00		3300	3300	1700	1750		18600	19500	0.32	0.30
BLT 12/10/01/01	03006.049	9.77 – 10.02	249.2	100.9	S	tri	2.47	6.63										
BLT 15/07/01	08021	6.00 – 6.19	190.2	101.7	S	mult	2.454											
BED-C 9/01/02/01	00011.080	1.00 – 1.16	157.50	68.95	S	tri	2.41			3400								
BED-C 9/01/02/02	00011.081	1.17 – 1.33	153.90	68.94	S	tri	2.42			3450								

Tab. 2 (continued)

core specification	unique specimen identifier	depth [m]	dimension		orien-tation	type of test	bulk density ρ [g/cm³]	water content [%]	ultrasonic velocities [m/s]				dynamic parameters			
			length [mm]	diameter [mm]					P-wave		S-wave		E_{dyn} [MPa]		ν_{dyn}	
									axial	radial ∥SS	radial ⊥SS	radial ∥SS	radial ⊥SS	radial ⊥SS	radial ∥SS	radial ⊥SS
BED-C 9/01/02/03	00011.082	1.52 – 1.70	175	68.92	S	tri	2.42			3500		2050		25200		0.24	
BED-C 9/01/02/04	00011.083	1.70 – 1.88	174.75	68.98	S	tri	2.41			3350		2000		23550		0.22	
BLT 12/11/01/01	03006.050	2.45 – 2.69	238.79	100.68	S	tri	2.46	5.71		3400	3400	2050	2050	25100	25100	0.21	0.21
BLT 12/13/01/01	03006.051	3.72 – 3.94	211.74	100.54	S	tri	2.47	6.20		3500	3400	2000	2000	24850	24400	0.26	0.24
BLT 5/02/01/01	02016.106	2.56 – 2.77	201.39	100.60	S	tri	2.41										
BLT 5/10/01/01	02016.097	4.40 – 4.65	247.5	100.3	S	tri	2.44										
BLT 5/13/01/01	02016.102	5.85 – 6.10	251.2	100.5	S	tri	2.41	6.53									
BLT 5/16/01/01	02016.090	6.85 – 7.05	199.05	100.20	S	tri	2.45	6.57									
BLT 5/20/01/01	02016.104	8.00 – 8.25	248.57	100.40	S	tri	2.46	6.38									
BLT 12/07/01/01	03006.056	7.48 – 7.72	238.55	100.82	S	tri	2.46	6.69		3300	3300	1750	1750	19650	19650	0.30	0.30
BLT 12/08/01/01	03006.055	7.76 – 8.01	249.70	100.86	S	tri	2.44	6.86		3400	3400	1750	1800	19700	20650	0.32	0.31
BLT 12/14/01/01	03006.052	5.55 – 5.78	227.28	100.61	S	tri	2.46	5.87		3600	3600	1950	1950	24200	24200	0.29	0.29
BLT 12/15/01/01	03006.053	7.20 – 7.45	248.75	100.52	S	tri	2.47	5.87		3400	3400	1950	1950	23550	23550	0.25	0.25
BLT 4/09/01	02009.045	3.29 – 3.53	239.2	100.9	Z	tri	2.44	7.13									
BLT 4/12/01	02009.044	3.95 – 4.16	210.6	101	Z	tri	2.41	7.56									
BLT 6/03/01/01	02016.092	2.00 – 2.20	201.8	100.4	Z	tri	2.44	6.80									
BLT 6/18/01/01	02016.094	8.62 – 8.82	199.68	101.20	Z	tri	2.36	6.86									
BED-C 10/01/03/01	00011.084	2.17 – 2.35	175.25	69.98	Z	tri	2.41			3250							
BED-C 10/01/02/01	00011.085	1.21 – 1.38	175.50	70.11	Z	tri	2.40			3300		2600		22150			
BED-C 10/01/02/02	00011.086	1.39 – 1.56	175.4	70	Z	tri	2.40			3250							
BED-C 10/01/02/03	00011.087	1.67 – 1.85	175.00	70.13	Z	tri	2.40			3400							
BED-C 10/01/02/04	00011.088	1.85 – 2.07	175.30	70.02	Z	tri	2.41			3350		2050		24350		0.20	
BLT 4/02/01	02009.043	0.57 – 0.79	221.6	100.7	Z	tri	2.44	6.56									
BLT 4/04/01	02009.049	1.59 – 1.84	249.5	100.7	Z	tri	2.43										
BLT 4/06/01	02009.048	2.20 – 2.45	251.2	100.8	Z	tri	2.43	7.07									
BLT 6/24/01/01	02016.105	10.02 – 10.22	192.48	100.40	Z	tri	2.44	6.92									
BLT 6/25/01/01	02016.093	10.60 – 10.80	199.33	101.30	Z	tri	2.36	6.54									
BLT 10/07/01	03060	4.45 - 4.65	200.05	101.5	P	cr_u	2.445		3225								
BLT 2/29/01	03035I	11.67 - 11.87	199.67	98.40	P	cr_u	2.522	6.99	3505								
BLT 10/17/01	03061	10.04 - 10.24	199.98	100.95	P	cr_u	2.429		3417								

Tab. 2 (continued)

core specification	unique specimen identifier	depth [m]	dimension		orien-tation	type of test	bulk density ρ [g/cm³]	water content [%]	ultrasonic velocities [m/s]						dynamic parameters			
			length [mm]	diameter [mm]					P-wave			S-wave			E_{dyn} [MPa]			ν_{dyn}
									axial	radial ∥SS	radial ⊥SS	radial ∥SS	radial ⊥SS		radial ∥SS	radial ⊥SS	radial ∥SS	radial ⊥SS
BLT 1/06/02	02009	2.88 - 3.13	250.06	99.85	P	cr_u	2.452											
BLT 11/03/01	03062	2.06 - 2.26	199.77	101.50	S	cr_u	2.396											
BLT 14/06/01	08018	4.38 - 4.59	210.02	99.54	P	cr_u	2.469		3459									
	08018A		209.86	99.49	P	cr_d	2.472											
BLT 14/09/01	08019	7.68 - 7.89	209.83	101.54	P	cr_u	2.483		4197									
	08019A		209.63	101.39	P	cr_d	2.489											
BLT 15/03/01	08020	1.92 - 2.13	209.56	100.95	S	cr_u	2.441											
	08020A		208.01	101.08	S	cr_d	2.450											
BLT 15/08/02	08022	7.38 - 7.59	209.64	98.22	S	cr_u	2.479											
	08022A		208.28	98.96	S	cr_d	2.455											
BLT 14/05/01	07001	3.00 - 3.22	220.00	99.91	P	cr_d	2.448		3320									
BLT 14/11/01	07002	9.74 - 9.96	220.03	99.90	P	cr_d	2.439		3325									
BLT 15/04/01	07004		218.19	99.80	S	cr_d	2.444											
BLT 15/08/01	07005		220.71	99.88	S	cr_d	2.447		2698									
BED C6/10c	03_00	3.96 - 4.02	cube 53 mm			tr_tri	2.40											
BED C6/10a	04_00	3.84 - 3.90	cube 53 mm			tr_tri	2.39											
BED C6/9a	05_00	3.66 - 3.72	cube 53 mm			tr_tri	2.38											
BED C6/9c	06_00	3.78 - 3.84	cube 53 mm			tr_tri	2.38											
BED C6/9b	07_00	3.72 - 3.78	cube 53 mm			tr_tri	2.38											
BLT 2/7/01	05_03	3.84 - 3.94	cube 53 mm			tr_tri	2.46											
BLT 2/7/03	06_03	4.05 - 4.15	cube 53 mm			tr_tri	2.46											
BLT 2/15/02	07_03	6.60 - 6.71	cube 53 mm			tr_tri	2.45											
BLT10/07/02	14_03	4.28 - 4.68	cube 53 mm			tr_tri	2.44											
BLT10/17/03	01_05	1.27 - 2.26	cube 53 mm			tr_tri	2.42	4.17										
BLT10/17/04	02_05	1.27 - 2.26	cube 53 mm			tr_tri	2.41	4.01										
BLT10/17/05	03_05	1.76 - 1.86	cube 53 mm			tr_tri	2.42	4.30										
BLT10/19/01	04_05	12.53 - 12.76	cube 53 mm			tr_tri	2.41	4.44										
BLT12/16/02	05_05	8.76 - 8.94	cube 53 mm			tr_tri	2.43	5.80										
BLT13/17/04	06_05	4.40 - 5.00	cube 53 mm			tr_tri	2.41	5.60										

Tab. 3 Results from triaxial creep tests. Any sample is identified by its unique file number (note that file numbers differing only by a letter denote the same sample used in different tests).

file no.	sample orientation	hydraulic mode	temperature [°C]	start of phase [d]	end of phase [d]	duration of phase [d]	confining pressure [MPa]	deviatoric stress [MPa]	deformation during load phase [%]	deformation at the end of phase [%]	stationary creep rate [10^{-6}/d]	type of calculation
02009	p	ud	50	3.9	459.0	455.0	0.5 – 10	10	0.179	0.557	1.98	tang
				459.0	580.0	121.0	1 – 3	12	0.028	0.602	2.38	tang
03035I	p	ud	40	12.0	376.0	364.0	12	10	0.131	0.464	0.865	tang
				376.0	594.9	218.9		15	0.089	0.564	1.25	tang
			50	595.0	838.2	243.2		15	0.039	0.606	1.14	tang
03060	p	ud	30	5.0	204.0	198.9	12	13	0.105	0.740	0.860	tang
				204.0	358.8	154.8		15	0.041	0.815	1.03	tang
				358.8	419.0	60.2		17	0.040	0.889	2.07	tang
				419.0	557.9	138.9		19	0.095	1.018	2.40	tang
				557.9	740.9	182.9		20	0.069	1.103	2.59	tang
03061	p	ud	50	27.2	167.0	139.9	12	5	0.035	0.401	0.880	tang
				167.0	213.0	46.0		7	0.012	0.432	0.842	tang
				213.0	321.9	108.9		9	0.025	0.476	0.814	tang
				321.9	382.1	60.2		11	0.016	0.511	0.976	tang
				396.1	544.0	147.9		15	0.047	0.601	1.15	tang
				544.0	703.9	159.9		17	0.034	0.653	1.50	tang
				704.0	803.1	99.1		20	0.033	0.716	1.66	tang
03062	s	ud	30	2.0	198.0	195.9	12	13	0.321	2.096	2.25	tang
				198.0	272.7	74.7		15	0.051	2.185	2.47	tang
07001	p	dr	30	20.0	54.8	34.8	10	5	0.000	-0.002	b.d.l.	
				54.9	104.8	50.0		8	-0.002	-0.005	b.d.l.	
				104.8	183.9	79.1		10	-0.001	-0.005	b.d.l.	
				184.0	252.9	68.9		13	0.002	-0.003	0.377	tang
07002	p	dr	30	20.0	54.8	34.8	10	5	-0.001	0.006	b.d.l.	
				54.9	104.8	50.0		8	0.000	0.006	b.d.l.	
				104.8	184.0	79.1		10	-0.001	0.005	b.d.l.	
				184.0	252.9	68.9		13	0.000	0.005	b.d.l.	
07004	s	dr	30	17.9	56.0	38.1	10	5	-0.003	-0.001	b.d.l.	
				56.0	108.1	52.1		10	0.001	0.000	0.140	tang
				108.1	177.0	68.9		13	0.004	0.004	0.437	tang
07005	s	dr	30	17.9	56.0	38.1	10	5	0.000	0.001	b.d.l.	
				56.0	108.1	52.1		10	0.002	0.003	0.206	tang
				108.1	177.0	68.9		13	0.001	0.004	0.148	tang
08018	p	ud	30	20.9	70.8	49.9	10	5	0.040	0.380	0.693	extr
				70.8	144.8	74.0		8	0.043	0.474	1.15	extr
08018A		dr	30	6.9	188.8	181.9	10	8	0.065	0.513	0.497	extr
				310.9	484.1	173.3		13	0.080	0.680	1.10	extr
08019	p	ud	30	20.9	70.8	49.9	10	5	0.033	0.318	0.685	extr
				70.8	138.9	68.1		8	0.038	0.396	1.35	extr
				138.9	250.7	111.9		13	0.085	0.552	2.66	extr
08019A		dr	30	1.6	82.8	81.2	10	1	0.085	0.552	< 0.10	extr
				82.8	204.9	122.1		8	0.045	0.435	0.610	extr
				281.9	378.7	96.9		13	0.069	0.578	1.61	extr
08020	s	ud	30	20.8	70.9	50.1	10	5	0.079	0.527	2.20	extr
				70.9	147.0	76.0		8	0.111	0.704	4.55	extr
				147.0	240.9	94.0		11	0.172	0.955	6.07	extr
08020A		dr	30	0.9	202.9	202.0	10	1	0.099	0.454	2.01	extr
				202.9	376.7	173.8		8	0.131	0.705	2.65	extr
08022	s	ud	30	19.9	69.8	50.0	10	5	0.141	0.815	5.06	extr
				69.8	137.9	68.0		8	0.286	1.207	7.05	extr
08022A		dr	30	26.8	323.8	297.0	10	1	0.115	0.488	0.552	extr
				323.9	476.7	152.8		8	0.233	1.074	2.94	extr

du = undrained
dr = drained
b.d.l. = below detection limit

tang = creep rate calculated as tangent slope at the end of the load phase
extr = creep rate calculated by extrapolation algorithm

Tab. 5 Detailed results from sample 02009 (p-geometry) tested at different values of confining pressure. The test was carried out in undrained mode at T=50°C.

start of phase [d]	end of phase [d]	duration of phase [d]	confining pressure [MPa]	deviatoric stress [MPa]	stationary creep rate [10^{-6}/d]
3.9	31.9	28	10	10	1.13
31.9	45.0	13	5		n.d.
45.0	52.9	8	2.5		n.d.
52.9	115.0	62	1.5		1.62
115.1	186.0	71	2.5		1.65
186.0	215.1	29	5		1.49
215.1	243.0	28	2.5		1.45
243.1	263.0	20	1		1.89
263.0	271.1	8	0.5		2.88
271.1	279.1	8	1		2.95
279.1	290.0	11	2		n.d.
290.0	299.9	10	2.5		1.41
300.0	339.1	39	3		1.38
339.1	388.1	49	2.5		2.61
388.2	419.9	32	2		n.d.
419.9	443.9	24	1.5		2.35
444.0	459.0	15	1		2.29
459.0	480.8	22	3	12	1.93
480.9	493.9	13	2.5		1.44
493.9	525.0	31	2		2.03
525.0	559.0	34	1.5		2.06
559.0	580.0	21	1		2.39

n.d. = not determined since data are too noisy or disturbed

Tab. 7 Results from indirect tensile strength tests (for sample orientation and direction of loading see Fig. 15).

sample specification	laboratory and specimen no.	sample orientation	direction of loading	tensile strength [MPa]
BLT-1/05/01/02	01017.112	P	∥SS	-0.66
BLT-1/02/01/02	01017.120	P	∥SS	-0.69
BLT-1/08/01/02	01017.117	P	⊥SS	-1.41
BLT-2/13/01/01	02003.005	P	⊥SS	-1.25
BLT-2/05/01/01	02003.006	P	⊥SS	-1.02
BLT-3/03/01/01	02009.040	S	⊥SS	-1.29
BLT-3/17/01/01	02009.042	S	⊥SS	-1.41
BLT-4/07/02	02009.047	Z	∥SS	-1.11

Tab. 8 Results from uniaxial and triaxial strength tests as well as from multistep triaxial strength tests.

core specification	laboratory + specimen no. resp. file no.	sample orien-tation	moisture state	type of test	T [°C]	strain rate $d\varepsilon/dt$ [10^{-6}/s]	conf. pressure σ_3 [MPa]	shear strength $\sigma_{dev,peak}$ [MPa]	strain at failure ε_{fail} [%]	residual strength $\sigma_{dev,res}$ [MPa]	Young's modulus E [MPa]	tangent modulus E_v [MPa]	residual deform. modulus E_{res} [MPa]
BHE-B 1/01/10/01	02073	P	moist	uni	30	50	0	12.4	0.35				
BLT 1/04/01/01	01017.113	P	moist	uni	24	10	0	8.1	0.35		5150	2750	
BLT 13/08/01	05001	P	moist	tri	30	1	3	20.1	0.55	10.2			
BLT 1/05/01/01	01017.111	P	moist	tri	33	10	10	22.8	0.51	9.1	8250	6550	5100
					33	10	7.5			8.5			
					33	10	5			6.5			
					33	10	2.5			4.5			
					33	10	1			2.8			
BLT 1/08/01/03	01017.118	P	moist	tri	32	10	3	21.9	0.37	7.2	8800	6350	5000
					32	10	2.5			6.5			
					32	10	1			4.1			
BLT 2/08/01/01	01017.124	P	moist	tri	31	10	1	16.5	0.29	4.2	7750	5350	4250
BLT 2/16/01/01	01017.126	P	moist	tri	35	10	6	20.7	0.43	8.7	6850	6000	4800
					35	10	5			7.6			
					35	10	2.5			4.9			
					35	10	1			3.1			
BLT 2/24/01/01	02007.025	P	moist	tri	32	10	6	17.2	0.42	6.2	7000	4150	4900
					32	10	5			5.8			
					32	10	2.5			4.3			
					32	10	1			2.7			
BLT 2/35/01/01	02009.039	P	moist	tri	35	10	6	11.9	0.53	5.6	7000	3950	4100
					35	10	5			5.1			
					35	10	2.5			3.4			
					35	10	1			2.0			

Moisture status: moist = water content >6.3% by weight, dry = water content <6.3%
Type of test: uni = uniaxial strength test, tri = triaxial strength test, mult = multistep triaxial strength test
Temperature: rT = room temperature (20 – 35°C)
Young's modulus = elastic modulus determined in an unloading-loading-loop (overconsolidated state)
Tangent modulus = modulus determined during the initial loading at $\sigma_{dev} = 0.5 \cdot \sigma_{dev,peak}$
Residual deformation modulus = elastic modulus determined in a post failure unloading-loading-loop

Tab. 8 (continued)

core specification	laboratory + specimen no. resp. file no.	sample orien-tation	moisture state	type of test	T [°C]	strain rate dε/dt [10^{-6}/s]	conf. pressure σ_3 [MPa]	shear strength $\sigma_{dev,peak}$ [MPa]	strain at failure ε_{fail} [%]	residual strength $\sigma_{dev,res}$ [MPa]	Young's modulus E [MPa]	tangent modulus E_v [MPa]	residual deform. modulus E_{res} [MPa]
BLT 9/03/01/01	03005.040	P	moist	tri	23	10	4.5	25.2	0.58		8850	4200	
BLT 9/07/01/01	03005.038	P	moist	tri	25	10	4.5	18.2	0.61	8.7	6340	3700	3000
BLT 9/10/01/01	03005.039	P	moist	tri	25	10	7.5	22.3	0.81	10.8	6460	3700	2500
BLT 10/02/01/01	03006.045	P	moist	tri	32	10	6	21.2	0.52	9.2		5000	3050
					32	10	5			8.1			
					32	10	2.5			5.0			
					32	10	1			2.9			
BLT 10/12/01/01	03006.043	P	moist	tri	31	10	1	12.1	0.29	4.1		4050	4200
BLT 10/13/01/01	03006.044	P	moist	tri	28	10	3	15.5	0.53	7.3	4900	3650	3100
					28	10	2.5			7.1			
					28	10	1			4.1			
BHE-B 1/01/15/01	02075	P	moist	mult	25	0.1	1	17.0	0.46		8610		
					25	0.1	2	18.4	0.65				
					25	0.1	3	20.1	0.78				
					25	0.1	4	21.3	0.88				
					25	0.1	1			3.9			
					25	0.1	2			5.7			
					25	0.1	3			7.3			
					25	0.1	4			9.0			
					25	0.1	6			12.7			
					25	0.1	8			15.4			
					25	0.1	10			16.9			
					25	0.1	12			18.3			
					25	0.1	15			19.8			
					25	0.1	18			21.4			
					25	0.1	21			23.1			

Tab. 8 (continued)

core specification	laboratory + specimen no. resp. file no.	sample orien-tation	moisture state	type of test	T [°C]	strain rate dε/dt [10^{-6}/s]	conf. pressure σ_3 [MPa]	shear strength $\sigma_{dev,peak}$ [MPa]	strain at failure ε_{fail} [%]	residual strength $\sigma_{dev,res}$ [MPa]	Young's modulus E [MPa]	tangent modulus E_v [MPa]	residual deform. modulus E_{res} [MPa]
					25	0.1	1	12.5	0.56		9630		
					25	0.1	5	16.5	0.64				
					25	0.1	15	21.0	0.75				
					25	0.1	30	21.3	0.78				
					25	0.1	1			4.3			
					25	0.1	1			4.3			
					25	0.1	2			6.1			
					25	0.1	3			7.8			
					25	0.1	4			9.0			
					25	0.1	6			12.4			
					25	0.1	8			13.8			
					25	0.1	10			15.7			
					25	0.1	12			15.3			
					25	0.1	15			17.1			
BLT 16/09/01	09001	P	moist	mult	25	0.1	20			17.3			
					25	0.1	25			18.0			
					25	0.1	35			18.0			
					25	0.1	28						10000
					25	0.1	30						10060
					25	0.1	33						9810
					25	0.1	6						9090
					25	0.1	8						9100
					25	0.1	1						7830
					25	0.1	12						8680
					25	0.1	1						7510
					25	0.1	3						8330
					25	0.1	4						8330
					25	0.1	5						8350
					25	0.1	20						8350

Tab. 8 (continued)

core specification	laboratory + specimen no. resp. file no.	sample orien-tation	moisture state	type of test	T [°C]	strain rate dε/dt [10^{-6}/s]	conf. pressure σ_3 [MPa]	shear strength $\sigma_{dev,peak}$ [MPa]	strain at failure ε_{fail} [%]	residual strength $\sigma_{dev,res}$ [MPa]	Young's modulus E [MPa]	tangent modulus E_v [MPa]	residual deform. modulus E_{res} [MPa]
					25	0.1	30						8510
					25	0.1	35						8390
					25	0.1	15						8050
					25	0.1	15						7730
					25	0.1	7						7460
					25	0.1	13						7610
					60	0.1	15						7900
BLT 1/02/01/01	01017.119	P	moist	uni	25	10	0	6.1	0.38			1650	
BLT 2/01/01/01	02003.007	P	moist	tri	60	10	6	13.1	0.46	4.7	5100	3000	3600
					60	10	5			4.5			
					60	10	2.5			3.2			
					60	10	1			2.0			
BLT 2/05/01/01	02003.008	P	moist	tri	80	10	6	13.4	0.37	5.5	4650	3350	3900
					80	10	5			5.0			
					80	10	2.5			3.3			
					80	10	1			1.9			
BLT 2/10/01/01	01017.122	P	moist	tri	80	10	10	16.1	0.35	6.6	8000	6100	5200
					80	10	7.5			5.6			
					80	10	5			4.3			
					80	10	2.5			2.9			
					80	10	1			1.6			
BLT 2/11/01/01	01017.121	P	moist	tri	80	10	3	15.9	0.35	4.9	7450	4500	4300
					80	10	2.5			4.4			
					80	10	1			2.8			
BLT 2/14/01/01	01017.125	P	moist	tri	80	10	1	12.0	0.26	2.9		4800	3600
BLT 2/25/01/01	02007.026	P	moist	tri	80	10	6	12.8	0.34	4.0	7100	4700	5000
					80	10	5			3.9			
					80	10	2.5			2.9			
					80	10	1			1.7			

Tab. 8 (continued)

core specification	laboratory + specimen no. resp. file no.	sample orien-tation	moisture state	type of test	T [°C]	strain rate dε/dt [10^{-6}/s]	conf. pressure σ_3 [MPa]	shear strength $\sigma_{dev,peak}$ [MPa]	strain at failure ε_{fail} [%]	residual strength $\sigma_{dev,res}$ [MPa]	Young's modulus E [MPa]	tangent modulus E_v [MPa]	residual deform. modulus E_{res} [MPa]
BLT 9/08/01/01	03005.041	P	moist	tri	80	10	4.5	13.2	0.52	6.3	4540	2450	3470
BLT 9/13/01/01	03005.042	P	moist	tri	80	10	7.5	13.6	0.59	7.8	4920	2450	2770
BLT 10/03/01/01	03006.046	P	moist	tri	80	10	1	12.1	0.21	3.5		6100	4350
BLT 10/04/01/01	03006.047	P	moist	tri	80	10	3	15.0	0.46	7.0	5200	3450	3250
					80	10	2.5			6.2			
					80	10	1			3.7			
BLT 10/06/01/01	03006.048	P	moist	tri	80	10	6	16.6	0.36	10.1	5250	4200	2650
BLT 15/25/01	07029	S	moist	uni	30	1 MPa/min	0	15.0	1.13				
BLT 19/06/01	08064	S	moist	uni	30	50	0	9.4	1.15				
BLT 12/06/01	04179	S	moist	tri	30	1	3	12.5	1.54				
BLT 3/23/01/01	02016.100	S	moist	tri	31	10	6			5.0			850
					31	10	5			4.7			
					31	10	2.5			3.9			
					31	10	1			2.5			
BLT 5/03/01/01	02016.096	S	moist	tri	32	10	10	13.5	2.15	11.6	2150	800	1450
					32	10	7.5			10.4			
					32	10	5			8.2			
					32	10	2.5			5.4			
					32	10	1			3.3			
BLT 5/05/01/01	02016.098	S	moist	tri	31	10	3	11.5	2.90	7.0	1800	500	800
					31	10	2.5			6.4			
					31	10	1			4.0			
BLT 5/15/01/01	02016.089	S	moist	tri	30	10	1	13.7	1.62	4.7	2650	1350	550
BLT 5/19/01/01	02016.091	S	moist	tri	31	10	6	16.6	2.56	10.1	2250	1000	950
					31	10	5			8.7			
					31	10	2.5			5.6			
					31	10	1			3.4			
BLT 5/22/01/01	02016.103	S	moist	tri	29	10	1	10.6	1.04	4.0	2400	1500	750

Tab. 8 (continued)

core specification	laboratory + specimen no. resp. file no.	sample orien-tation	moisture state	type of test	T [°C]	strain rate dε/dt [10^{-6}/s]	conf. pressure σ_3 [MPa]	shear strength $\sigma_{dev,peak}$ [MPa]	strain at failure ε_{fail} [%]	residual strength $\sigma_{dev,res}$ [MPa]	Young's modulus E [MPa]	tangent modulus E_v [MPa]	residual deform. modulus E_{res} [MPa]
BLT 5/27/01/01	02016.101	S	moist	tri	30	10	0	12.4	1.05		2650	2100	1250
					30	10	10			10.7			
					30	10	7.5			9.8			
					30	10	5			8.1			
					30	10	2.5			5.4			
					30	10	1			3.3			
BLT 12/03/01/01	03006.054	S	moist	tri	32	10	6	11.5	1.33	7.2	2700	1250	950
					32	10	5			6.5			
					32	10	2.5			4.5			
					32	10	1			2.9			
BLT 12/10/01/01	03006.049	S	moist	tri	33	10	3	13.0	1.62	6.3	2400	1000	900
					33	10	2.5			5.8			
					33	10	1			3.9			
BLT 15/07/01	08021	S	moist	mult	25	0.1	1	10.7	0.59		5480		
					25	0.1	5	13.9	0.59				
					25	0.1	15	15.5	0.97				
					25	0.1	25	16.1	1.14				
					25	0.1	1			3.7			
					25	0.1	5			9.3			
					25	0.1	9			11.9			
					25	0.1	10			11.3			
					25	0.1	13			12.9			
					25	0.1	15			13.6			
					25	0.1	17			13.6			
					25	0.1	19			13.7			
					25	0.1	21			13.0			
					25	0.1	23			13.8			
					25	0.1	25			13.5			
					25	0.1	27.5			13.9			
					25	0.1	30			13.8			

Tab. 8 (continued)

core specification	laboratory + specimen no. resp. file no.	sample orien-tation	moisture state	type of test	T [°C]	strain rate dε/dt [10^{-6}/s]	conf. pressure σ_3 [MPa]	shear strength $\sigma_{dev,peak}$ [MPa]	strain at failure ε_{fail} [%]	residual strength $\sigma_{dev,res}$ [MPa]	Young's modulus E [MPa]	tangent modulus E_v [MPa]	residual deform. modulus E_{res} [MPa]
BED-C 9/01/02/01	00011.080	S	dry	tri	24	10	0.5	21.5	0.27	6.7		9850	9800
					24	10	7.5			20.9			14200
					24	10	5			17.2			
					24	10	2.5			10.1			
					24	10	1			5.5			
BED-C 9/01/02/02	00011.081	S	dry	tri	24	10	2	29.7	0.43	10.1	12650	8150	12050
					23	10	20			36.0			8950
					23	10	17.5			33.9			
					23	10	15			29.6			
					23	10	12.5			25.8			
					23	10	10			22.6			
					23	10	7.5			20.4			
					23	10	5			15.5			
					23	10	2.5			8.9			
					23	10	1			4.6			
BED-C 9/01/02/03	00011.082	S	dry	tri	23	10	6	39.9	0.90	18.5	12600	7100	7350
					23	10	15			30.9			7700
					24	10	12.5			28.4			
					24	10	10			22.8			
					24	10	7.5			18.2			
					24	10	5			14.8			
					24	10	2.5			10.8			
					24	10	1			6.2			
BED-C 9/01/02/04	00011.083	S	dry	tri	24	10	10	45.7	1.04	25.5	13250	8050	9700
					24	10	7.5			22.4			
					24	10	5			17.3			
					23	10	2.5			11.0			
					23	10	1			5.7			
BLT 12/11/01/01	03006.050	S	dry	tri	23	10	1	24.4	1.51	5.9	4050	2150	1800

Tab. 8 (continued)

core specification	laboratory + specimen no. resp. file no.	sample orien-tation	moisture state	type of test	T [°C]	strain rate $d\varepsilon/dt$ [10^{-6}/s]	conf. pressure σ_3 [MPa]	shear strength $\sigma_{dev,peak}$ [MPa]	strain at failure ε_{fail} [%]	residual strength $\sigma_{dev,res}$ [MPa]	Young's modulus E [MPa]	tangent modulus E_v [MPa]	residual deform. modulus E_{res} [MPa]
BLT 12/13/01/01	03006.051	S	dry	tri	23	10	10	29.4	1.69	18.3	5320	2300	1900
					23	10	7.5			14.6			
					23	10	5			10.7			
					23	10	2.5			6.8			
					23	10	1			3.8			
BLT 5/02/01/01	02016.106	S	moist	tri	80	10	10	9.0	1.99	6.9	1500	600	850
					80	10	7.5			6.4			
					80	10	5			5.5			
					80	10	2.5			3.7			
					80	10	1			2.1			
BLT 5/10/01/01	02016.097	S	moist	tri	80	10	3	8.8	1.45		1950	850	
BLT 5/13/01/01	02016.102	S	moist	tri	80	10	0	3.9	1.75			200	1380
					80	10	10			8.6			
					80	10	7.5			6.7			
					80	10	5			5.2			
					80	10	2.5			3.2			
					80	10	1			1.7			
BLT 5/16/01/01	02016.090	S	moist	tri	80	10	6	12.0	1.94	7.3	1550	750	800
					80	10	5			6.9			
					80	10	2.5			4.7			
					80	10	1			2.7			
BLT 5/20/01/01	02016.104	S	moist	tri	80	10	1	8.4	0.94	3.0	2100	1950	1200
BLT 12/07/01/01	03006.056	S	moist	tri	80	10	6	9.8	1.20	6.9	2400	1200	1000
					80	10	5			6.7			
					80	10	2.5			4.9			
					80	10	1			3.0			
BLT 12/08/01/01	03006.055	S	moist	tri	80	10	3	8.4	0.99	5.5	1800	1150	1000
					80	10	2.5			5.1			
					80	10	1			3.1			

Tab. 8 (continued)

core specification	laboratory + specimen no. resp. file no.	sample orien-tation	moisture state	type of test	T [°C]	strain rate dε/dt [10^{-6}/s]	conf. pressure σ_3 [MPa]	shear strength $\sigma_{dev,peak}$ [MPa]	strain at failure ε_{fail} [%]	residual strength $\sigma_{dev,res}$ [MPa]	Young's modulus E [MPa]	tangent modulus E_v [MPa]	residual deform. modulus E_{res} [MPa]
BLT 12/14/01/01	03006.052	S	dry	tri	80	10	1	17.7	1.03	6.0	4900	1950	1150
BLT 12/15/01/01	03006.053	S	dry	tri	80	10	10	23.7	1.78	15.4		1750	1550
					80	10	7.5			9.9			
					80	10	5			7.4			
					80	10	2.5			4.5			
					80	10	1			2.4			
BLT 4/09/01	02009.045	Z	moist	tri	35	10	6	5.0	0.42	2.9	3150	1150	1800
					35	10	5			3.0			
					35	10	2.5			2.6			
					35	10	1			1.8			
BLT 4/12/01	02009.044	Z	moist	tri	34	10	1			2.6			850
BLT 6/03/01/01	02016.092	Z	moist	tri	30	10	0	8.4	1.34		1850	1300	1700
					30	10	10			9.9			
					30	10	7.5			9.3			
					30	10	5			7.9			
					30	10	2.5			5.6			
					30	10	1			3.6			
BLT 6/18/01/01	02016.094	Z	moist	tri	33	10	3						2600
					33	10	10			10.3			2400
					33	10	7.5			9.8			
					33	10	5			8.5			
					33	10	2.5			6.3			
					33	10	1			3.8			
BED-C 10/01/03/01	00011.084	Z	moist	tri	23	10	0.5			4.2			3100
					23	10	7.5			16.9			4150
					23	10	5			12.3			
					23	10	2.5			9.6			
					23	10	1			5.4			

Tab. 8 (continued)

core specification	laboratory + specimen no. resp. file no.	sample orien-tation	moisture state	type of test	T [°C]	strain rate dε/dt [10^{-6}/s]	conf. pressure σ_3 [MPa]	shear strength $\sigma_{dev,peak}$ [MPa]	strain at failure ε_{fail} [%]	residual strength $\sigma_{dev,res}$ [MPa]	Young's modulus E [MPa]	tangent modulus E_V [MPa]	residual deform. modulus E_{res} [MPa]
BED-C 10/01/02/01	00011.085	Z	moist	tri	23	10	2			6.6			2450
					23	10	20			24.7			3700
					23	10	17.5			22.9			
					23	10	15			22.7			
					23	10	12.5			21.4			
					23	10	10			18.9			
					23	10	7.5			15.1			
					23	10	5			13.6			
					23	10	2.5			7.7			
					23	10	1			6.4			
BED-C 10/01/02/02	00011.086	Z	moist	tri	24	10	6	15.9	1.19	14.7	7750	4150	5950
					24	10	15			23.1			4000
					24	10	12.5			22.5			
					24	10	10			19.5			
					24	10	7.5			16.7			
					24	10	5			12.1			
					24	10	2.5			9.1			
					24	10	1			5.9			
BED-C 10/01/02/03	00011.087	Z	moist	tri	22	10	10	20.0	1.42	19.7	5550	3800	5500
					22	10	7.5			17.6			
					22	10	5			14.3			
					22	10	2.5			9.8			
					22	10	1			5.8			

Tab. 8 (continued)

core specification	laboratory + specimen no. resp. file no.	sample orien-tation	moisture state	type of test	T [°C]	strain rate dε/dt [10^{-6}/s]	conf. pressure σ_3 [MPa]	shear strength $\sigma_{dev,peak}$ [MPa]	strain at failure ε_{fail} [%]	residual strength $\sigma_{dev,res}$ [MPa]	Young's modulus E [MPa]	tangent modulus E_v [MPa]	residual deform. modulus E_{res} [MPa]
BED-C 10/01/02/04	00011.088	Z	moist	tri	23	10	20	29.7	2.04	25.2	8700	2600	3200
					23	10	30			28.0			2350
					23	10	27.5			27.2			
					23	10	25			26.4			
					23	10	22.5			25.7			
					23	10	20			23.9			
					23	10	17.5			21.4			
					23	10	15			21.0			
					23	10	12.5			18.2			
					23	10	10			17.2			
					23	10	7.5			13.0			
					23	10	5			10.1			
					23	10	2.5			6.4			
					23	10	1			3.2			
BLT 4/02/01	02009.043	Z	moist	tri	80	10	1	4.9	0.45	1.7	2450	1500	1350
BLT 4/04/01	02009.049	Z	moist	tri	80	10	7	5.3	0.72	3.2	2950	1100	1350
BLT 4/06/01	02009.048	Z	moist	tri	80	10	2.05	3.8	0.45	3.6	2050	1150	1900
					80	10	1			2.2			
BLT 6/24/01/01	02016.105	Z	moist	tri	80	10	6	7.8	1.01	5.8	2450	1050	1100
					80	10	5			5.4			
					80	10	2.5			4.0			
					80	10	1			2.5			
BLT 6/25/01/01	02016.093	Z	moist	tri	80	10	0	1.4	1.20		2650	100	1600
					80	10	6			6.9			
					80	10	5			6.3			
					80	10	2.5			4.3			
					80	10	1			2.7			